Smart Water for Enhanced Oil Recovery from Seawater and Produced Water by Membranes

by

Remya Ravindran Nair

Thesis submitted in fulfilment of
the requirements for the degree of
PHILOSOPHIAE DOCTOR
(PhD)

Faculty of Science and Technology
Department of Chemistry, Bioscience and Environmental Engineering
2018

University of Stavanger
NO-4036 Stavanger
NORWAY
www.uis.no

ISBN: Click to enter ISBN.
ISSN: Click to enter ISSN.
PhD: Thesis UiS No. Click to enter PhD No.

Acknowledgements

I would like to address my utmost gratitude to my main supervisor Professor Torleiv Bilstad for his support and guidance throughout this research. Professor Torleiv Bilstad is a great inspiration for all the students and I would like to thank him for giving me the opportunity to present my work at several national and international conferences.

I am deeply grateful to Dr. Skule Strand for his advice and guidance as my co-supervisor. The friendly, supportive, long technical discussions with Dr. Skule have been inspiring. I highly appreciate my former colleague Evgenia Protasova for constructive reviewing my papers and assisting in the lab and for creating such a wonderful working atmosphere.

Special thanks to the National IOR Centre of Norway for the financial support of my Ph.D. project. Special mention to Professors Merete Vadla Madland and Aksel Hiorth for proper guidance. It has been a great experience working with the Centre. I am also grateful to emeritus Professor Aud Berggraf Sæbø for lessons on presentations.

I also appreciate the time, effort and commitment of all the people at the faculty. Special thanks to Liv Margaret Aksland for her advice and timely supply of my research equipment, Lyudmyla Nilson for using her lab and equipment during experiments, Kåre Bredeli Jørgensen for his help with the IR. I would also like to thank Reidar Inge Korsnes for guiding me with the IC experiments. Special mention to John Grønli, Jan Magne Nygård and Tor Gulliksen from the Mechanical Engineering. Thanks to Terje Jåsund at Statsbygg for always arranging transportation of seawater from Mekjarvik. The administrative support from the faculty is also highly appreciated.

Many Ph.D. students at the University have helped with my experiments. A special thanks to Mona Wetrus Minde for helping me with SEM

analyses. I am also thankful to the master and bachelor students for their assistance in the lab.

I want to express my deepest gratitude to my parents and sister for all their support and encouragement.

Lastly, I want to express my sincere gratitude to my husband Anil for moral support and my kids, Hemant and Nandita for their love and patience through all these years.

Remya Ravindran Nair

Summary

Sustainable use of scarce water resources and stringent environmental regulations are currently moving the focus towards environmentally friendly and cost-effective injection methods in the offshore oil industry. Water injection is used for most oil reservoirs as pressure support and improved displacement of oil. Most water-based enhanced oil recovery (EOR) techniques consist of chemical injection into reservoirs resulting in hazardous flow back of chemicals and produced water (PW). Smart water injection is an alternative and simultaneously represents a sustainable environmental and economic EOR flooding technique. The optimized ionic composition of injection water improves the initial wetting towards more water-wet conditions, which improves displacement efficiency due to increased capillary forces.

Smart water improves oil recovery by wettability alteration in both carbonate and sandstone reservoirs. Seawater is the main injection brine offshore and when enriched in divalent ions such as SO_4^{2-} and Ca^{2+} and depleted in Na^+ and Cl^- is considered smart water in carbonates. Injection brine with salinity below 5,000 mg/L and low in divalent cations are considered suitable as smart water in sandstone reservoirs.

Nanofiltration membranes (NF) are efficient in performing partial desalination of seawater and PW at low feed pressures resulting in high flux and low power consumption. The main focus of this research was to determine appropriate technical conditions and limitations of NF membranes for producing smart water from seawater and PW.

Special focus was on exploring NF membrane performance in terms of flux and rejection under varying feed compositions, pressures, pH and recoveries of polyamide and sulfonated polyethersulfone membranes. Both permeate and retentate streams from NF membranes are used for producing smart water. The divalent ion rich retentate could be used in carbonate reservoirs, whereas the permeate with low divalent ion

concentrations is optimal for sandstone reservoirs with seawater as membrane feed.

Produced water re-injection (PWRI) as smart water was evaluated as an alternative to PW discharge in terms of environmental and economic advantages. One of the main concerns in membrane treatment of PW is the presence of organics that cause membrane fouling. De-oiling of synthetic PW by media filtration upstream NF membranes eliminated fouling during short-term membrane experiments.

Additionally, the presence of barium and strontium ions in PW cause scaling if mixed with seawater. Membrane removal of Ba^{2+} and Sr^{2+} was optimized by increasing the concentration of scaling ions in the feed which resulted in efficient removal of Ba^{2+} and Sr^{2+} during NF experiments. However, the main challenge in reusing PW as smart water is low flux through NF membranes.

Experiments with altering pH of seawater were performed within pH limitations of the membrane materials to determine the effect of pH on membrane performance. A comparison between pH tolerance on polyamide and sulfonated polyethersulfone membranes were conducted during the experiments. A significant change in ion rejection was observed even with small changes in pH.

Another limitation with NF membrane separation with PW is the high total dissolved solids (TDS) in PW yielding high osmotic and operating pressures. Dilution of PW with NF permeate with seawater as feed reduces TDS.

Artificial neural network (ANN) was used to predict ion rejection based on multiple variable experimental data for feed pH, pressure and flux. An ANN structure was designed that were in close agreement between ANN predictions and experimental data, exceeding 95 % agreement for the tested membranes.

Based on experimental data, a predictive model was developed to quantify individual ion rejection by polyamide membranes using

Spiegler-Kedem model based on non-equilibrium thermodynamics and steric hindrance pore model. These models using rejection and flux values from six commercially available membranes determined the membrane transport parameters that included reflection coefficient and solute permeability. Membrane characterization was also accomplished by determining the effective pore radius of each membrane based on steric hindrance pore model for individual ions present in seawater. Experimental data were implemented for modeling the rejection characteristics of polyamide NF membranes with pure water permeabilities suitable for smart water production. Equations were formulated from plots of pure water permeability versus reflection coefficient and solute permeability which enable end users to choose suitable NF membranes without performing extensive membrane experiments.

Power consumption analysis of membrane operations was evaluated for smart water production in carbonates and sandstones using both seawater and PW as membrane feed. Power consumed per cubic meter of smart water produced for carbonates was 0.7 kWh/m^3 and 5.2 kWh/m^3 for sandstones using seawater as feed. A power consumption analysis using PW as feed was 0.88 kWh/m^3 for carbonate reservoirs. For sandstone reservoirs, the power required for smart water production was 13.99 kWh/m^3.

List of Articles

Paper I

Membrane Performance Analysis for Smart Water Production for Enhanced Oil Recovery in Carbonate and Sandstone Reservoirs

Remya R. Nair, Evgenia Protasova, Skule Strand and Torleiv Bilstad
Energy & Fuels, 2018, 32 (4), pp 4988-4995
DOI: 10.1021/acs.energyfuels.8b00447

Paper II

Evaluation of Nanofiltration Membranes for Smart Water Production in Carbonate Reservoirs from De-Oiled Produced Water and Seawater

Remya R. Nair, Evgenia Protasova, Skule Strand and Torleiv Bilstad
SPE Productions and Operations (Under Review)

Paper III

Effect of pH on Produced Water Treatment Using Nanofiltration Membranes: Artificial Neural Network for Performance Assessment and Steric Hindrance Pore Model for Flux Variation Evaluation

Remya R. Nair, Evgenia Protasova, Skule Strand and Torleiv Bilstad
Desalination and Water Treatment (Under Review)

Paper IV

Implementation of Spiegler - Kedem and Steric Hindrance Pore Models for Analyzing Nanofiltration Membrane Performance for Smart Water Production

Remya R. Nair, Evgenia Protasova, Skule Strand and Torleiv Bilstad
Membranes, 2018, 8 (3), 78

DOI:org/10.3390/membranes8030078

Conference Presentations and Proceedings

1. "Produced Water Treatment with Membranes for Enhanced Oil Recovery in Carbonate and Sandstone Reservoirs", 19th European Symposium on Improved Oil Recovery, Stavanger, Norway from 24-27th April 2017, DOI:10.3997/2214-4609.201700296.
2. "Reuse of Produced Water by Membranes for Enhanced Oil Recovery", SPE Annual Technical Conference and Exhibition, Dubai, September 26-28, 2016, ISBN 978-1-61399-463-4. DOI: 10.2118/181588-MS.
3. "Applicability and Costs of Nanofiltration for Produced Water Reinjection for EOR", Industrial and Hazardous Waste Management, organized by Technical University of Crete, September 27-30, 2016, extended abstract is published (ISSN 2241-3138. ISBN: 978-960-8475-24-3. p. 265-266).
4. "Oily Waste Regulations and Best Available Technologies for Sustainable Development", Industrial and Hazardous Waste Management, organized by Technical University of Crete, September 27-30, 2016, (ISSN 2241-3138. ISBN: 978-960-8475-24-3. p. 357-358).
5. "Re-injection of Produced Water for Enhanced Oil Recovery by Membranes", European Desalination Society, Desalination for the Environment: Clean Water and Energy, Rome, Italy, May 22-26, 2016.
6. "Evaluation of NF membrane characteristics and ionic selection from produced water for IOR", AWWA/AMTA Membrane Technology Conference, San Antonio, Texas, USA, February 1-5, 2016.
7. "Evaluation of NF membrane characteristics and ionic selection from seawater for IOR", AWWA/AMTA Membrane Technology Conference, San Antonio, Texas, USA, February 1- 5, 2016.

8. "Ionic selection from seawater using membranes for IOR", 2nd International Conference on Desalination using Membrane Technology, July 2015, Singapore.
9. "Improved oil production by membranes", 26th Drilling-Oil-Gas AGH 2015 Conference, June 2015, Poland, – Paper published, (AGH Drilling Oil Gas 2015; Volume 32 (1) p. 221-231. ISSN 2299-4157, dx.doi.org/10.7494/drill.2015.32.1.221
10. "Produced Water Treatment with Membranes for Enhanced Oil Recovery in Carbonate and Sandstone Reservoirs", NFiP (Petroleum Research School of Norway), Stavanger Oil Museum, November 2017
11. "Cost Effective Smart Water Production for Enhanced Oil Recovery by Membranes", NORWEP (Norwegian energy partners), Energy seminar: Efficiency in the oil industry, Norwegian Energy Partners, 6 April 2017, Jakarta, Indonesia.
12. "Smart water production from seawater and produced water by membranes", 6th annual November conference for Norwegian / Brazilian Energy Research, 12-13th November 2018, Rio de Janeiro, Brazil.

Poster Presentations

1. Modification of seawater by membranes for enhanced oil recovery", European Desalination Society, Desalination for the Environment: Clean Water and Energy, Rome, Italy, May 22-26, 2016.
2. 'Smart Water for EOR by Membranes' at The National IOR Centre Annual Conference, Stavanger, Norway, April 26-27, 2016.
3. *"*Ionic Selection from Seawater for IOR*"*, IDA World Congress 2015 Technical Program, San Diego, California, August 30, 2015 – September 4, 2015.

4. “Ionic selection from produced water using NF membranes for IOR” as co-author, 2nd International Conference on Desalination using Membrane Technology, July 2015, Singapore.

Abbreviations and Symbols

ANN	Artificial Neural Network
A	Membrane Area or Feed Channel Cross-section
a	Membrane Width
$A_k/\Delta x$	Ratio of Membrane Porosity to Membrane Thickness
b	Channel Spacer Height
CoBR	Crude Oil-Brine-Rock
CP	Concentration Polarization
C_f	Feed Concentration
C_p	Permeate Concentration
C_c	Retentate Concentration
C_m	Concentration at the Membrane Surface
D	Hydraulic Diameter
EDS	Energy Dispersive X-Ray spectroscopy
EOR	Enhanced Oil Recovery
E_{oil}	Hydrocarbon Removal Efficiency
FW	Formation Water
h_{ch}	Channel Height
IR	Infrared
J_v, J_s	Solvent and solute flux, respectively
k	Mass Transfer Coefficient
L_p	Pure Water Permeability
LS	Low Salinity
LSE	Low Salinity Effect
MF	Microfiltration
MWCO	Molecular Weight Cut-off
MSE	Mean Square Error
NF	Nanofiltration
NTU	Nephelometric Turbidity Unit
OOIP	Original Oil in Place

PV	Pore Volume
PW	Produced Water
PWRI	Produced Water Reinjection
P_s	Solute Permeability Coefficient
Δp	Pressure Difference
PV	Pore Volume
Q_f	Feed Flow Rate
Q_p	Permeate Flow Rate
Q_r	Retentate Flow Rate
RO	Reverse Osmosis
R_{obs}	Observed Rejection
r_p	Pore Radius
S_D	Steric Hindrance Factor for Diffusion
S_F	Steric Hindrance Factor for Filtration Flow
SHP	Steric Hindrance Pore Model
SI	Spontaneous Imbibition
SK	Spiegler-Kedem Model
t	Filtration Time
TDS	Total Dissolved Solids
TFC	Thin Film Composite
UF	Ultrafiltration
v	Permeate Volume
VF	Viscous Flooding
w_{ch}	Channel Width
η	Efficiency of the pump
μ	Feed Viscosity or dynamic viscosity
π_F	Feed Osmotic Pressure
$\Delta\pi$	Osmotic Pressure Difference
σ	Reflection Coefficient
υ	Cross-flow Velocity
ρ	Density of Feed Water
Ø	Flow Channel Porosity
ν	Kinematic Viscosity

Table of Contents

Acknowledgements iii

Summary v

List of Articles ix

Abbreviations and Symbols xiii

List of Figures xvii

List of Tables xix

1 Introduction 1

1.1 Oil Recovery Methods 1

1.2 EOR by Smart Water 3

1.3 Smart Water Production from PW 3

1.4 Smart Water Production by Membranes 4

2 Objectives and Scope 7

3 Literature Review 9

3.1 Smart Water 9

3.2 Membrane Technology 18

3.3 Factors Affecting NF Membrane Performance 21

3.4 Separation Mechanisms 23

3.5 Kedem - Katchalsky Permeability Equations 24

3.6 Spiegler - Kedem Model 25

3.7 Steric Hindrance Pore Model 25

3.8 Artificial Neural Network (ANN) Theoretical 27

3.9 Membrane Regeneration 28

4 Experiments and Methods 29

4.1 Membrane Selection 29

4.2 Membrane Testing 30

4.3 Chemicals, Analytical Instruments and Feed Compositions 31

4.4 Membrane Cleaning and Preservation 32

4.5 Media Filtration for Oil Removal 32

4.6 Infrared (IR) Analysis 34
4.7 Scanning Electron Microscopy (SEM) 35
4.8 Modeling of Membrane Experiments 35
5 Results and Discussion 37
5.1 Pure Water Permeability 37
5.2 Reynolds Number 38
5.3 Effect of Applied Pressure on Ion Rejection 38
5.4 Effect of Increased Feed Concentration on Ion Rejection 42
5.5 Produced Water Treatment 45
5.6 Spiegler - Kedem Model 55
5.7 Steric Hindrance Pore Model 55
5.8 Power Consumption Analysis 60
6 Concluding Remarks 65
6.1 Conclusions 65
6.2 Future Work 67
References 69
Appendices 79
Appendix 1 – Paper I 79
Appendix 2 – Paper II 81
Appendix 3 – Paper III 83
Appendix 4 – Paper IV 85

List of Figures

Figure 1. Schematic of smart water production from seawater using NF membranes 5
Figure 2. Oil recovery tests on sandstone cores at 60 °C by secondary and tertiary LS injection [21, 22] 10
Figure 3. Smart water mechanisms with LSE on sandstone reservoirs [20] ... 12
Figure 4. Schematic of mechanisms for wettability alteration in carbonates a) Mechanisms when monovalent ions are present b) Mechanisms with increased Ca^{2+} and SO_4^{2-} and decreased Na^+ and Cl^- concentrations [28]. 13
Figure 5. Effect of smart water on carbonate core at 110 °C [19] 14
Figure 6. Spontaneous imbibition of brines with varying SO_4^{2-} concentrations into fractional intermediate wetted chalk cores [30] 15
Figure 7. Spontaneous imbibition of brines with varying Ca^{2+} concentrations into chalk cores at 70 °C [30] 16
Figure 8. SI experiments with modified seawater containing only SO_4^{2-} and NaCl (without Ca^{2+} and Mg^{2+}) [31] 17
Figure 9. Spontaneous imbibition of brines into oil saturated chalk cores at 90 °C with VB (FW), seawater (SW), and modified seawater (SW0NaCl, and SW0NaCl- 4 × SO_4^{2-}) [32] 18
Figure 10. Schematic of the membrane system used for the experiments [63] 30
Figure 11. Schematic of the lab-scale media filtration unit 34
Figure 12. Ion rejection with increasing pressure with NANO-SW 39
Figure 13. Cl^- rejection for six NF membranes 40
Figure 14. Na^+ rejection for six NF membranes 40
Figure 15. Comparison of SO_4^{2-} rejection with pressure for six membranes .. 41
Figure 16. Flux variations with increased SO_4^{2-} concentrations in the feed ... 43
Figure 17. Cl^- rejection with increased SO_4^{2-} concentration 44
Figure 18. Comparison of influent and effluent samples a) before extraction b) after extraction 45
Figure 19. Rejection of Ba^{2+} and Sr^{2+} with NANO-SW 46
Figure 20. Flux versus pressure with Ba^{2+} and Sr^{2+} in the feed 47
Figure 21. SEM image of NF membrane on the feed side 48

Figure 22. EDS analysis of Spot 1 48
Figure 23. SEM image on the permeate side of the membrane 49
Figure 24. Flux variations with a change in pH with ESNA membrane..... 50
Figure 25. Effect of pH on Cl^- rejection for NF 270..... 51
Figure 26. Effect of pH on Na^+ rejection with NF 270..... 52
Figure 27. Variations in pore size with feed pH 53
Figure 28. ANN design with 7 neurons to predict ion rejections at varying feed pH..... 54
Figure 29. Rejection versus flux for Na^+ for ESNA 55
Figure 30. Pure water permeability versus (a) reflection coefficient (b) solute permeability of chloride 58
Figure 31. Schematic for smart water production from seawater 61
Figure 32. Schematic for smart water production from PW for carbonate and sandstone reservoirs 62

List of Tables

Table 1. EOR classifications [2] 2
Table 2. Ion Properties [56, 57, 58, 49] 26
Table 3. Membrane specifications according to manufacturers [61, 62] 29
Table 4. Ion compositions of feed analyzed by IC 32
Table 5. Pure water permeabilities of tested membranes 37
Table 6. Effective ion pore radius r_p calculated using SK and SHP models for different membranes 56

1 Introduction

Global energy requirements will rise 30 % and the demand for oil will reach 105 million barrels/day by 2040 [1]. Environmentally friendly and cost-effective recovery mechanisms are preferred to mitigate the demand-supply balance. A range of approaches has been developed over the years to meet this increasing energy demand. Most oil reservoirs implement waterflooding and water-based EOR. Ionic modification of seawater and PW by membranes is such an appropriate energy-efficient method for hydrocarbon recovery.

1.1 Oil Recovery Methods

In classic reservoir engineering, oil recovery is classified as primary, secondary and tertiary processes [2].

Primary recovery results from natural pressures in reservoirs transporting oil to the well surface [3]. Typical recoveries for primary production are 5-20 % of the original oil in place (OOIP). Secondary recovery methods are applied when reservoir pressures decrease during production. Water or gas is injected to retain reservoir pressure and sustain the flow of hydrocarbons towards the production wells. Water forces oil through the reservoir rocks towards the production wells. Seawater is readily available offshore in large quantities and with its incompressible nature requires less energy compared to gas injection. Secondary recovery is pursued until injected fluid appears in considerable amount in the production wells making oil production uneconomical. Primary and secondary recoveries from reservoirs produce 20 - 50 % of OOIP depending on the properties of oil and reservoirs [2] .

Tertiary recovery is also referred to as enhanced oil recovery (EOR) and is implemented following primary and secondary recoveries. EOR

includes techniques for improving oil displacement leading to further increase in hydrocarbon production.

EOR methods are classified into four different categories relating to the mechanisms of oil displacement as shown in Table 1.

Table 1. EOR classifications [2]

Thermal EOR processes	Steam flooding Hot waterflooding In-situ combustion Cyclic steam stimulation
Chemical EOR processes	Surfactant flooding Polymer flooding Alkaline flooding Solvent flooding Micellar
Gas EOR processes	Hydrocarbon injection CO_2 flooding Nitrogen flooding Flue gas injection Water - Alternating - Gas (WAG)
Emerging EOR processes	Smart water Low salinity waterflooding Carbonated waterflooding Microbial EOR Foam

EOR methods recover 50 – 80 % of OOIP [2, 3]. In modern reservoir management, pressure maintenances are mostly achieved through water injection and it is generally accepted that EOR should be implemented as early as possible for optimizing the EOR effect.

1.2 EOR by Smart Water

Increased awareness of chemicals added to the environment is a major concern in the oil and gas industry. EOR by smart water is both cost-effective and environmentally friendly compared with alternative methods in Table 1. Recent extensive studies and experiments have confirmed that initial wetting equilibrium in reservoirs between pore surface minerals, crude oil and formation water (FW) could be changed by injecting brines with different ion compositions compared with FW. Smart water facilitates wettability alteration towards more water-wet conditions. Increased positive capillary forces improve the microscopic sweep efficiency in heterogeneous pore systems, which increase oil recovery. Both field observations and laboratory studies confirm significant EOR potentials using smart water.

Wettability is defined as the ¨*tendency of one fluid to spread on or to adhere to a solid surface in the presence of other immiscible fluids*¨ [4]. Reservoir mineralogy has a fundamental property which regulates the type of interactions controlling adsorption of polar organic compounds in crude oil. Carbonate and sandstone reservoirs differ as the carbonate surface charge is positive whereas sandstones are negatively charged due to the presence of minerals such as clays, quartz, feldspar, and silicate [5].

Injected brine composition is of utmost importance in a wettability alteration process. Ion composition, pH and salinity of the brines are the determining factors [6]. An injected brine with an ion composition different from FW could be capable of modifying the chemical equilibrium between mineral - FW - crude oil [7].

1.3 Smart Water Production from PW

PW is the largest wastewater stream from oil production and is a mixture of FW, injected water, production chemicals, and crude oil. The content is mainly hydrocarbons, inorganic salts, metals and naturally occurring

radioactive materials [8]. Salinity of PW varies between 1000 and 250,000 mg/L [9].

Generally, treatment of PW involves removal of organics such as dissolved and emulsified oil components, dissolved inorganic ions, and particulates such as sand and clay. PW is treated by physical and chemical means before discharging to the environment. Numerous treatment technologies are used to reduce oil in water before discharge where maximum allowed concentration is 40 mg/L of oil in water in several countries [10]. The official threshold for oil in water discharges in Norway is 30 mg/L [11]. Treatment technologies are selected based on PW chemistry, available space, cost, discharge and reuse options.

Reuse of PW as smart water by modifying the ionic composition with membranes is a new approach. A number of pre-treatment steps upstream of membrane treatment are required to prevent membrane fouling. Pre-treatment involves de-oiling, disinfection to avoid biofouling, and suspended solids removal to avoid membrane pore blockage.

1.4 Smart Water Production by Membranes

Membranes are defined as selective barriers that permit passage of certain components while retaining others in a feed [12]. Membrane desalination processes were investigated for producing injection water with required smart water ionic composition. Most onshore oil fields use surface or aquifer water for pressure maintenance and oil displacement. NF and reverse osmosis (RO) membranes are two pressure-driven membrane desalination technologies of interest offshore for smart water production.

During cross flow membrane operations, the feed stream is split into retentate (reject) and permeate [13]. The retentate from an NF membrane with seawater as feed becomes enriched in divalent ions and meet criteria for smart water in carbonate reservoirs. The NF permeate, depleted in

divalent ions and enriched in monovalent ions, may be used as smart water in sandstone reservoirs. A schematic of an NF membrane process is shown in Figure 1.

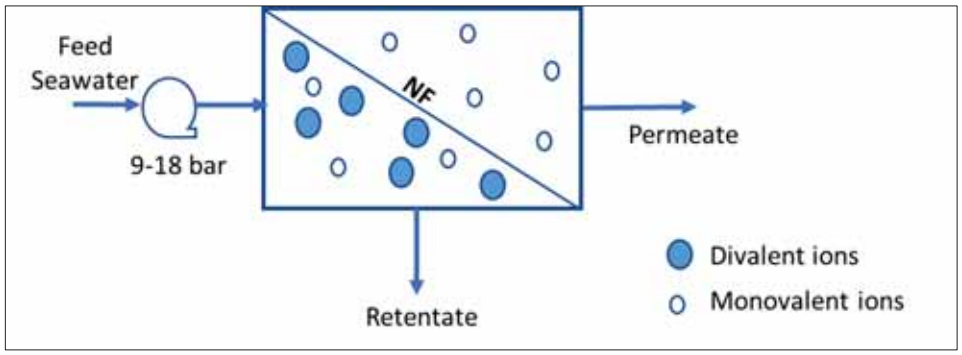

Figure 1. Schematic of smart water production from seawater using NF membranes

NF membranes are easy to operate and are without phase change during operation. Membrane systems are readily combined with supplemental separation processes. Another potential advantage of NF membrane is that performance changes with temperature, pH and feed concentrations [14]. Membrane-based technologies are more suitable for offshore applications due to relatively compact footprint as well as low weight and power requirements compared to alternative desalination technologies [15].

NF and RO membrane desalination processes are widely used both onshore and offshore for desalination and sulfate removal for scale prevention.

- In Marathon Oil Co.UK Ltd. developed together with FilmTec a thin film composite membrane (TFC) for sulfate removal with a capacity of 40,000 barrels per day on South Brae platform installed in November 1988. GE Power and Water reported in 2015 that there are over 80 sulfate removal membrane units globally [16].

- Major seawater desalination plants for potable water production include 330,000 m^3/day in Ashkelon, Israel and a 136,000 m^3/day Tuas in Singapore [17].

2 Objectives and Scope

The main objective of this research was to evaluate the potential of using RO and NF membranes for producing smart water by using seawater and de-oiled synthetic PW as membrane feed.

In Paper I, production of smart water from seawater for carbonate and sandstone reservoirs was evaluated. Seawater was spiked with divalent ions to determine the effect of increased concentrations of SO_4^{2-}, Ca^{2+}, and Mg^{2+} on flux and ion rejection. The energy consumed by major desalination technologies was compared. It was concluded that the use of membranes was optimal for the production of smart water. The power consumed for producing 1 m^3/h of smart water from seawater using membranes was evaluated.

Paper II evaluates the possibility of reusing de-oiled PW as smart water in carbonate reservoirs. Research on PWRI as smart water is an innovative idea and experiments with de-oiled PW were performed to determine membrane separation efficiencies. De-oiling of synthetic PW was performed using a media filtration unit. Rejection of Ba^{2+} and Sr^{2+} were also determined during the experiments. The NF permeate with PW as feed was subjected to equilibration experiments to analyze whether the permeate is compatible with chalk. Power consumed for different water sources used to produce smart water from PW was calculated. The paper concluded that NF is the best available option to produce smart water in carbonates without use of chemicals.

At neutral pH, most NF membranes are negatively charged. Hence, electrostatic interactions between charged solutes and membrane play a role in ion rejection and this interaction depends on feed pH. During reuse of PW as smart water, pH of PW is one of the main concerns that affect NF membrane performance. In **Paper III**, the effect of pH on NF membrane performance was discussed. Experiments were performed on three NF membranes with varying feed pH values from 2.5 to 10.2. The

corresponding ion rejections and flux were measured. Spiegler - Kedem and steric hindrance pore models were used to determine the variations in pore size with pH. An artificial neural network (ANN) was designed with pH, flux and pressure as inputs to the model to quantitatively predict ion rejection. Results can be implemented in industrial scale-up when PW and saline water with different pH are used.

In **Paper IV** correlations were developed for selecting porous polyamide membranes with high feed ionic concentrations for smart water production using Spiegler - Kedem and steric- hindrance pore models. Ten correlations were suggested which could predict the reflection coefficient and solute permeability of individual ions when pure water permeability of a specific membrane was known. This guides the selection of polyamide NF membranes for smart water production.

3 Literature Review

Initial reservoir wetting is controlled by polar acidic and basic organic components present in crude oil. These components can be quantified by acid or base number analysis. The unit of measurement is mg KOH/g for both cases. In acid number analysis, the measurement unit represents the amount of KOH required to neutralize the acidic components in one gram of oil. For basic number measurement, the unit represents the equivalent concentration of basic organic material present in one gram of crude oil.

These acidic materials are generally represented by the carboxylic functional group, -COOH and naphthenic acids where the basic material are typically nitrogen in aromatic molecules and is represented by R_3N:.

Acid and basic material present at the oil-water interface undergoes fast proton exchange reaction that is affected by the pH of the aqueous media and is presented in Equation 1 and Equation 2.

$$R_3NH^+ \rightleftarrows H^+ + R_3N: \quad (1)$$

$$RCOOH \rightleftarrows H^+ + RCOO^- \quad (2)$$

Acid material control initial wetting in carbonates and have alkaline pH due to $CaCO_3$ dissolution, and positively charged mineral surfaces interact with negatively charged acidic components.

3.1 Smart Water

Smart water has an ion composition and salinity different from FW and can alter the established equilibrium between crude oil, FW and pore surface minerals thereby modifying the wetting properties of reservoirs [18]. Smart water is easily implementable, environment-friendly and cost-effective compared to other water-based chemical EOR methods. Optimized smart water compositions have to be evaluated for individual

reservoirs depending on initial wetting, FW composition and reservoir temperature.

3.1.1 Smart Water in Sandstone Reservoirs

Injection water with salinities less than 5,000 mg/L is defined as smart water in sandstones [19]. Mineral surfaces in sandstone reservoirs are generally negatively charged [5]. The wettability in sandstones can change from strongly water-wet to strongly oil-wet. Silica or clay minerals contribute with a large surface area with permanent localized negative charges. Clays undergo CoBR interactions through cation exchange processes and it is confirmed that they have an affinity for crude oil components. It has been suggested that low salinity effect (LSE) in sandstones is controlled by desorption of the polar compounds from the silicate surfaces [20], and is pH dependent. The degree of oil wetness is related to the affinity of polar components at a certain pH, temperature and brine salinity [20].

Figure 2 shows the effect of low salinity brine on sandstone cores at 60 °C confirming that increased oil recovery was observed during low salinity waterflooding.

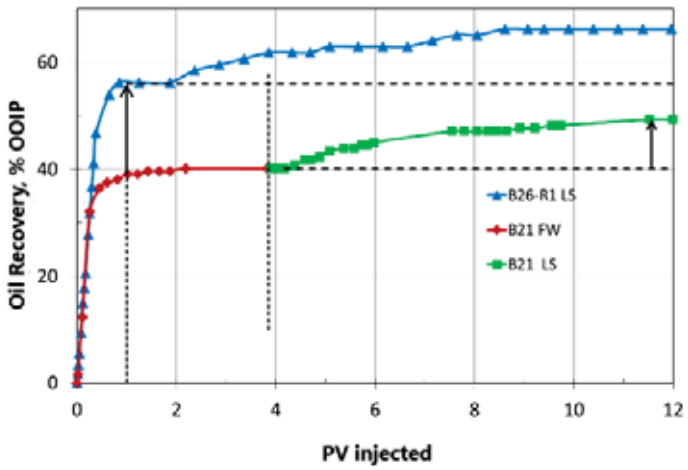

Figure 2. Oil recovery tests on sandstone cores at 60 °C by secondary and tertiary LS injection [21, 22]

The core was initially injected with FW resulting in 40 % OOIP. This was followed by LS brine injection resulting in an OOIP increase to 50 %. However, when the core was injected with LS brine from start resulted in a plateau of 60 - 65 % OOIP by less PV injection.

LSE reported by Tang and Morrow [23] indicated that oil recovery in sandstones increased during spontaneous imbibition (SI) and waterflooding with low salinity water. However, several authors have argued to the existence of different thresholds of salinity that aids in positive salinity effects [24, 25]. It was argued that the presence of divalent ions in low salinity brines have mixed results [26]. Austad et al. [19, 20] suggested that the presence of divalent ions in low salinity brines is not advantageous as it may hinder the rise in pH which is essential to obtain LSE. However, recent research shows that EOR effects with 25,000 mg/L NaCl are possible [27].

Figure 3 presents an explanation for smart water effect in sandstones according to Austad et al. [20]. Figure 3 explains how the acidic and basic components adsorbed onto the clay minerals are desorbed from the clay surface by an in-situ pH increase.

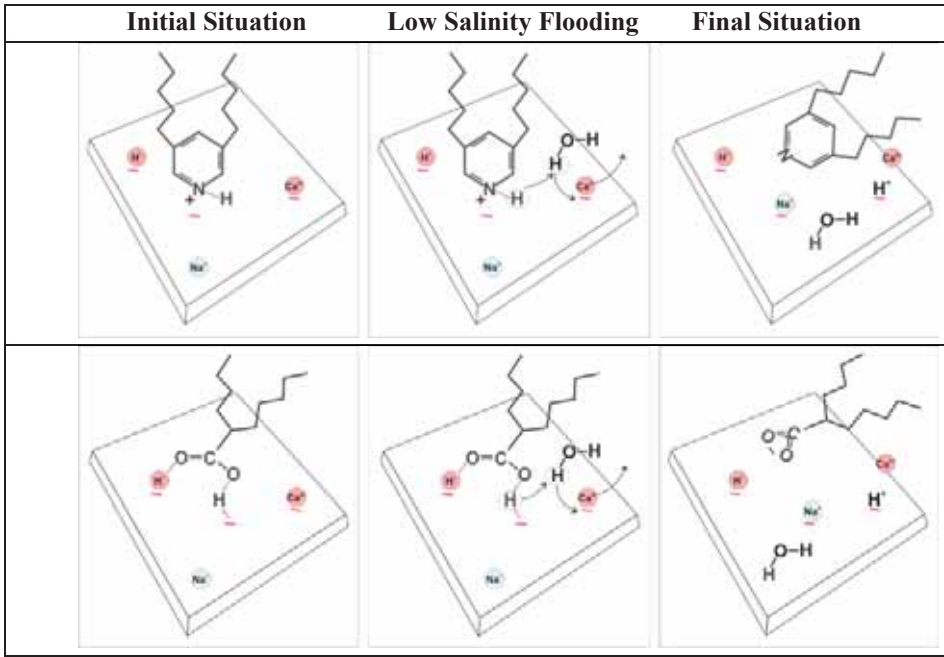

Figure 3. Smart water mechanisms with LSE on sandstone reservoirs [20]

Clays have permanent negative charges and behave as the main wetting mineral in sandstone reservoirs. Equilibrium established with formation water is disturbed when low salinity brine is injected into the reservoir. This results in desorption of Ca^{2+} from the surface to establish a new equilibrium which creates negative charges on the clay surfaces. This negative charge is balanced by adsorption of H^+ at the negative site located on the clay surface. The adsorbed H^+ creates a local pH rise and is the basis for desorption of organic components from clay. Equation 3 explains the reaction.

$$Clay - Ca^{2+} + H_2O \rightarrow Clay - H+ + Ca^{2+}\ OH^- + heat \qquad (3)$$

Presence of divalent ions can reduce the rise in pH by precipitation of hydroxides as shown in Equation 4 and Equation 5 and resulting in reducing possible LSE in sandstones.

$$Mg^{2+}{}_{(aq)} + 2OH^-{}_{(aq)} \rightleftarrows Mg\ (OH)_{2\ (s)} \qquad (4)$$

$$Ca^{2+}_{(aq)} + 2OH^{-}_{(aq)} \rightleftarrows Ca(OH)_{2(s)} \quad (5)$$

3.1.2 Smart Water in Carbonate Reservoirs

The mechanisms by which modified brines or smart water change the wettability of carbonate reservoirs are explained in Figure 4. The initial wetting in carbonates is controlled by negatively charged acidic polar components adsorbed to positive sites at the mineral surface. The wettability alterations are promoted by desorption of acids from the mineral surface.

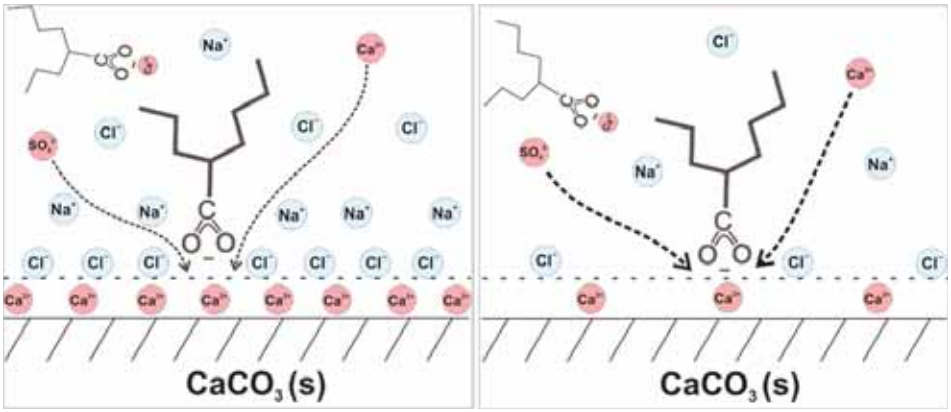

a) b)

Figure 4. Schematic of mechanisms for wettability alteration in carbonates a) Mechanisms when monovalent ions are present b) Mechanisms with increased Ca^{2+} and SO_4^{2-} and decreased Na^+ and Cl^- concentrations [28].

The wettability alterations are triggered by chemical adsorption of SO_4^{2-} and Ca^{2+} [19] present in seawater. Hence, seawater can act as smart water in carbonates and shift the wettability from mixed-wet to water-wet state.

Injection of fluids with salinities between 6,000 and 28,000 mg/L is suitable for carbonate reservoirs. Smart water enriched in sulfate and divalent cations but depleted in monovalent ions are desired in carbonates. Smart water should be enriched with 2 - 4 × SO_4^{2-} and 1 - 2 × Ca^{2+} concentrations compared to seawater for EOR [18, 19, 29].

Figure 5 shows increased oil recovery when seawater was injected into a carbonate core.

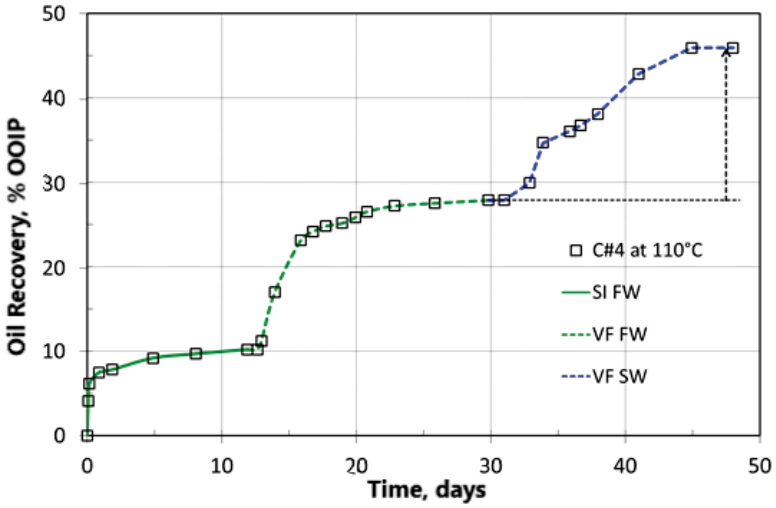

Figure 5. Effect of smart water on carbonate core at 110 °C [19]

The core is subjected to spontaneous imbibition with FW for 12 days resulting in 10 % OOIP confirming initial mixed wetting (Figure 5). Viscous flooding (VF) of the core with FW after SI increased the recovery to 28 %. Switching to seawater after 30 days resulted in an increase to 45 % OOIP. Figure 5 confirms the positive impact of seawater or smart water injection in carbonate reservoirs.

The established chemical equilibrium of a carbonate system is disrupted when a brine with a different ion composition is injected. Negatively charged SO_4^{2-} interacts with positively charged carbonate surface, lowering the surface charge. Due to less electrostatic repulsion, more Ca^{2+} approach the surface and displaces the carboxylic material from the mineral surface. This symbiotic SO_4^{2-} - Ca^{2+} interaction initiates desorption of active polar organic components from the carbonate surface, resulting in wettability alteration [19, 30]. At temperatures above 90 °C, in the absence of Mg^{2+} in the brine, $CaSO_4$ anhydrite precipitation occurs, decreasing the concentration of active ions. If Mg^{2+}

is present in the brine, the ion stabilizes SO_4^{2-} by forming an ion pair between Mg^{2+} and SO_4^{2-}.

Strand et al. [18] and Zhang et al. [30] described the effect of varying sulfate and calcium concentrations in a brine based on seawater and concluded that the oil recovery increased as SO_4^{2-} and Ca^{2+} concentrations in the imbibing fluid increased. The results are presented in Figure 6 and Figure 7.

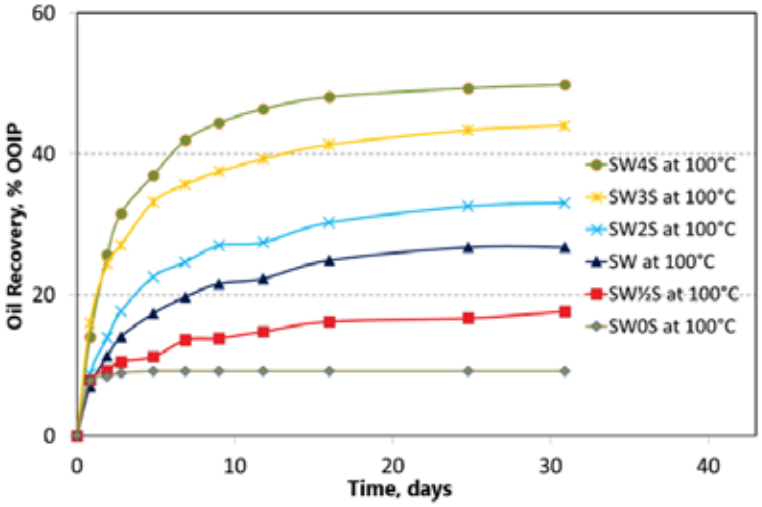

Figure 6. Spontaneous imbibition of brines with varying SO_4^{2-} concentrations into fractional intermediate wetted chalk cores [30]

SO_4^{2-} acts as a catalyst for wettability alteration as presented in Figure 6. The figure demonstrates that brine with no sulfate had the least oil recovery and the recovery increased with increasing SO_4^{2-} concentrations. The result confirms that seawater act as smart water in carbonates [30].

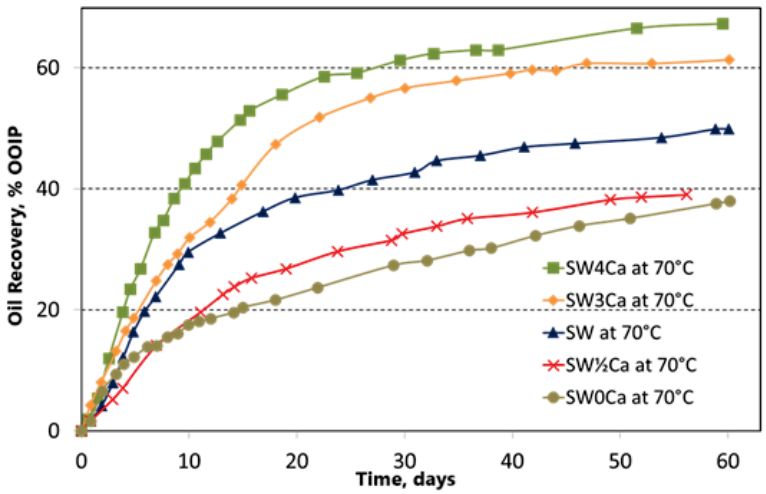

Figure 7. Spontaneous imbibition of brines with varying Ca^{2+} concentrations into chalk cores at 70 °C [30]

Increased wettability alteration with increased calcium concentration occurs as confirmed in Figure 7. Mineral dissolution could not explain the EOR effect due to the common ion effect. Increased Ca^{2+} concentrations reduce $CaCO_3$ dissolution.

Figure 8 shows the oil recovery effect when modified seawater with only divalent SO_4^{2-} and NaCl were used [31].

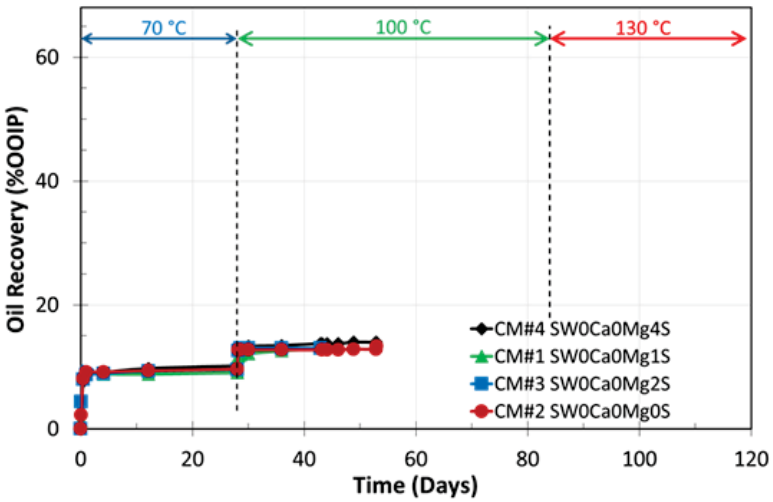

Figure 8. SI experiments with modified seawater containing only SO_4^{2-} and NaCl (without Ca^{2+} and Mg^{2+}) [31]

Figure 8 demonstrated that modified seawater with only sulfate is not smart water even though sulfate could change the mineral surface charge. Presence of Ca^{2+} and Mg^{2+} in the brine is required for wettability alteration and further oil displacement.

Smart water EOR is temperature dependent. EOR brines at high temperature should have only reduced NaCl concentration or low salinity without any increase in SO_4^{2-}/ Ca^{2+} since an increase in these ions will result in precipitation. At low reservoir temperature, low NaCl concentration and increased SO_4^{2-}/ Ca^{2+} concentration will improve the efficiency compared to seawater.

The results confirm that seawater can act as an EOR fluid in chalk reservoirs [19]. However, seawater could be made even smarter and result in further increase in oil recovery. Figure 9 shows the impact of modified brines when spontaneously imbibed into the chalk core [32].

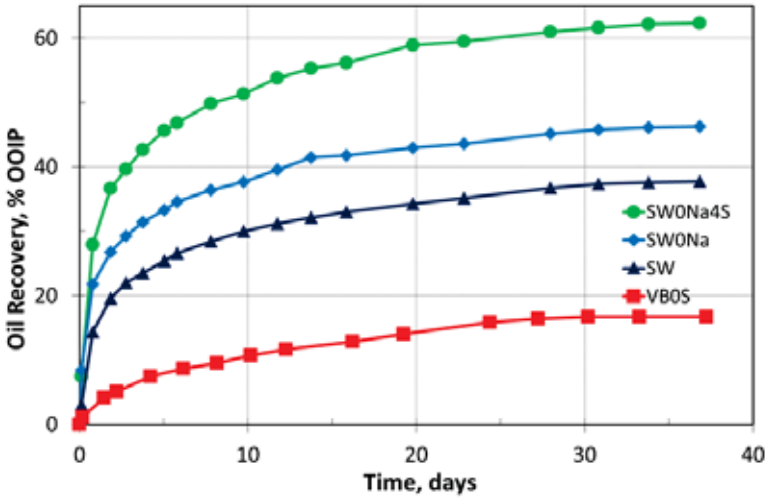

Figure 9. Spontaneous imbibition of brines into oil saturated chalk cores at 90 °C with VB (FW), seawater (SW), and modified seawater (SW0NaCl, and SW0NaCl- 4 × SO_4^{2-}) [32]

FW gave an ultimate recovery of 18 %, seawater behaved as a smart water and improved the oil recovery to 38 %. Seawater depleted in Na (SW0Na) resulted in a maximum oil recovery of 47 % of OOIP, and further spiked four times with sulfate (SW0Na4S), the oil recovery increased to 62 % OOIP. Hence, the imbibition rate was improved when NaCl was removed and when sulfate concentration was increased. This behavior is in line with the mechanism explaining the increased concentration of active ions in the double layer at the chalk surface. The results confirm that wettability alteration in carbonate reservoirs is sensitive to the ionic composition and concentration of ions in the injected brine.

3.2 Membrane Technology

Membrane desalination processes are designed based on the ability of semipermeable membranes to selectively separate or minimize the passage of certain ions. Microfiltration (MF), ultrafiltration (UF), NF

and RO are pressure-driven membrane processes and is classified according to pore sizes. MF membranes have pores in the range 0.1-10 μm with operating pressure 0.1-2 bar. UF membranes have pores from 1-100 nm with operating pressures 1-10 bar [13]. Removal of substances by MF and UF is based on sieving mechanisms. UF rejects colloids, viruses, and macromolecules from solution but allows the passage of dissolved ionic species. The separation based on sieving in UF depends on molecular weight cut-off (MWCO) of solutes [12]. The cut-off value is defined as the molecular weight of the solute where 90 % is rejected by the membrane [33].

NF and RO membranes are both pressure-driven and diffusion-controlled membrane processes and are mainly used when small organic molecules such as glucose or low molecular weight solutes such as inorganic salt separation are required. For NF membranes, the pore size ranges from 0.1 to 1 nm whereas RO membranes are considered non-porous [13]. The operating pressure of NF membranes is 3-20 bar whereas for RO the operating pressure varies from 10 to 100 bar depending on the osmotic pressure of feed solutions. The main difference between RO and NF is based on selectivity. RO membranes work on the solution-diffusion mechanism and reject all ions including monovalent ions with only water molecules passing through the membrane. NF rejects divalent ions and allows passage of monovalent ions. Thus, due to a change in pore size, the operating pressure for all membranes varies significantly and increases with a decrease in pore size.

NF membranes are mostly TFC consisting of active polyamide or polysulfone layer deposited on a microporous polysulfone layer supported by a reinforcing fabric. Membrane separation is solely by the active layer.

Membrane performance is evaluated by determining rejection, flux, and recovery.

3.2.1 Rejection

Rejection measurements are performed to determine the separation characteristics of membranes. Observed rejection R_{obs} is calculated using Equation 6.

$$R_{obs} = 1 - \frac{C_p}{C_f} \quad (6)$$

where C_p is the solute concentration in the permeate, C_f is the solute concentration in the feed.

3.2.2 Flux

Flux J_v is defined as volume flowing through a membrane per unit area and time and is generally presented as L m^{-2} h^{-1} [13]. Flux is calculated using Equation 7.

$$J_v = \frac{V}{t \times A} \quad (7)$$

where V is permeate volume during time t and A is membrane area.

For a semipermeable membrane, the flux is also defined as in Equation 8.

$$J_v = L_p(\Delta P - \Pi_F) \quad (8)$$

where L_p is water permeability, ΔP is pressure and Π_F is the osmotic pressure of the feed. The plot of pressure against pure water flux Jv results in a straight line if no membrane fouling occurs. The slope of the line corresponds to the pure water permeability of the membrane.

The pure water permeability is also expressed by the Hagen-Poiseuille equation and is defined by Equation 9.

$$L_P = r_p^2(\frac{A_k}{\Delta x})/8\mu \quad (9)$$

where r_p is pore radius, $A_k/\Delta x$ is the ratio of membrane porosity to membrane thickness and μ is the feed viscosity.

3.2.3 Permeate Recovery

Permeate recovery is an important parameter in the design and operation of membranes. Recovery is the fraction of feed flowing through the membrane and defined by Equation 10.

$$Recovery\ (\%) = {}^{Q_p}\!/_{Q_f} \times 100 \qquad (10)$$

where Q_p and Q_f are the permeate and feed flow rates, respectively.

3.3 Factors Affecting NF Membrane Performance

The main factors influencing the performance of NF membranes are:

1. Feed - Solids retention and water flux through NF membranes are strongly dependant on the concentration of feed. The higher the feed concentration the lower will be the ion retention and flux. This is a typical characteristic of charged membranes [34].
2. Pressure - Flux increases linearly with operating pressure provided no membrane fouling occurs.
3. pH - Numerous studies have focussed on the effect of pH on separation of ions with NF membranes [35, 36]. NF membranes normally contain functional groups that are strongly pH dependent that protonate or deprotonate with changing pH. At low pH, a high proton concentration is present in the solution leading to protonation of the functional group, resulting in positive membrane charge below the membrane isoelectric point [36]. At high pH, the proton concentration is low and leads to deprotonation of the functional group resulting in negative membrane charge. Thus, the feed pH can change the nature of the membrane surface charge [37] and pore size and thus affect the membrane separation efficiency.
4. Temperature - Feed viscosity decreases with increasing temperature and reduces membrane resistance resulting in higher

water flux and solute passage through the membrane. An increase in temperature also reduces concentration polarization (CP) due to reduced viscosity. Hence, total resistance to filtration decreases reducing necessary transmembrane pressure at a constant flux [38].

5. Membrane - Variations in membrane performance occur depending on membrane material. A wide range of polymers is used for manufacturing membranes that include cellulose acetate, polyamide, and sulfonated polyethersulfone. The hydrophilic or hydrophobic properties of membrane materials affect performance. Hydrophilic membranes made from polyamide and cellulose acetate are less prone to fouling in comparison to more hydrophobic membranes such as polyethersulfone. Polyethersulfone, however, has a wider pH tolerance [12].
6. Turbulence - Spiral wound membranes operate in turbulent flow [12]. Turbulence has a large effect on flux through membranes. Turbulent flow reduces formation of a gel layer or concentration polarization near the membrane surface. The turbulence in the system is calculated by measuring cross-flow velocity. The velocity in feed channel is calculated by dividing the volumetric flow rate by cross-sectional area.
   The cross-flow velocity (υ) in ms^{-1} is calculated by Equation 11 [39].

$$\upsilon = \frac{Q_f}{A} = \frac{Q_f}{W_{ch} \times h_{ch} \times \emptyset} \qquad (11)$$

where Q_f is feed flow rate in Lh^{-1}, A is feed channel cross-section which is the product of channel width w_{ch}, channel height h_{ch} and flow channel porosity ($\emptyset$).

Porosity of a material is a measure of voids. For spiral-wound membranes, feed channel porosity is measured as the ratio of void volume over total spacer volume and varies between 0 and 1 [39].

For flow velocity calculations in this research, the porosity is assumed to be 0.89.

Reynolds number *Re* is calculated to determine whether the flow is in laminar or turbulent regions and is calculated by Equation 12.

$$Re = \frac{\rho v D}{\mu} \quad (12)$$

where ρ is the density of feed water in kg m^{-3}, v is the kinematic viscosity in $m^2\ s^{-1}$, μ is the dynamic viscosity in Ns m^{-2}, D is the hydraulic diameter (m) calculated by Equation 13.

$$D = \frac{2ab}{a+b} \quad (13)$$

where a is membrane width and b is channel spacer height (m).

3.4 Separation Mechanisms

Nanoscale pores and charged membrane surfaces make the partitioning and transport mechanisms in NF complex. Separation in NF is based on sieving or steric hindrance, Donnan or electrostatic effects and dielectric exclusion [40, 41].

Removal of uncharged solutes is mainly due to steric or size exclusion in which shape and solute size are predominant factors. Solutes with a larger size than membrane pores are rejected due to sieving. Smaller solutes pass through the membrane [42].

The Donnan effect results from charged nature of membranes where most NF membranes are negatively charged at neutral pH. Solutes with the same charge as the membrane, co-ions, are repelled while counter-ions are attracted to the membrane [43]. Due to the Donnan effect, distribution of charged ions between the membrane and solution is affected by interactions between ions in solution and membrane surface charge. Hence, high retention of SO_4^{2-} occurs while retention of Na^+ is

low. However, the separation mechanism is dependent on feed pH since the membrane surface charge can vary due to dissociation of functional groups on membrane surface with changing pH [44, 45].

Dielectric exclusion occurs due to the difference between interfaces of solution and membrane with different dielectric constants [46, 47].

Hydration energy of ions also plays a role in ion separation. Ions with higher hydration energy are more efficiently retained. More energy is required to remove ions with high hydration energy compared with ions having low hydration energy [48, 49].

3.5 Kedem - Katchalsky Permeability Equations

Transfer of solutes through a charged membrane is described using the principles of nonequilibrium thermodynamics. In a two-component system consisting of a solute and water with two fluxes J_v and J_s, respectively, is related by three membrane coefficients [50]

1. The hydraulic permeability L_p
2. The solute permeability P_s
3. The reflection coefficient σ

Kedem and Katchalsky [51] proposed a set of equations to define the volume flux J_v and the solute flux J_s and membrane coefficients in Equation 14 and Equation 15.

$$J_V = L_p(\Delta P - \sigma\Delta\pi) \quad (14)$$

$$J_s = P_s\Delta C_s + (1-\sigma)J_v\, C_m \quad (15)$$

where $\Delta C_s = C_m - C_p$, with C_m the solute concentration at the membrane surface. ΔP the pressure difference and $\Delta\pi$ the osmotic pressure difference across the membrane.

3.6 Spiegler - Kedem Model

An important aspect of membrane modeling involves characterizing membranes in terms of parameters that allow the membrane to be defined by simplified mathematical models. The Spiegler - Kedem Model (SK) [50] is based on principles of irreversible thermodynamics and is used to determine transport parameters of NF membranes. This model considers a membrane as a black box [52] with no insight into structure and morphology of the membrane [53]. The relation between observed rejection R_{obs} and volume flux J_v with regard to this model is given by Equation 16 and Equation 17.

$$R_{obs} = \sigma \frac{(1-F)}{1-\sigma F} \tag{16}$$

where

$$F = \exp\left(-\frac{1-\sigma}{P_s} J_{v)}\right) \tag{17}$$

and σ is the reflection coefficient and P_s the solute permeability coefficient.

The membrane parameters σ and P_s are determined by fitting the SK model by using flux and rejection values from experiments.

The reflection coefficient σ is a measure of the selectivity of a membrane. If $\sigma = 1$, the membrane is semipermeable whereas if $\sigma = 0$, the membrane is unselective with no ion separation [54].

3.7 Steric Hindrance Pore Model

The first step in membrane characterization involves the estimation of membrane effective pore size. The steric hindrance pore model (SHP) was developed by Nakao et al. [55], and later applied by researchers [34] to predict separation performance of NF membranes. According to this model, the reflection coefficient σ and the solute permeability P_s obtained from the SK model is linked to the membrane morphological

parameters pore radius r_p and the ratio of membrane porosity to membrane thickness $A_k/\Delta x$.

The membrane parameters σ and P_s are related to the membrane structural parameters according to Equations 18 - 22.

$$\sigma = 1 - S_F \{1 + (16/9)q^2\} \quad (18)$$

$$P_s = D.S_D.(A_k/\Delta x) \quad (19)$$

where

$$S_D = (1-q)^2 \quad (20)$$

$$S_F = 2(1-q)^2 - (1-q)^4 \quad (21)$$

and $$q = r_s/r_p \quad (22)$$

where S_D and S_F are the steric hindrance factors for diffusion and filtration flow, respectively, D is diffusivity and r_s is the Stokes radius of the solute. Stokes radii and ion diffusivity of solutes are provided in Table 2.

Table 2. Ion Properties [56, 57, 58, 49]

Ions	**Cl^-**	**Na^+**	**SO_4^{2-}**	**Ca^{2+}**	**Mg^{2+}**
Stokes Radius (nm)	0.121	0.184	0.231	0.310	0.348
Ion Diffusivity, D_∞ ($m^2/s \times 10^{-9}$)	2.03	1.33	1.06	0.792	0.706
Hydration free energy (KJ/mol)	-340	-365	-1145	-1592	-1922

3.8 Artificial Neural Network (ANN) Theoretical

ANN's are computational models inspired by structural and functional aspects of biological neural networks. ANN's can effectively create a relation between input and output variables without considering any detailed physical interaction between variables. ANN's are capable of mapping non-linear relationships between inputs and outputs in a system through interconnected groups of artificial neurons. A multi-layer perceptron ANN structure may consist of a single layer or multiple layers of neurons.

Weight coefficients and biases connect the neurons and to generate a neuron output, an activation or transfer function is established on the summation of weights and bias input of neurons in each layer. Each neuron is a computational processor that has a summing junction operator and a transfer function. The transfer function converts the net inputs into an output. Generally used transfer functions for solving regression problems include the log-sigmoid transfer function (logsig), the hyperbolic tangent sigmoid transfer function (tansig), and the linear transfer function (purelin) [59].

Feed-forward backpropagation algorithm was used for data training. The method by which the input neurons and the outputs are connected is known as the architecture of the neural network. The neuron networks are usually grouped into several layers such as input, hidden and output layers. Number of neurons in the input layer corresponds to the number of inputs provided to the neural network and are considered as passive and only transmits signal to the next layer. Neurons present in the hidden layer are active and take part in signal modification. The number of neurons in the output layer are also active and corresponds to the number of outputs in the network. ANN works through a training process where the network trains the neurons how to produce an output within the desired accuracy corresponding to an input pattern.

For evaluation of ANN accuracy, the mean square error (MSE) and statistical coefficient of determination R^2 were used after training performance of the network. The MSE is expressed in Equation 23.

$$MSE = \frac{\sum_{i=1}^{n}(t_i - a_i)^2}{n} \quad (23)$$

where t_i is the i-th target value, a_i is the predicted output value and n is the number of samples.

3.9 Membrane Regeneration

Adequate pre-treatment is required to slow down or prevent membrane fouling and to maintain the production capacity of a membrane. According to the guidelines, membranes should be cleaned in any of the following cases; when a 10 % drop in permeate flow is observed, when a 15 % increase in operating pressure is observed for identical flow rate or when the permeate salt content increases by 10 % [60]. The frequency of cleaning influences the operating lifetime of a membrane.

Chemical cleaning is commonly the main requirement of a cleaning procedure and that cleaning should be able to restore membrane flux and be effective against the foulants as well as sustain membrane retention characteristics. Cleaning agents are chosen based on the type of foulants, thermal and chemical properties of the membrane material [13]. Acidic cleaners are used to reduce inorganic foulants whereas alkaline cleaners are used for organic foulants [12].

4 Experiments and Methods

4.1 Membrane Selection

Eight commercially available membranes were chosen for this research. Seawater and synthetic PW were used as membrane feed. Dow FilmTec provided FilmTec NF 270 and SR 90 and Nitto Hydranautics provided other six membranes. The membranes used for the experiments are negatively charged. The main specifications of these membranes are provided by the manufactures in Table 3.

Table 3. Membrane specifications according to manufacturers [61, 62]

Membranes	**Material**	**Area (m^2)**	**pH range**
HYDRACORe10*	Sulfonated polyethersulfone	2.3	2-11
HYDRACORe50*			
NF 270	Composite polyamide	2.6	3-10
SR90			
ESNA		2.3	2-10
NANO-SW			3-9
LFC3			2-10.6
HYDRApro501			2-11

* MWCO of HYDRACoRe10 and HYDRACoRe50 are 3000 and 1000 Daltons, respectively.

The maximum operating pressures of all membranes are from 41 to 41.6 bar. All membranes except for HYDRApro 501 has a maximum operating temperature of 45 °C. The operating temperature is pressure dependent for HYDRApro 501 and may be operated at 41 bar and 14 bar at 65 °C and at 90 °C, respectively.

4.2 Membrane Testing

The operating pressures were gradually changed from 9 bar to 18 bar with 25 minutes membrane stabilization time between pressure changes. A schematic of the membrane set-up for experiments is shown in Figure 10. The pressure vessel had one spiral-wound membrane module.

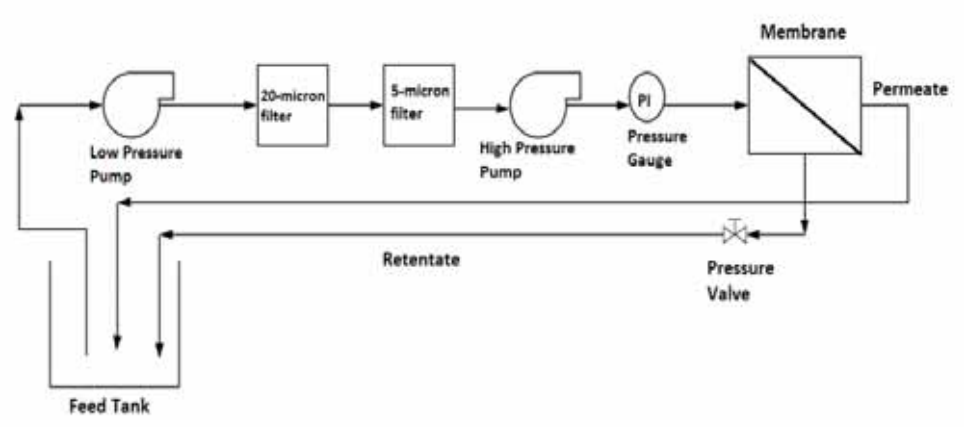

Figure 10. Schematic of the membrane system used for the experiments [63]

Retentate and permeate were recirculated to a feed tank to maintain identical feed concentrations over time. Equation 24 exemplifies the mass flow through the membrane.

$$Q_f C_f = Q_p C_p + Q_c C_c \quad (24)$$

where Q_f, Q_p, and Q_c are feed, permeate and retentate flow rates, respectively.

C_f, C_p and C_c are feed, permeate and retentate concentrations, respectively.

The permeate and retentate flow rates were manually measured by using a calibrated cylinder and a stopwatch. pH, TDS, conductivity and temperature were recorded for all samples.

4.3 Chemicals, Analytical Instruments and Feed Compositions

Analytical grade chemicals were used for all experiments. pH was recorded by VWR Phenomenal pH 1100L. TDS and conductivity were measured using TDS meter VWR collection CO3100N. Individual ion concentrations in the feed, permeate and retentate was determined using ion chromatography (Dionex ICS-5000^{+} DP). Turbidity of the samples was measured in nephelometric turbidity unit (NTU) using a turbidimeter. At each pressure, temperature, conductivity, salinity, TDS, pH and flow rates of retentate and permeate were determined.

Different feeds were used during the experiments. Filtered normal seawater with a conductivity of 49 mS/cm and pH 8 was used.

The ionic composition of PW and seawater are similar, however, with difference in salinity. For ease of experiments, all synthetic PW experiments were performed with seawater at different concentrations.

- For determining Ba^{2+} and Sr^{2+} rejection, seawater was used as feed for NF. Permeate without SO_4^{2-} was collected and mixed with $BaCl_2$ and $SrCl_2$.
- Synthetic PW was produced by mixing Ekofisk oil with seawater at 0.1, 0.2, 0.3, 1, 2- and 3-mL/L oil in seawater at 19,000 rpm using *Polytron PT 300 Mixer* from *Kinematica*.
- During PW pH experiments for reuse of PW as smart water, it was assumed that PW was diluted to seawater concentrations and analytical grade HCl and NaOH were thus added to normal seawater. 12 feed pH values were used; 2.5, 3, 3.5, 4, 4.5, 5, 6, 7, 8.5, 9.2, 9.7 and 10.2. Experiments were also performed with normal seawater at pH 8.

Brine compositions used for experiments and analyzed by IC are reported in Table 4.

Table 4. Ion compositions of feed analyzed by IC

Ions	Concentrations, mM	
	Seawater	Synthetic PW for Ba^{2+} and Sr^{2+} experiments
HCO^{3-}	2	0.00
Cl^{-}	525	352
SO_4^{2-}	24	0.00
Mg^{2+}	51	7.1
Ca^{2+}	9.3	5.67
Na^{+}	450	396
K^{+}	10	7
Ba^{2+}	-	1.6
Sr^{2+}	-	1.6
Li^{+}	-	

4.4 Membrane Cleaning and Preservation

The interval for cleaning of membranes depends on the type of feed. Membranes were routinely cleaned with pure water at 9 bar after each experiment to prevent accumulation of irreversible foulant on the membranes. HCl and NaOH cleaning solutions recirculated for 30 - 45 minutes through the membranes after each set of experiments. The membranes were first washed with HCl diluted with tap water at pH 3 followed by NaOH washing at pH 10 - 11. At the end of each cleaning, the membranes were immediately rinsed with clean water until the permeate conductivity was as pure water. Metabisulfite was used to preserve membranes when not used for more than a week.

4.5 Media Filtration for Oil Removal

A lab-scale media cylindrical filtration unit of diameter 25 cm and height 120 cm was constructed to remove oil from synthetic PW. The media

was powdered activated carbon and anthracite. Anthracite was placed on top followed by activated carbon. Pebbles were placed at the bottom to provide support. Backwashing was performed with a 350 W pump at a maximum flow rate of 2500 L/h. Synthetic PW was used as feed and the effluent was collected and immediately used as NF feed. Three trials were performed for each concentration. The unit was backwashed with tap water after experiments for each concentration. Samples were collected from the influent, effluent and backwashed water in regular intervals to check concentrations of oil in water. The media was replaced when the backwash water contained oil droplets even after prolonged washing.

Hydrocarbon removal efficiency E_{oil} (%) was calculated using Equation 25.

$$E_{Oil} = 1 - {}^{C_{p(oil)}}\Big/_{C_{f(oil)}} \times 100 \qquad (25)$$

where $C_{p(oil)}$ and $C_{f(oil)}$ are the oil concentrations in the effluent (permeate) and influent (feed), respectively.

A schematic of the filtration unit is shown in Figure 11.

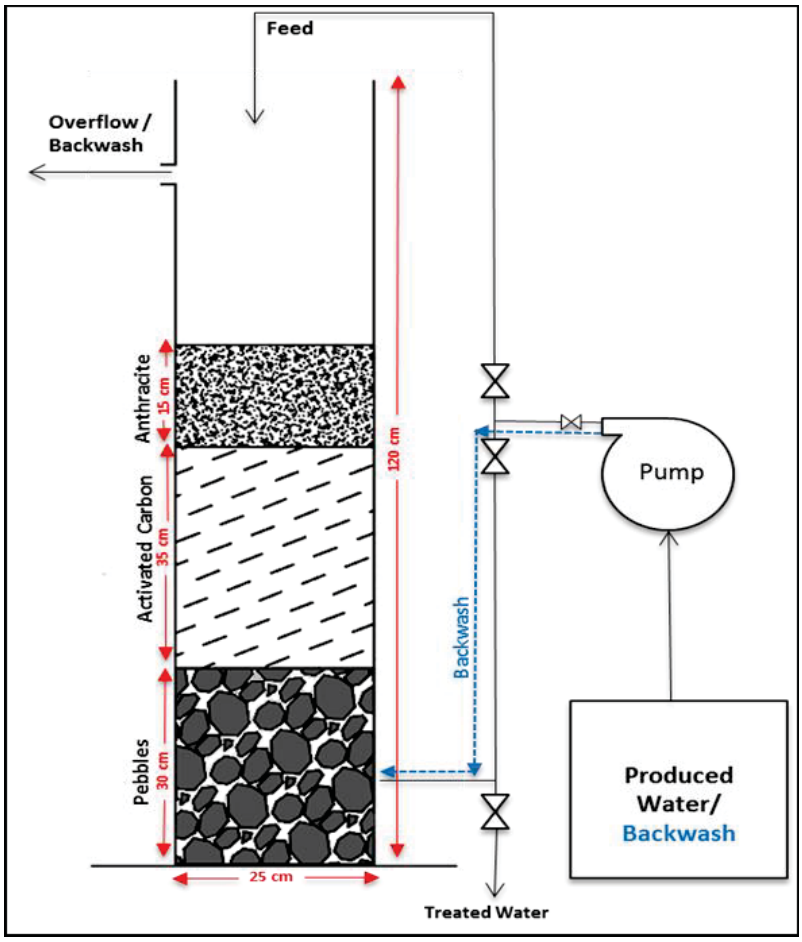

Figure 11. Schematic of the lab-scale media filtration unit

4.6 Infrared (IR) Analysis

Oil in synthetic PW was analyzed by IR spectrometer (Agilent Cary 630 FTIR). Extraction of media filter influent, effluent and de-oiled NF feed and permeate were performed immediately using cyclohexane according to ASTM D7678-17 [64].

4.7 Scanning Electron Microscopy (SEM)

SEM was used in this research to analyze the membrane surface after a year of operation. While using SEM, the membrane surface must be conductive to produce signals and avoid charging when the electron beam impinges on the membrane surface. Thus, a conductive coating of palladium was applied. However, SEM could only give information on the macroscopic structure of the NF membranes, as the maximum resolution obtained was 200 nm. The analysis was performed at 10 mm working distance with an accelerating voltage of 15 kV and aperture size of 30 μm.

4.8 Modeling of Membrane Experiments

Modeling based on experiments were performed using Spiegler - Kedem and steric hindrance pore models. ANN was used during experiments with PW. Flux, pressure and pH from three NF membranes were used as input and rejection of Cl^-, Na^+, Mg^{2+} and Ca^{2+} were the output.

4.8.1 Models-based on Spiegler - Kedem and SHP models

A predictive model helps users obtain membrane characteristics, predict process performance and aid in improving the process. Beginning with the SK model for filtration through a porous membrane, equations were derived to compute NF reflection coefficient and solute permeability within a particular pure water permeability range and possible rejection for individual ions in seawater. For this purpose, the transport parameters were obtained using a nonlinear least squares method by fitting the experimentally obtained rejection and flux data to the SK model. The SHP model determined the pore radius of membranes by using the Stokes radius of ions from Table 2.

4.8.2 Data Training by Artificial Neural Network

Rejection of ions was predicted using ANN when feed pH was varied. A feed-forward back propagation ANN was used that works with a set of

input and output data. Feed pH, pressure and flux data were used as input. A number of neurons were altered to design the best ANN structure for predicting ion rejection. The number of hidden neurons was selected after evaluating the neurons performance by calculating the mean square error (MSE). The set of neurons with least MSE was selected for the ANN structure. The training of the ANN model was carried out by using the Levenberg - Marquardt algorithm. For proper network training, and to avoid overfitting, the experimental data were randomly divided into three sets of 70 %, 15 % and 15 % for training, validation, and testing, respectively. A set of 65 samples were provided for each membrane with varying pH and operating pressures. Hence, 45 samples were used for training and 10 each for validation and testing of the proposed ANN design.

5 Results and Discussion

Performance of NF, based on brine composition, concentrations, pressure and pH, was determined by measuring permeability, flux and rejection. Major results obtained during the research are explained in this section.

5.1 Pure Water Permeability

Membrane flux from pure water feed and applied pressure was obtained for the membranes prior to testing of seawater and PW. The membranes were washed with tap water until all preservatives were removed. The permeate and retentate were recirculated to the feed tank during washing until the conductivity of the feed water equals the conductivity of tap water. Water flux from eight membranes was recorded. Pure water permeability is used as a baseline to evaluate cleaning efficiency of membranes.

Pure water permeabilities of individual membranes are presented in Table 5.

Table 5. Pure water permeabilities of tested membranes

Membranes	**Pure water permeability ($Lh^{-1} m^{-2} bar^{-1}$)**
HYDRACoRe 10	13.56
ESNA	10.52
NF 270	9.38
HYDRACoRe 50	5.15
SR 90	4.46
NANO-SW	3.27
LFC3	2.85
HYDRApro 501	1.32

Pure water permeability is related to the structural parameters of the membrane according to Hagen Poiseuille as shown in Equation 9. Thus, a membrane with higher permeability has a larger pore size. According to Table 5, the effective pore size of the membranes is in the descending order HYDRACoRe 10 > ESNA > NF270 > HYDRACoRe 50 > SR 90 > NANO-SW > LFC3 > HYDRApro 501.

5.2 Reynolds Number

Reynolds number was calculated to determine whether the flow was laminar or turbulent. Equations 11, 12 and 13 were applied with seawater as membrane feed with density, kinematic viscosity and dynamic viscosity of seawater at 25 °C used for calculations. The spacer height was obtained from membrane manufacturers.

The Reynolds number was 261. Theoretically, this value is in the laminar region. However, the feed spacers between the membranes act as turbulence promoters and contribute additional turbulence.

5.3 Effect of Applied Pressure on Ion Rejection

Ion rejection from NF membranes with seawater as feed showed high divalent and low monovalent ion rejection. Rejection varied with membrane pore size. Figure 12 shows rejection by NANO-SW membrane, a tight membrane according to the pure water permeability values in Table 5.

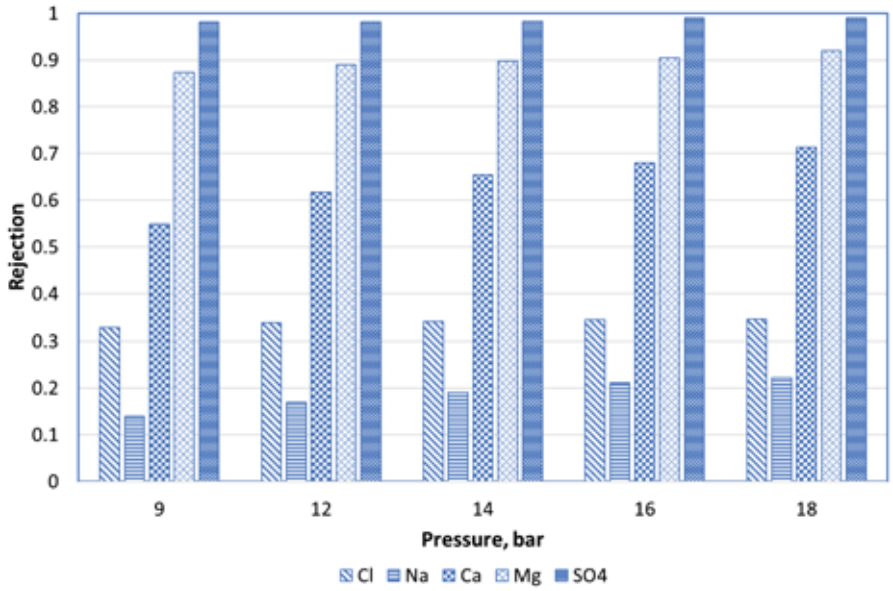

Figure 12. Ion rejection with increasing pressure with NANO-SW

Ion rejection for NANO-SW in Figure 12 shows that rejection increased in the order $Na^+ < Cl^- < Ca^{2+} < Mg^{2+} < SO_4^{2-}$ and is explained by differences in hydration free energy of ions. Na^+ and Cl^- have a hydration free energy of -365 KJ/mol and -340 KJ/mol, respectively. Na^+ is attracted by the membrane and is rejected the least as observed in Figure 12. Ions with lower hydration energies permeate easier through the membrane. However, the effect of negative membrane charge plays a major role in separation. Cl^- will be rejected by the membrane even with a lower hydration energy. Cl^- rejection is higher than Na^+ due to its charge. Hydration free energy of Ca^{2+} (-1592 KJ/mol) is lower than Mg^{2+} (-1922 KJ/mol) and has accordingly the lower rejection of the two. The negatively charged divalent sulfate has the highest rejection by NF membranes. Hydration free energy of SO_4^{2-} is -1145 KJ/mol [49].

Rejections of Cl^- and Na^+ with a change in pressures are demonstrated in Figure 13 and Figure 14, respectively.

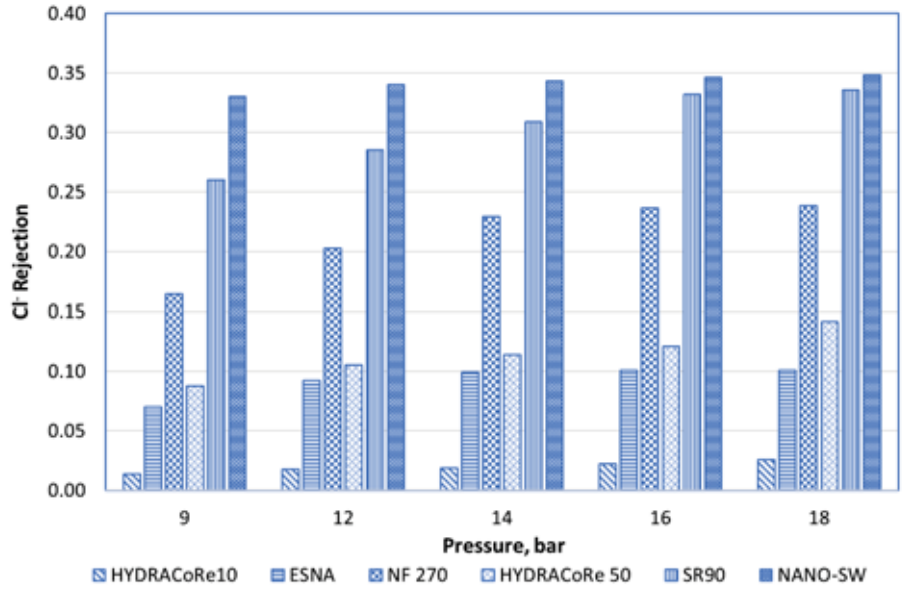

Figure 13. Cl^- rejection for six NF membranes

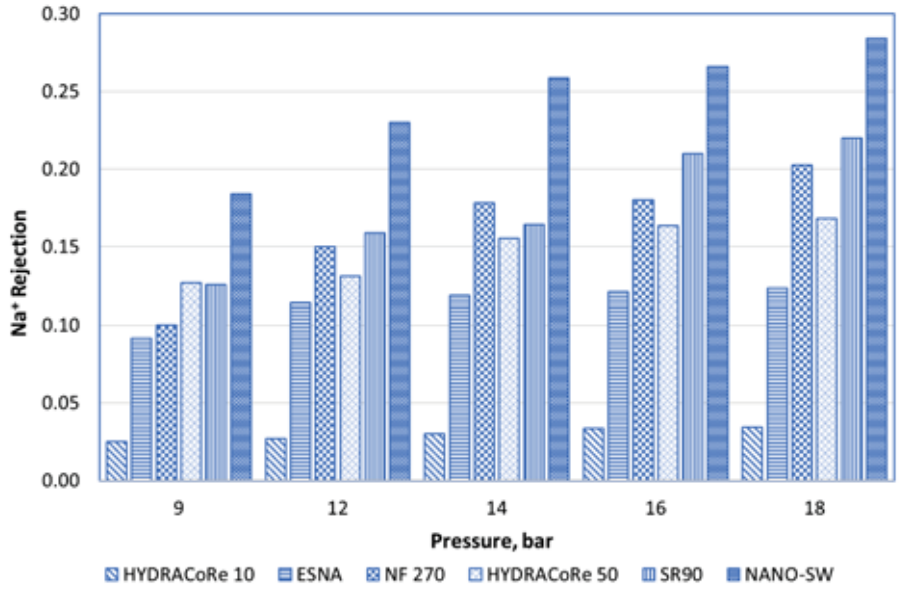

Figure 14. Na^+ rejection for six NF membranes

Figure 13 shows that Cl^- rejection is higher than Na^+ rejection at all pressures except for HYDRACoRe 10 and HYDRACoRe 50. Anions will be rejected more than cations when a negatively charged membrane is used. However, for both HYDRACoRe membranes, the rejection is opposite, perhaps due to a comparatively lower surface charge.

SO_4^{2-} rejection with increasing pressure for six membranes are shown in Figure 15.

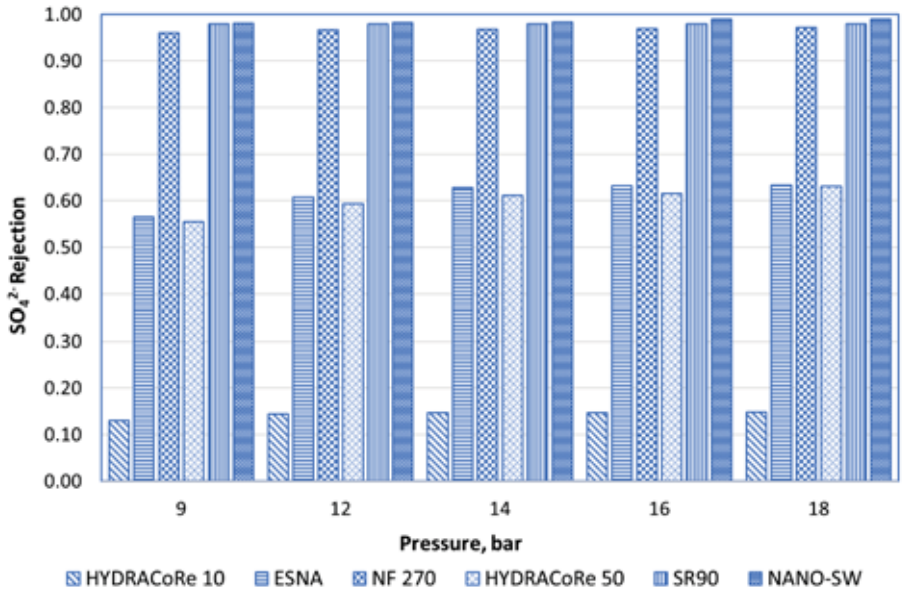

Figure 15. Comparison of SO_4^{2-} rejection with pressure for six membranes

Rejection presented in Figure 15 confirms that NANO-SW, SR 90 and NF270 are highly negatively charged and have smaller effective pore sizes yielding high divalent anion rejection. ESNA is likewise a negatively charged membrane, however, with larger pore size. Both HYDRACoRe membranes showed lower SO_4^{2-} rejection due to lower surface charge. The overall results show that retention of multivalent ions was higher than the retention of monovalent ions though the tighter membranes also retained monovalent ions. The results are supporting

reported values of Stokes radius and confirms that ions with a relatively larger diffusivity have lower rejection. Ion permeability through NF membranes has strong correlations to their radius of hydration and hydration energy. Mg^{2+} and Ca^{2+} have larger Stokes radius and higher hydration energy as reported in Table 2. These ions hold their hydration shells more strongly, thus are more effectively removed by membranes.

5.4 Effect of Increased Feed Concentration on Ion Rejection

Experiments with seawater spiked with chemicals using NANO-SW were performed to investigate the effects of increased divalent ion concentrations on rejection of ions. Several researchers have reported a decrease in salt retention with increasing feed concentrations [65, 66].

Concentrations of SO_4^{2-}, Ca^{2+} and Mg^{2+} were increased individually by addition of Na_2SO_4, $CaCl_2$ and $MgCl_2$ to seawater. Spiking with divalent ions was performed as smart water for carbonates includes high divalent ion concentrations.

SO_4^{2-} was added in doses of 54 mM (dose 1), 76 mM (dose 2) and 95 mM (dose 3) to seawater. Three trials at each dose were performed and samples were collected for IC analysis. Pressures were increased from 8 bar to 16 bar. Membrane stabilization time was 25 minutes for each pressure change. Washing with pure water was performed after each dose. The NANO-SW membrane was rinsed with seawater before another spiking. Figure 16 shows flux behavior with increasing feed concentration, dose 1 to dose 3, by addition of Na_2SO_4 to seawater.

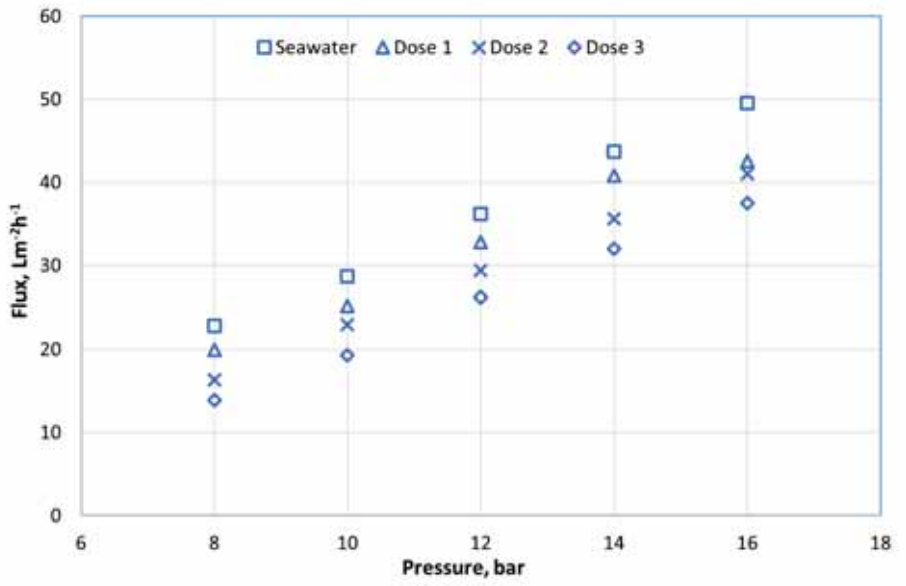

Figure 16. Flux variations with increased SO_4^{2-} concentrations in the feed

The results confirm that volume flux increases linearly with applied pressure and decreases with an increase in feed concentration. This behavior is due to an increasing osmotic pressure difference across the membrane as the ion concentration increases.

Figure 17 shows the effect of increased SO_4^{2-} concentration on Cl^- rejection using NANO-SW.

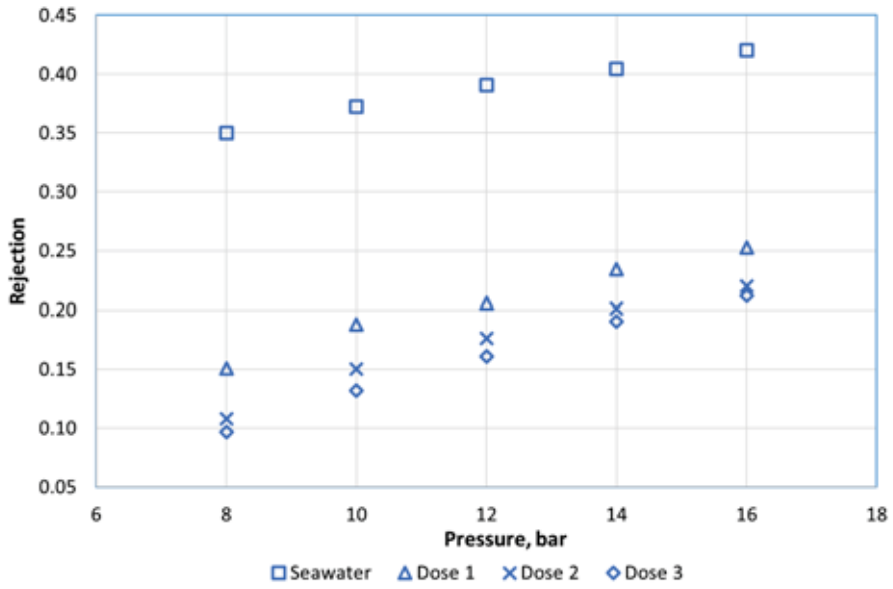

Figure 17. Cl^- rejection with increased SO_4^{2-} concentration

According to Figure 17, with increased SO_4^{2-} concentrations in the feed, retention of Cl^- decreased for a fixed pressure. This variation is explained by electrostatic and steric hindrance effect. At low feed concentrations, membrane charge has a dominant role in ion rejection and the negatively charged membrane rejects Cl^-. When SO_4^{2-} concentration in feed increased, effective membrane charge reduces and the dominant separation mechanism becomes steric hindrance increasing permeation of Cl^-. Similar effects are observed in the literature [66, 67, 68]. Further explanation for the observed decrease in Cl^- rejection is due to the increased concentration of Na^+ added to the solution with SO_4^{2-} as Na_2SO_4. For maintaining electroneutrality, one of the co-ions has to permeate with the counterion. This results in a preferential permeation of Cl^- rather than SO_4^{2-} due to high hydration energy and Stokes radius of SO_4^{2-}.

According to Figure 16 and Figure 17, it will be advantageous to spike divalent ions in the feed rather than to the retentate for producing smart

water in carbonates. This assist in increased permeation of Cl^- with increasing SO_4^{2-}.

5.5 Produced Water Treatment

Oily wastewater contains impurities resulting in membrane fouling and scaling, affecting the filtration process and shortening membrane life. Though the RO membrane provides better water quality, NF membranes are more cost-effective for reuse of PW in the oil and gas industry. However, real and synthetic PW must be evaluated carefully as real PW makes the membrane process less effective due to fouling.

5.5.1 De-oiling of Synthetic PW by Media Filtration Unit

Synthetic PW with oil was filtered through a media filtration unit. The influent and effluent samples were extracted according to ASTM D7678-17 with cyclohexane and the extracted samples were analyzed with IR Spectrometer. 96 - 98 % hydrocarbon removal efficiency was calculated according to Equation 25. A visual comparison of the influent and effluent samples from media filtration unit before and after extraction with cyclohexane is shown in Figure 18.

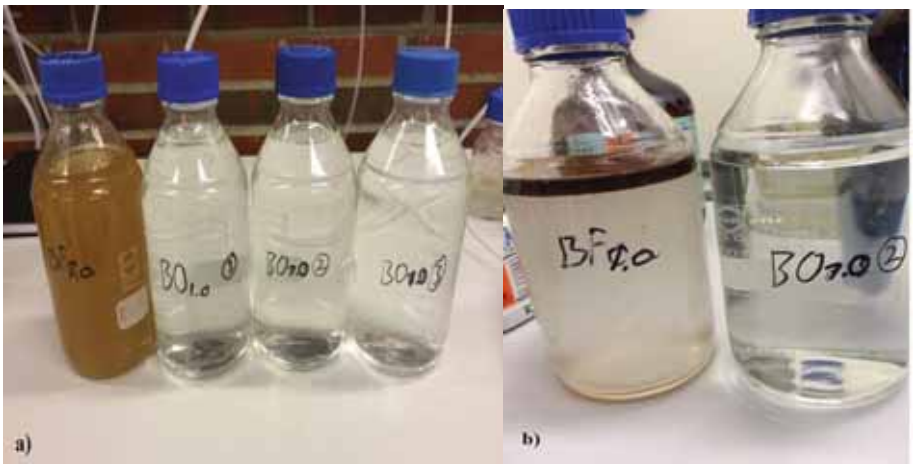

Figure 18. Comparison of influent and effluent samples a) before extraction b) after extraction

5.5.2 Barium and Strontium Removal

Synthetic PW spiked with Ba^{2+} and Sr^{2+} was treated with NANO - SW at room temperature. The results are shown in Figure 19.

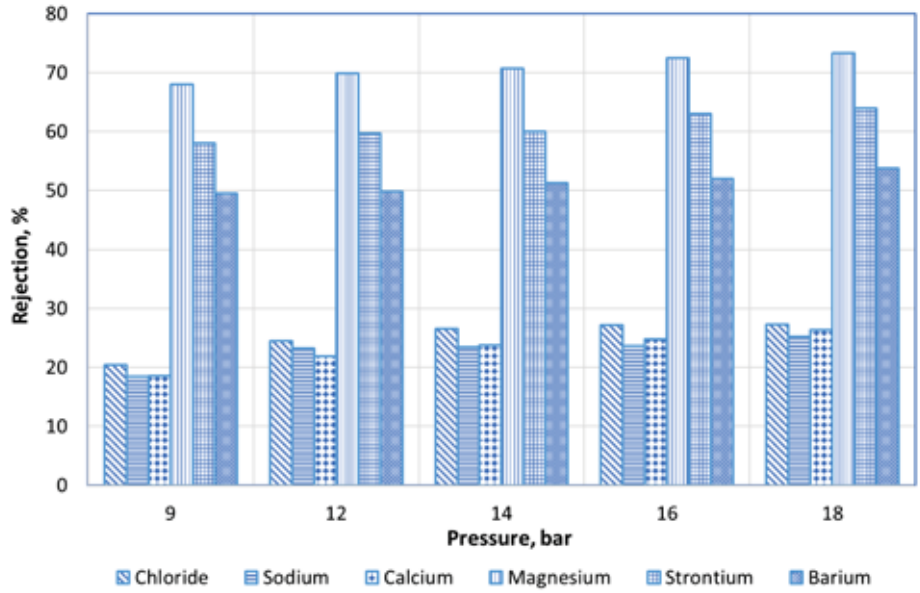

Figure 19. Rejection of Ba^{2+} and Sr^{2+} with NANO-SW

The results show that the membrane rejected 64 % Sr^{2+} and 53 % Ba^{2+}. The hydration free energy of Ba^{2+} is -1273 KJ/mol [69] whereas that of Sr^{2+} is -1395.7 KJ/mol [70] The difference in hydration free energy explains the higher rejection of Sr^{2+} compared to Ba^{2+}. Figure 20 shows flux versus pressure when Ba^{2+} and Sr^{2+} were spiked in the feed. The linear relation confirms that no fouling occurred during the operation.

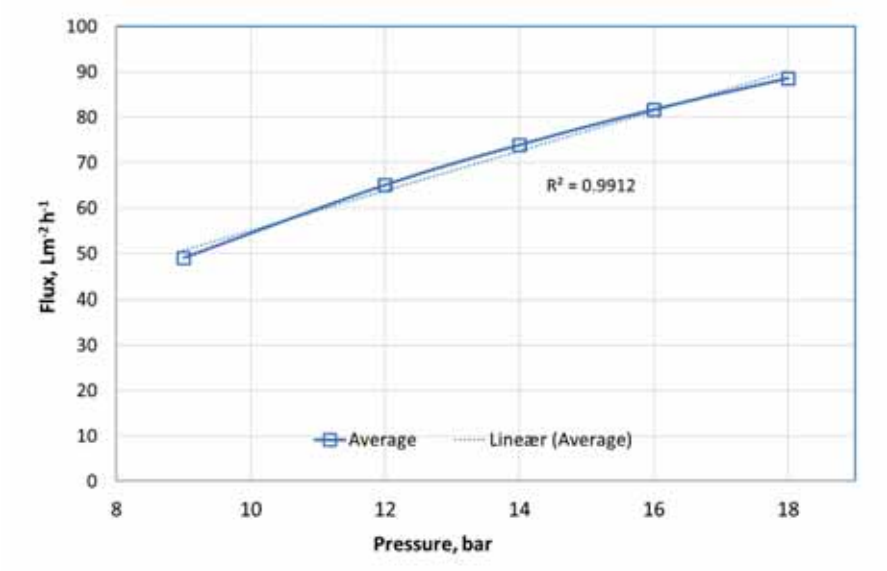

Figure 20. Flux versus pressure with Ba^{2+} and Sr^{2+} in the feed

5.5.3 Importance of Adequate Membrane Cleaning

The polyamide NF membrane (NANO-SW) after operation for a year was analyzed using SEM. The SEM experiments were performed after several experiments with synthetic PW containing Ba^{2+} and traces of SO_4^{2-} (6 mg/L) in the feed. No chemical treatment or washing was conducted on the membrane after the experiments in order to analyze the amount of Ba^{2+} precipitation during membrane separation.

The SEM images revealed that ion precipitation occurred and was largely seen on the feed side of the membrane. The SEM images of the membrane are presented in Figure 21.

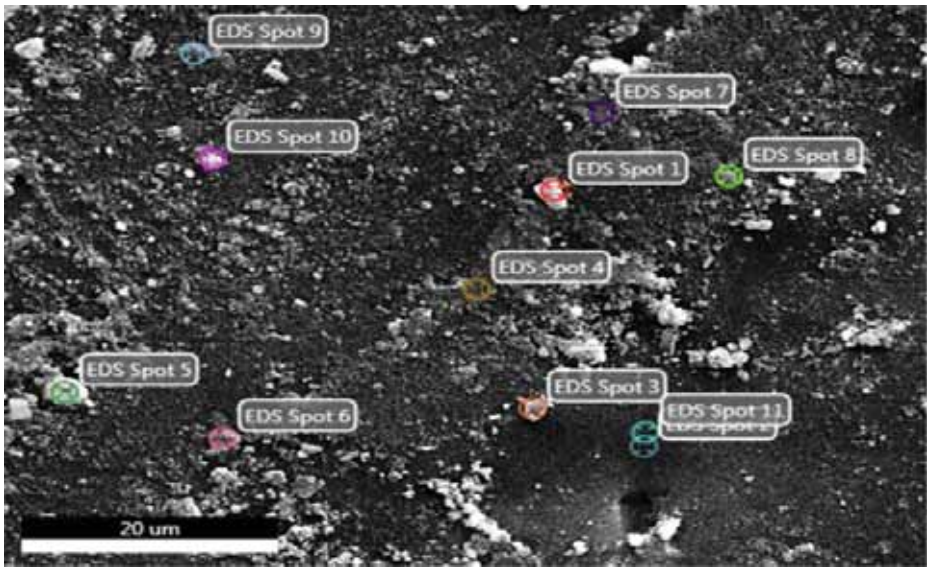

Figure 21. SEM image of NF membrane on the feed side

The energy dispersive X-ray spectroscopy (EDS) resulted in an analysis of the elements present on the surface. EDS analysis of Spot 1 in Figure 21 is presented in Figure 22.

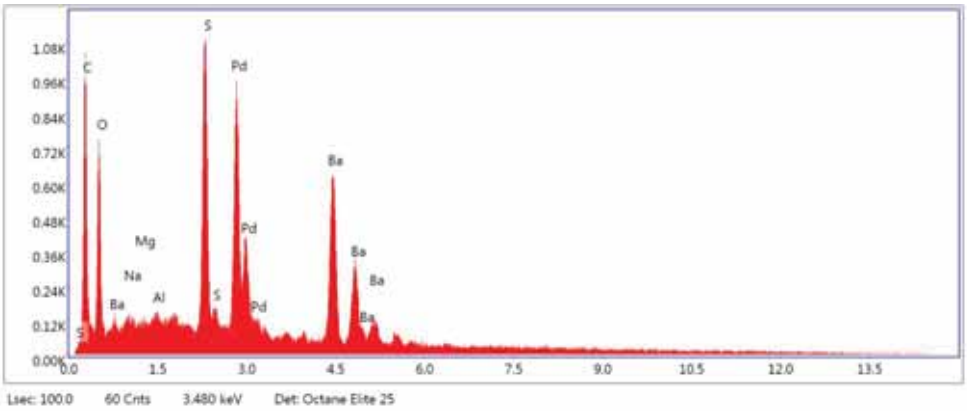

Figure 22. EDS analysis of Spot 1

The SEM-EDS analysis revealed the accumulation of inorganic precipitates on NF membrane surface. It is evident that Ba^{2+} and SO_4^{2-}

are present on the surface due to high concentration of Ba, S, and O in the spectrum. Figure 23 demonstrates the SEM image on the permeate side of the membrane. Precipitation of ions on the permeate side is less than on the membrane feed side.

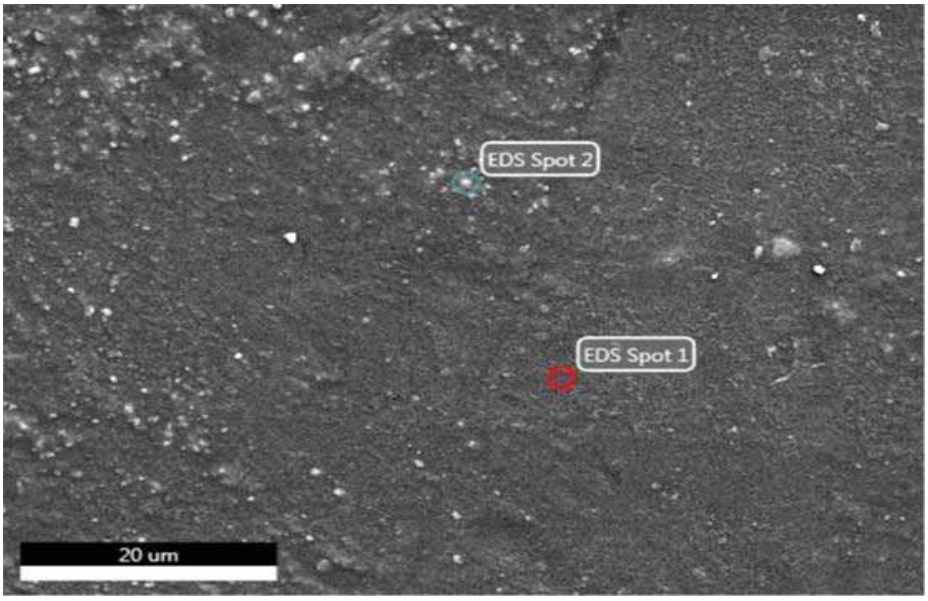

Figure 23. SEM image on the permeate side of the membrane

Analysis of SEM images suggests that proper chemical membrane cleaning is required during treatment of PW with scale causing ions, which could otherwise lead to permanent scaling and membrane production loss.

5.5.4 Effect of Produced Water pH on NF Membrane Performance

pH of synthetic PW was varied from 2.5 to 10.2 and pressure increasing from 9 to 18 bar. Experiments were performed for three NF membranes; ESNA, NF 270 and HYDRACoRe50. Three trials each was performed at all pH concentrations.

A significant change in flux and rejection was observed with variations in pH. Flux was higher in basic environments. When flux increased with an increase in pH, the rejection of charged ions decreased. Highest flux was observed for ESNA indicating a larger pore size than for HYDRACoRe and NF 270. A change in ion rejection was noticeable between acidic and alkaline environments for divalent ions. A sharp decrease in Mg^{2+} rejection was observed in the basic environment for ESNA and NF 270. It was confirmed that pore size decreased with a decrease in feed pH using SK and SHP models (Equation 16 - Equation 22).

Effect of feed pH on flux with ESNA is shown in Figure 24.

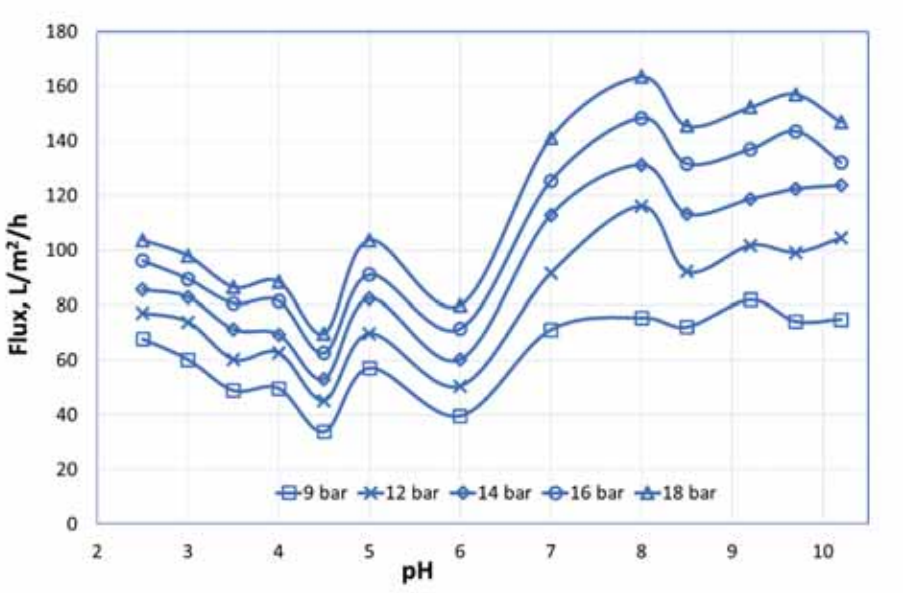

Figure 24. Flux variations with a change in pH with ESNA membrane

According to the Donnan effect, negatively charged membranes attract positively charged ions. NF membrane acquires charges in the presence of an ionic solution due to the association or dissociation of functional groups on the membrane surface that strongly depends on the pH of the solution.

Polyamide NF membranes consist of both carboxyl group (≡ COO^-) and amino groups (≡ NH^{3+}) and exhibit positive and negative surface charges depending on pH. At acidic conditions, protonation of amine occurs (≡NH_2 → ≡NH_3^+) resulting in increased pore size and increasing flux. This explains a slight peak in flux in an acidic environment at pH 5 in Figure 24. At alkaline pH, polyamide membrane matrix appears to be more expanded due to deprotonation of carboxyl group (≡COOH → ≡COO-) resulting in increased flux [36, 44] as for ESNA and NF 270.

Figure 25 shows Cl^- rejection for NF 270 when feed pH varied from 2.5 to 10.2. A rejection minimum at acidic pH was observed between pH 4 and pH 5 and a maximum Cl^- rejection was observed at pH 3.

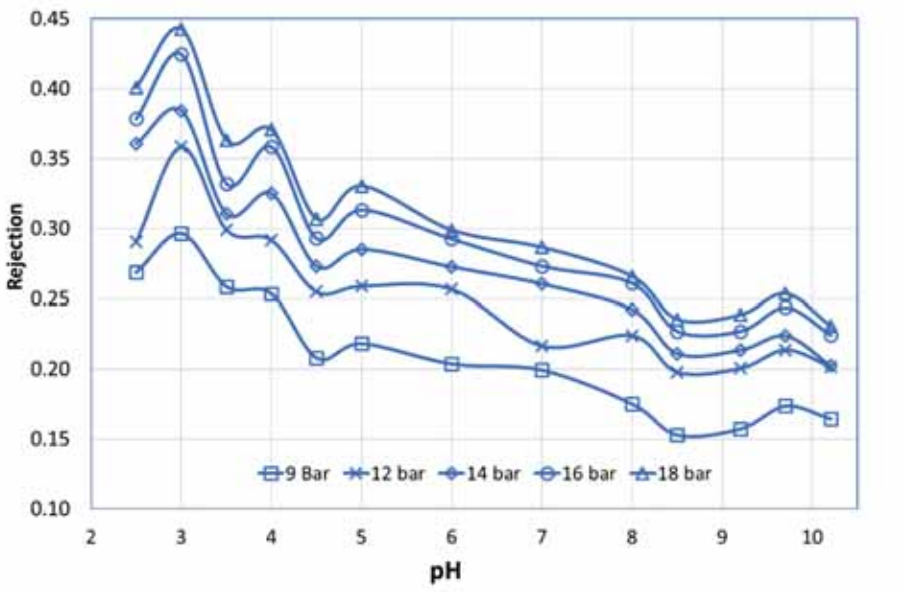

Figure 25. Effect of pH on Cl^- rejection for NF 270

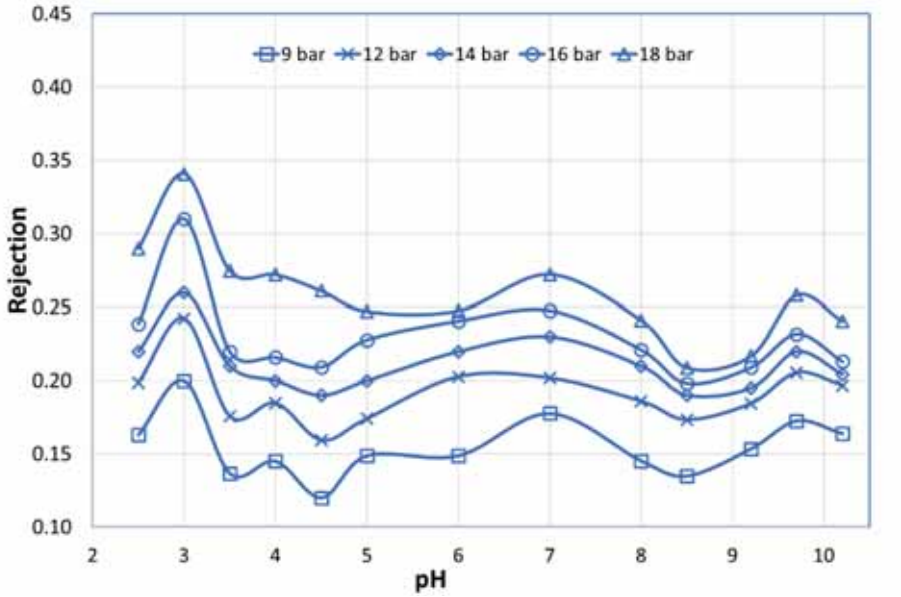

Figure 26. Effect of pH on Na^+ rejection with NF 270

Figure 26 shows Na^+ rejection at varying feed pH. The results show that Na^+ rejection coincides with Cl^- rejection at varying pH. At pH 3, a Na^+ rejection maximum is observed which confirms that monovalent cation is also rejected enabling electroneutrality in solution.

Positive charges of a membrane increase with a decrease in pH below the isoelectric point of the membrane [44] and results in more Na^+ rejected by the membrane. The isoelectric point is the point where rejection of Na^+ and Cl^- is the lowest. The membrane charge is considered positive below the isoelectric point and is negative above the isoelectric point [36, 44, 71]. Since anions and cations do not act independently, Cl^- is also rejected to maintain electroneutrality. Similarly, at pH 9.7, when the membrane is more negatively charged, Cl^- experiences an electrostatic repulsion from the membrane and thus more Cl^- is rejected and explains the peak at pH 9.7 in Figure 25. This results in a subsequent increase in Na^+ rejection to maintaining the electroneutrality of the permeate as observed in Figure 26.

Change in pore size with varying pH was determined using SK and SHP model and is presented in Figure 27. The pore size was calculated based on the solute - to - pore size ratio of Mg^{2+} for the three NF membranes.

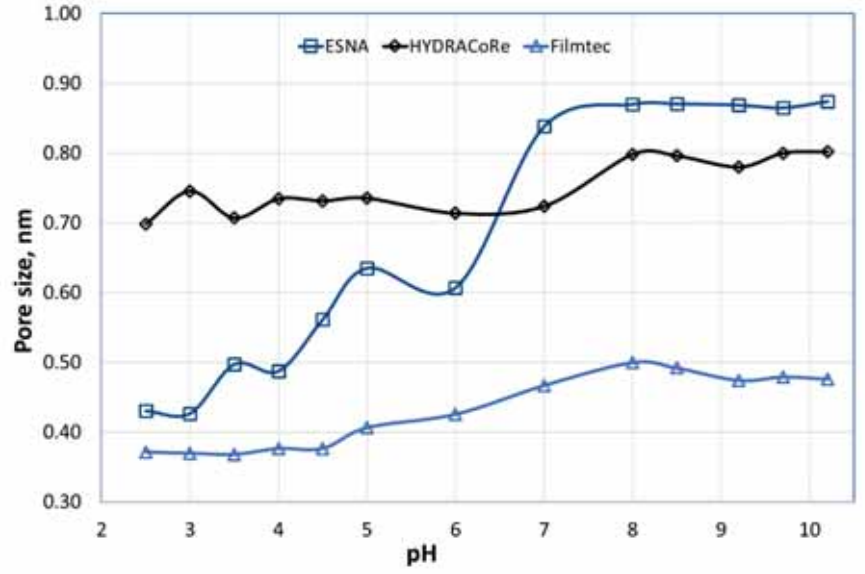

Figure 27. Variations in pore size with feed pH

Figure 27 shows that the separation performance of membranes varies with membrane material. Variations between acidic and basic pH are more obvious in polyamide membranes since they are more hydrophilic and are prone to ionization and hydration in aqueous solutions. This results in changes on the conformation of polymer chains, especially at different pH. Since the NF membranes have nanoscale pore dimensions, even a small change in pore size would have a clear impact on membrane performance. ESNA and FilmTec NF 270 are hydrophilic polyamide membranes whereas HYDRACoRe membranes are made of hydrophobic polyethersulfone with a high pH tolerance [12]. This explains the relative stable behavior of HYDRACoRe with pH.

5.5.5 Predicting Ion Rejection by Artificial Neural Network

After providing the necessary data, the neural network model was created using MATLAB software. The number of neurons used for the network in this research is seven where the calculated MSE values were the least along with the highest R^2 values. It was observed that the training of input and output data was well performed with an R^2 value of 0.996 for training. R^2 value for test data is also greater than 0.99 confirming that ANN predicted rejection values and experimental values are in close agreement. These values signify the ability of ANN in predicting major ion rejection if flux, pH and pressure are available and simulation can be used for entering new inputs. Figure 28 shows the ANN structure used for ion predictions with varying input variables.

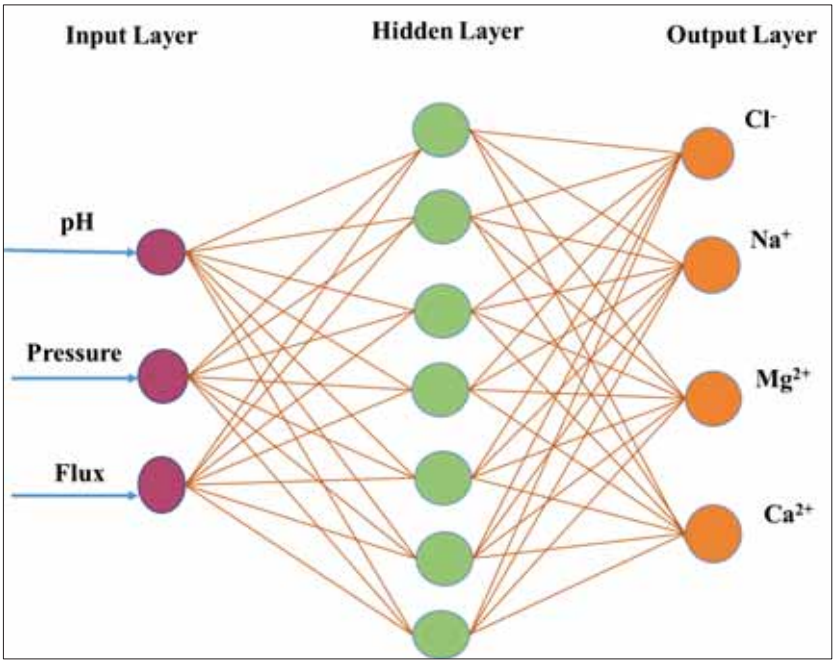

Figure 28. ANN design with 7 neurons to predict ion rejections at varying feed pH

5.6 Spiegler - Kedem Model

Estimation of transport parameters σ and P_s was by using the SK model. Equations 16 and 17 were independently fitted to each set of experimentally obtained values for R_{obs} and J_v, corresponding to each major ion in seawater, which did yield the transport coefficients specific for individual ions. The procedure was repeated for six NF membranes. The transport parameter σ confirmed that with an increase in ion rejection, the reflection coefficient increased and with an increase in ion permeability coefficient, P_s increased. Figure 29 shows rejection versus flux for Na^+ with ESNA when the values were fitted using the SK model. The data points present the rejection values from the experiment and the solid line presents the values obtained using the SK model with the best-fitted σ and Ps values. Figure 29 shows that the theoretical curves are in close agreement with experimental values.

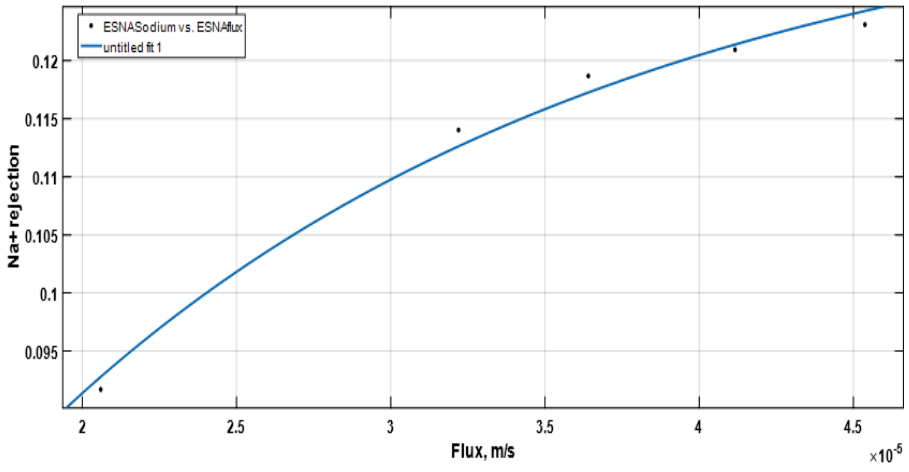

Figure 29. Rejection versus flux for Na^+ for ESNA

5.7 Steric Hindrance Pore Model

Evaluation of effective pore size r_p of the membranes was determined using steric hindrance pore model. The value of such measurements

enables determining the pore size based on a single ion rather than using an uncharged molecule such as glucose for measuring the effective pore radius. This increase proper understanding of real case scenario using membranes for desalination.

Transport parameters for each ion with NF membranes were determined by fitting R_{obs} versus J_v according to the SK model. The estimated σ and P_s values for each ion were substituted in Equations 18 - 22 to determine the pore radius specific to a particular ion and is presented in Table 6. This method assumes that only steric effects cause ion rejection and that ions with Stokes radius larger than the membrane pore size are rejected. The SK model used to analyze the experimental rejection data versus flux showed a good fitting for all ions investigated.

Table 6. Effective ion pore radius r_p calculated using SK and SHP models for different membranes

Ions	**ESNA**	**NF 270**	**SR 90**	**HYDRACoRe 10**	**HYDRACoRe 50**	**NANO-SW**
	r_p (nm)					
Cl^-	0.41	0.35	0.24	-	0.37	0.24
Na^+	0.63	0.52	0.45	1.42	0.46	0.42
SO_4^{2-}	0.34	0.25	0.24	0.73	0.33	0.24
Ca^{2+}	0.71	0.58	0.39	0.99	0.67	0.37
Mg^{2+}	0.86	0.62	0.41	2.15	0.68	0.40

Negative reflection coefficients were obtained for Cl^- with HYDRACoRe 10. This could be due to negative rejection of Cl^-. However, during experiments with HYDRACoRe10, negative rejections were not observed. This could be mainly due to the fact that the experiments were performed at operating pressures between 9 and 18 bar and negative rejection is generally observed at lower pressures and rejection becomes positive with increasing pressure [72, 73, 74].

The estimated r_p values confirm that the effective pore size was lowest for NANO-SW and HYDRACoRe10 had the largest pore size. Hence, the pore size of the tested membranes was in the sequence HYDRACoRe10 > ESNA > HYDRACoRe 50 > NF 270 > SR 90 > NANO-SW. This order is valid when Cl^-, Ca^{2+} and Mg^{2+} effective pore radius of each ion is compared for six membranes. While comparing the r_p values for Na^+, results were slightly different; HYDRACoRe50 was tighter than NF 270. The r_p values for SO_4^{2-} cannot be compared due to several mechanisms affecting the ion. SO_4^{2-} is a divalent anion and will be rejected by the negatively charged membrane though the hydration energy of SO_4^{2-} is low (-1145 KJ/mol).

Ten model correlations were developed using results from four polyamide NF membranes, which could determine the rejection, reflection coefficient and solute permeability of individual ions in seawater. The four membranes chosen were ESNA, NF 270, SR 90, and NANO-SW.

The pure water permeability chosen for the model is in the range required for smart water production. The only variables required for this model is the pure water permeability and membrane flux with seawater as feed.

Figure 30 shows the pure water permeability of polyamide membranes versus σ and P_s of chloride for four NF membranes mentioned earlier.

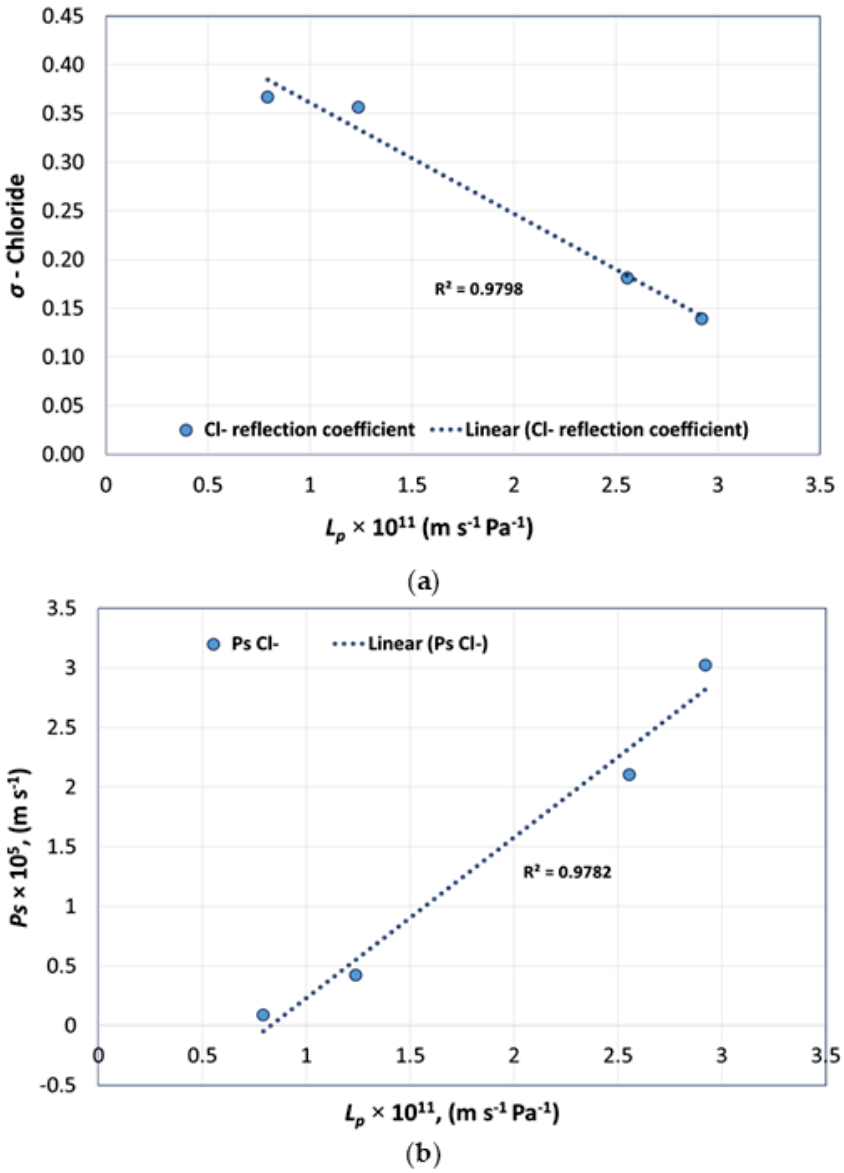

Figure 30. Pure water permeability versus (a) reflection coefficient (b) solute permeability of chloride

Figure 30 (a) shows that with an increase in water permeability, the reflection coefficient of ions decreased whereas Figure 30 (b) shows that

the solute permeability increased. This confirms that when the effective membrane pore radius increases, permeability increases, resulting in low ion rejection.

A close correlation between the model and experimental values of σ, P_s, and rejection of ions were obtained. The correlations are valid if the feed is seawater with no change in viscosity and ionic concentration for all four tested polyamide membranes. Equations 26 – 35 determines σ and P_s of each ion with a given pure water permeability L_{p0}.

$$\sigma_{Cl^-} = -1 \times 10^{10} \times L_{p0} + 0.4749 \quad (26)$$

$$\sigma_{Na^+} = -6 \times 10^{9} \times L_{p0} + 0.3318 \quad (27)$$

$$\sigma_{SO_4{}^{2-}} = -1 \times 10^{10} \times L_{p0} + 1.118 \quad (28)$$

$$\sigma_{Ca^{2+}} = -3 \times 10^{10} \times L_{p0} + 1.1354 \quad (29)$$

$$\sigma_{Mg^{2+}} = -3 \times 10^{10} \times L_{p0} + 1.2559 \quad (30)$$

$$P_{s_{Cl^-}} = 1 \times 10^{11} \times L_{p0} - 1.1144 \quad (31)$$

$$P_{s_{Na^+}} = 6 \times 10^{10} \times L_{p0} - 0.0147 \quad (32)$$

$$P_{s_{SO_4{}^{2-}}} = 4 \times 10^{31} \times L_{p0}{}^{3.0496} \quad (33)$$

$$P_{s_{Ca^{2+}}} = 1 \times 10^{11} \times L_{p0} - 0.7388 \quad (34)$$

$$P_{s_{Mg^{2+}}} = 9 \times 10^{30} \times L_{p0}{}^{2.9414} \quad (35)$$

The correlations can be used for calculating σ and P_s of polyamide membranes with a pore size between 0.4 to 0.86 nm and with pure water permeabilities between 5×10^{-12} to 3×10^{-11} m/s/Pa.

5.8 Power Consumption Analysis

A power consumption analysis of membrane performance for smart water production from seawater and de-oiled PW for both carbonate and sandstone reservoirs were performed.

5.8.1 Power Consumption Analysis with Seawater as Feed

Retentate from NF membrane is rich in divalent ions and suitable for smart water for carbonates. NF and RO in parallel are suitable for smart water production for sandstones. The experiments were conducted at room temperature with an assumed pump efficiency of 80 %. The NF and RO membranes for smart water production with seawater as feed operated at 16 bar and 55 bar, respectively. Experimental results are directly available for full-scale applications. Normal seawater was feed to commercially available NF membranes with a surface area of 2.3 -2.6 m^2.

Pre-filtered seawater at 1 m^3/h was used as feed in crossflow NF membranes, which resulted in two streams with different ionic compositions. The permeate is rich in monovalent ions (TDS 20,800 - 21,000 mg/L) suitable for sandstones after dilution, whereas the retentate is rich in divalent ions such as SO_4^{2-}, Ca^{2+}, and Mg^{2+} and therefore suitable for carbonates. TDS in retentate depends on pore size and charge of the chosen NF membrane, applied pressure, and temperature.

Smart water for sandstone reservoirs should be low in divalent ions with TDS less than 5,000 mg/L. TDS in NF permeate with seawater as feed is 21,000 mg/L and should be diluted with low TDS water for sandstone applications. Thus, an RO membrane is recommended to be used in parallel to dilute the smart water stream. RO retentate, rich in both divalent and monovalent ions is recirculated to the feed tank.

Total power consumed is calculated using Equation 36.

$$Power(W) = \frac{Feed\ flow\ rate\left(\frac{m^3}{s}\right) \times Feed\ pressure\ (Pa)}{Efficiency\ \eta\ (\%)} \qquad (36)$$

Power consumed for smart water production in sandstones is higher than smart water in carbonates due to higher operating pressure for RO when compared with NF. With an energy recovery factor of 50 % for RO, 50 % of the required energy for the feed pump is recovered from the retentate stream. The RO membrane used for power consumption calculations assumed 8 % permeate recovery i.e., the ratio of permeate flow rate to feed flow rate. The RO permeate flow rate can be increased by selecting an alternative RO membrane with higher recovery.

Figure 31 presents a schematic for smart water production in carbonate and sandstone reservoirs showing flow rates and TDS concentrations. Power consumed per cubic meter of smart water produced for carbonates was 0.70 kWh/m^3 and 5.21 kWh/m^3 for sandstones using seawater as feed.

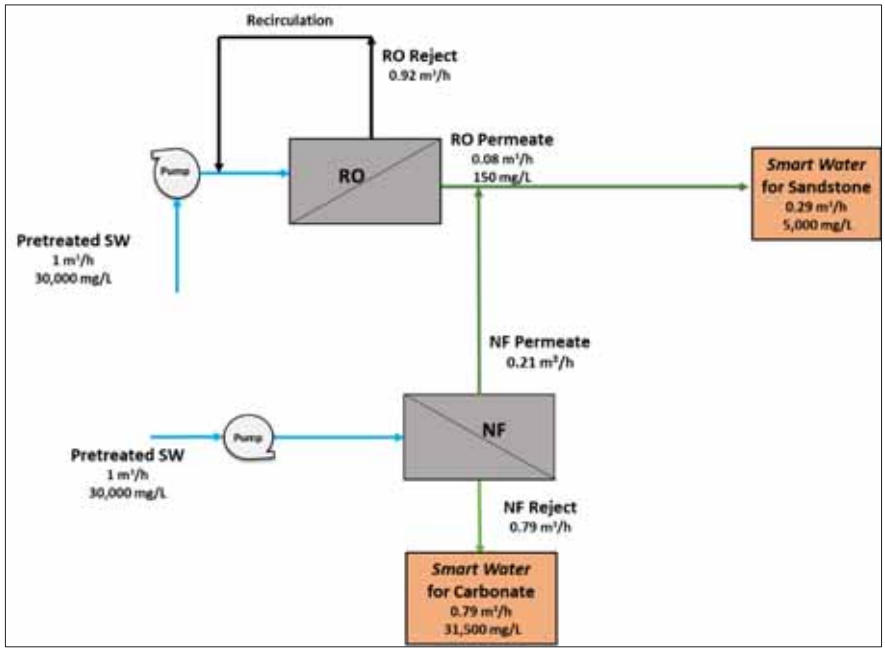

Figure 31. Schematic for smart water production from seawater

5.8.2 Power Consumption Analysis with PW as Feed

Reuse of PW for smart water production is salinity dependant. PW with TDS of 90,000 mg/L was assumed in this research for calculations. A TDS of 90,000 mg/L must be diluted before used as feed for NF. Feed pressures of 9 bar and 55 bar were used for NF and RO membranes, respectively. A diluted PW feed of 40,000 mg/L was used for power calculations. Utilizing retentate as smart water for carbonates has a benefit in reducing concentrate disposal issues.

Figure 32 shows a model for smart water production from PW for both sandstone and carbonate reservoirs. The model presents calculations for a single NF and RO unit. To achieve the required smart water flow rate for injection, multiple membrane stages should be used.

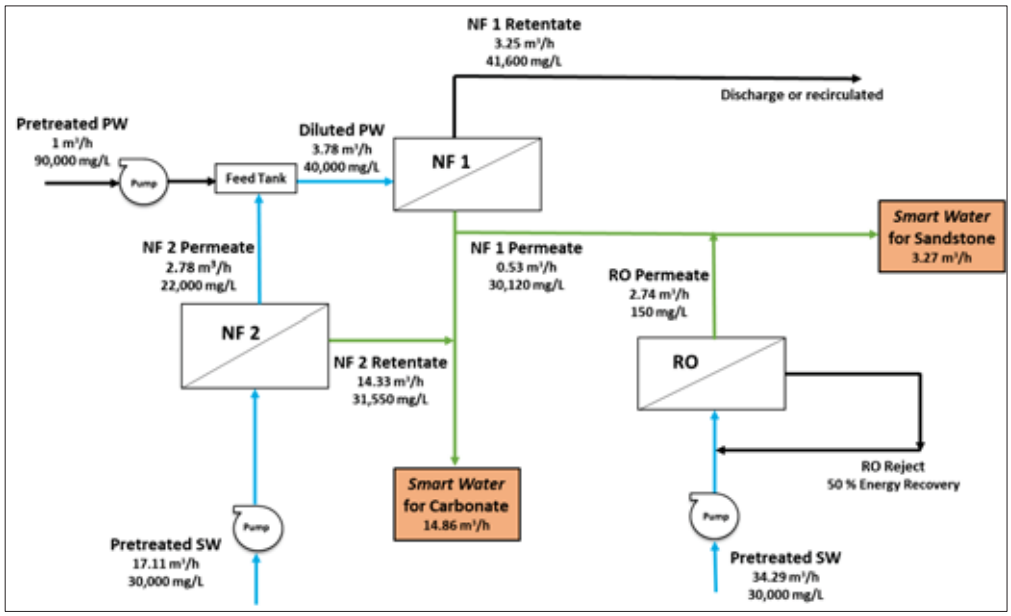

Figure 32. Schematic for smart water production from PW for carbonate and sandstone reservoirs

Smart water TDS of 5,000 mg/L for sandstone reservoirs is produced from permeate from NF and mixed with permeate from RO with

seawater as feed. The energy consumption of RO is directly proportional to ion concentrations due to changes in osmotic pressure. This increases the total power consumption for smart water production for sandstone compared to carbonate reservoirs. An energy recovery factor of 50 % was applied to the RO process.

The power consumed for carbonate reservoirs with PW as feed is calculated to 0.88 kWh/m^3 whereas the total power consumed calculated for an NF and RO membrane in parallel for smart water production in sandstone reservoirs from PW feed is 13.99 kWh/m^3. The power consumed could be lower if the initial TDS of PW is in the range of 40,000 mg/L instead of an initial TDS of 90,000 mg/L. Likewise, increased permeate flow rate could also reduce power consumption. This is possible by selecting NF membranes yielding higher flow rates and with appropriate ion separation efficiency. From the proposed model, it is evident that most of the power is consumed for dilution of feed. Nevertheless, comparing with other desalination techniques, this option is most cost-efficient. One main challenge in PW reuse by membranes is the degree of fouling. Fouling affects the frequency of cleaning and therefore process cost.

The disposal of NF1 retentate is another concern. The retentate is diluted from 90,000 mg/ L to approximately 41,600 mg/L and has an ionic composition similar to seawater. This de-oiled retentate can either be discharged to sea, recirculated to feed tank or reused for pressure support in oil reservoirs.

However, TDS varies with the type of PW. If increased water is produced after secondary injection, PW will nearly have equal concentration to that of injected seawater and makes PW reuse feasible. However, if more concentrated PW is produced, PWRI after required treatment to sub-surface is practicable.

6 Concluding Remarks

This research concluded that smart water suitable for both carbonate and sandstone reservoirs can be produced from seawater and PW by nanofiltration membranes. The advantage of using membranes is ease of operation, no chemicals added and defined as environmentally friendly and sustainable.

6.1 Conclusions

1) Flux and ion retention increased with an increase in applied pressure indicating no fouling of membranes during the experiments.
2) Experiments confirm that membrane pore size and charge are the main factors determining ion rejection.
3) Negative rejection of monovalent ions was observed when the concentration of divalent ions with the same charge was increased in the feed to maintain charge electroneutrality.
4) The NF retentate with seawater as feed is for carbonates and eliminates concentrate disposal issues compared to alternative desalination technologies, distillation and reverse osmosis whereas the permeate is intended as smart water for sandstones.
5) Increased divalent ion concentrations for carbonates resulted by spiking chemicals to membrane feed. Results confirmed that adding divalent ions in the feed was more beneficial than adding it to retentate.
6) No fouling was initiated during short-term membrane separation with synthetic PW with traces of organic compounds. Sr^{2+} and Ba^{2+} concentrations were efficiently reduced which could prevent scaling when PW was used as membrane feed.
7) Experiments with different membrane feed pH confirmed the occurrence of protonation and deprotonation of membrane

functional groups, which lead to pore expansion resulting in increased flux. At very low pH, pore shrinkage occurred resulting in decreased flux. Membrane properties can be manipulated by changing feed pH during smart water production for modifying flux and ion rejection to either type of reservoirs.

8) Smart water production by nanofiltration has two concerns:
   - Retentate with high concentrations of divalent ions also contains monovalent ions due to counterion effects.
   - Only a small percentage of PW could be reused as smart water due to low membrane recovery from high PW feed TDS.
9) An ANN model for predicting ion rejection was presented. The model considers the effect of varying feed pH and increasing operating pressure for different flux and ion rejection. The model showed a close agreement with experimental data.
10) A power consumption analysis is proposed, along with a schematic for smart water production, with flow rates and compositions for each stream. This provides the end-users a choice of membrane configurations for industrial use.
11) Smart water production in carbonates with seawater as feed showed a power consumption of 0.70 kWh/m^3. For sandstones, the power consumed is higher at 5.21 kWh/m^3. This is due to a combination of NF and RO membranes used to dilute NF permeate to TDS < 5,000 mg/L.
12) The total power consumed by 2 NF membranes in parallel for smart water production in carbonates from PW feed is calculated to 0.88 kWh/m^3.
13) The total power consumed by NF and RO membranes in parallel for smart water production in sandstones from PW feed is calculated to 13.99 kWh/m^3.
14) Correlations were developed to determine reflection coefficient and solute permeability of ions for polyamide NF membranes to predict ion rejection. Transport parameters were determined

based on Spiegler -Kedem and steric hindrance pore models. The proposed correlations predict rejection, reflection coefficient and solute permeability with close accuracy. The main advantage of these correlations is that they require few input data that can be easily obtained from simple experiments.

6.2 Future Work

- Smart water produced by membranes for carbonate and sandstone reservoirs was not tested on cores. Further process improvements should be made after core testing.
- The fate of production chemicals present in PW has to be verified. Experiments analyzing the type of chemicals permeating through NF should be identified for reuse.
- Reuse of PW retentate in a more efficient way by forward osmosis or membrane distillations.

References

[1] IEA, "World Energy Outlook," 2017.

[2] E. Donaldson, G. Chilingarian and T. Yen, Enhanced oil recovery, II processes and operations, Elsevier, 1989.

[3] D. Green and G. Willhite, "¨Enhanced Oil Recovery¨ SPE Textbook Series Vol.6," 1998.

[4] F. Craig, The reservoir engineering aspects of waterflooding, H.L.Doherty Memorial Fund of AIME, 1971.

[5] M. Jaafar, N. Mohd and M. Hamid, "Measurement of isoelectric point of sandstone and carbonate rock for monitoring water encroachment," *Journal of Applied Sciences,* no. 14, pp. 3349-3353, 2014.

[6] W. Anderson, "Wettability literature survey- part 2," *Journal of Petroleum Technology,* pp. 1246-1262, 1986.

[7] J. Buckley, "Effective wettability of minerals exposed to crude oil," *Current Opinion in Colloid and Interface Science,* pp. 191-196, 2001.

[8] K. Lee and J. Neff, Produced Water- Environmental risks and advances in mitigation technologies, Springer Science + Business Media, 2011.

[9] F.-R. Ahmadun, A. Pendashteh, L. C. Abdullah, D. R. A. Biak, S. S. Madaeni and Z. Z. Abidin, “Review of technologies for oil and

gas produced water treatment," *Journal of Hazardous Materials,* no. 170, pp. 530-551, 2009.

[10] S. Munirasu, M. A. Haija and F. Banat, "Use of membrane technology for oil field and refinery produced water treatment- A review," *Process Safety and Environmental Protection,* 2016.

[11] Environmental Report, "Environmental Report- Environmental work by the Oil and Gas Industry," Norsk Olje and Gass, 2016.

[12] M. Cheryan, Ultrafiltration and Microfiltration Handbook, CRC Press:Boca Raton, FL, 1998.

[13] M. Mulder, Basic principles of membrane technology, Kluwer Academic Publishers, 1996.

[14] M. Nilsson, G. Tragårdh and K. Ostergren, "The influence of pH, salt and temperature on nanofiltration performance," *Journal of Membrane Science,* pp. 97-106, 2008.

[15] A. Al-Karaghouli and L. Kazmerski, "Energy consumption and water production cost of conventional and renewable - energy - powered desalination processes," *Renewable Sustainable Energy Rev.,* pp. 343-356, 2013.

[16] L. W. Jye and A. F. Ismail, Nanofiltration membranes: Synthesis, Characterization and Applications, CRC Press, Taylor and Francis Group, 2017.

[17] A. Pérez- González, A. Urtiaga, R. Ibáñez and I. Ortiz, "State of the art and review on the treatment technologies of water reverse osmosis concentrates," *Water Research,* 2012.

[18] S. Strand, E. Høgnesen and T. Austad, "Wettability alteration of carbonates- Effects of potential determining ions (Ca2+ and SO42-) and temperature," *Colloids and Surfaces A: Physiochem. Eng. Aspects,,* pp. 1-10, 2006.

[19] T. Austad, "Water-based EOR in carbonate and sandstone: New chemical understanding of the EOR- potential using ¨Smart water¨.," in *Enhanced Oil Recovery Field Case Studies*, Sheng. J, Gulf Professional Publishing: Houston, TX, 2013, pp. 301-335.

[20] T. Austad, A. Rezaeidoust and T. Puntervold, "Chemical mechanism of low salinity water flooding in sandstone reservoirs," *SPE 129767,* 2010.

[21] I. D. Torrijos, T. Puntervold, S. Strand, T. Austad, H. I. Abdullah and K. Olsen, "Experimental study of the response time of the low - salinity enhanced oil recovery during secondary and tertiary low salinity waterflooding," *Energy and Fuels,* no. 30, pp. 4733-4739, 2016.

[22] I. D. P. Torrijos, Enhanced oil recovery from sandstone and carbonates with ¨ Smart Water¨, ISBN: 978-82-7644-708-8: Unversity of Stavanger, 2017.

[23] G. Tang and N. Morrow, "Salinity, temperature, oil composition, and oil recovery by waterflooding," *SPE Reservoir Engineering,* no. 12(4), pp. 269-276, 1997.

[24] N. Morrow and J. Buckley, "Improved oil recovery by low-salinity waterflooding," *Journal of Petroleum Technology,* no. 63(5), 2011.

[25] G. Jerauld, K. Webb, C. Lin and J. Seccombe, "Modelling low-salinity waterflooding, SPE 102239," *SPE Annual Technical*

Conference and Exhibition, San Antonio, Texas, 24-27 September, 2006.

[26] Y. Zhang and N. Morrow, "Comparison of secondary and tertiary recovery with change in injection brine composition for crude oil/sandstone combinations," *SPE 99757 presented at the SPE/DOE Symposium on Improved Oil recovery,* 2006.

[27] I. D. P. Torrijos, T. Puntervold, S. Strand and A. Rezaeidoust, "Optimizing the low salinity water for EOR effects in sandstone reservoirs- Composition vs salinity," in *78th EAGE Conference and Exhibition*, 2016.

[28] S. Fathi, T. Austad and S. Strand, "Water-based enhanced oil recovery (EOR) by ¨Smart Water¨: Optimal ionic composition for EOR in carbonates," *Energy and Fuels,* pp. 5173-5179, 2011.

[29] T. Puntervold, S. Strand, R. Ellouz and T. Austad, "Modified seawater as a smart water fluid in chalk," *Journal of Petroleum Science and Engineering,* no. 133, pp. 440-443, 2015.

[30] P. Zhang and T. Austad, "Wettability and oil recovery from carbonates: Effects of temperature and potential determining ions," *Colloids and Surfaces A: Physiochem and Eng. Aspects,* no. 279, pp. 179-187, 2006.

[31] P. Zhang, M. T. Tweheyo and T. Austad, "Wettability alteration and improved oil recovery by spontaneous imbibition of seawater into chalk: Impact of the potential determining ions Ca2+, Mg2+, and SO42-," *Colloids and Surfaces A. Physicochem. Eng. Aspects,* no. 301, p. 199.208, 2007.

[32] S. Fathi, T. Austad and S. Strand, "Water-based enhanced oil recovery (EOR) by ¨Smart Water¨ in carbonate reservoirs," *SPE*

154570 presented at the SPE EOR Conference at Oil and Gas West Asia, Muscat, Oman, 16-18 August, 2012.

[33] R. W. Baker, Membrane Technology and Applications, John Wiley & Sons, Ltd, 2004.

[34] X.-L. Wang, T. Tsuru, M. Togoh, S.-I. Nakao and S. Kimura, "Evaluation of pore structure and electrical properties of nanofiltration membranes," *Journal of Chemical Engineering of Japan,* 1994.

[35] S. Bandini, J. Drei and D. Vezzani, "The role of pH and concentration on the ion ejection in polyamide nanofiltration membranes," *Journal of Membrane Science,* no. 264, pp. 65-74, 2005.

[36] J. Luo and W. Yinhua, "Effect of pH and salt on nanofiltration- A critical review," *Journal of Membrane Science,* no. 438, pp. 18-28, 2013.

[37] J.-J. Qin, M. H. Oo, H. Lee and B. Coniglio, "Effect of feed pH on permeate pH and ion rejection under acidic conditions in NF process," *Journal of Membrane Science,* no. 232, pp. 153-159, 2004.

[38] J. Luo, L. Ding, Y. Su, ShaopingWei and Y. Wan, "Concentration polarization in concentrated saline solution during desalination of iron dextran by nanofiltration," *Journal of Membrane Science,* no. 363, pp. 170-179, 2010.

[39] A. Siddiqui, S. Lehmann, V. Haaksman, J. Ogier, C. Schellenberg, M. van Loosdrecht, J. Kruithof and J. Vrouwenvelder, "Porosity of spacer-filled channels in spiral - wound membrane systems:

Quantification methods and impact on hydraulic characterization," *Water Research,* no. 119, pp. 304-311, 2017.

[40] N. Hilal, H. Al-Zoubi, N. Darwish, A. Mohammad and M. Abu Arabi, "A comprehensive review of nanofiltration membranes: Treatment, pretreatment, modeling, and atomic force microscopy," *Desalination,* no. 170, pp. 281-308, 2004.

[41] R. Epsztein, E. Shaulsky, N. Dizge, D. M. Warsinger and M. Elimelech, "Role of ionic charge density in Donnan exclusion of monovalent anions by nanofiltration," *Environmental Science and Technology,* pp. 4108-4116, 2018.

[42] W. Bowen, A. Mohammad and N. Hilal, "Characterisation of nanofiltration membranes for predictive purposes/use of salts, uncharged solutes and atomic force microscopy," *Journal of Membrane Science,* no. 126, pp. 91-105, 1997.

[43] F. Donnan, "Theory of membrane equilbria and membrane potentials in the presence of non-dialysing electrolytes. A contribution to physical,chemical physiology," *Journal of Membrane Science,* no. 100, pp. 45-55, 1995.

[44] A. E. Childress and M. Elimelech, "Effect of solution chemistry on the surface charge of polymeric reverse osmosis and nanofiltration membranes," *Journal of Membrane Science,* no. 119, pp. 253-268, 1996.

[45] A. E. Childress and M. Elimelech, "Relating nanofiltration membrane performance to membrane charge (electrokinetic) characteristics," *Environmental Science and Technology,* no. 34, pp. 3710-3716, 2000.

[46] A. E. Yaroshchuk, "Dielectric exclusion of ions from membranes," *Advances in Colloid and Interface Science,* no. 85, pp. 193-230, 2000.

[47] S. Bandini and D. Vezzani, "Nanofiltration modeling: The role of dielectric exclusion in membrane characterization," *Chemical Engineering Science,* no. 58, pp. 3303-3326, 2003.

[48] L. A. Richards, B. S. Richards, B. Corry and A. I. Schafer, "Experimental energy barriers to anions transporting through nanofiltration membranes," *Environmental Science & Technology,* no. 47, pp. 1968-1976, 2013.

[49] B. Tansel, "Significance of thermodynamic and physical characteristics on permeation of ions during membrane separation: Hydrated radius, hydration free energy and viscous effects," *Separation and Purification Technology,* no. 86, pp. 119-126, 2012.

[50] K. Spiegler and K. O., "Thermodynamics of hyperfiltration (reverse osmosis): Criteria for efficient membranes," *Desalination,* vol. 1, pp. 311-326, 1966.

[51] O. Kedem and A. Katchalsky, "Thermodynamical analysis of the permeability of biological membranes to non-electrolytes," *Biochimica et Biophysica Acta,* pp. 229-246, 1958.

[52] C. K. Diwara, S. Lo, M. Rumeau, M. Pontie' and O. Sarr, "A phenomenological mass transfer approach in nanofiltration of halide ions for a selective defluorination of brackish drinking water," *Journal of Membrane Science,* pp. 103-112, 2003.

[53] S. Jain and S. K. Gupta, "Analysis of modified surface force pore model with concentration polarization and comparison with

Spiegler-Kedem model in reverse osmosis systems," *Journal of Membrane Science,* no. 232, pp. 45-61, 2004.

[54] Z. Murthy and S. Gupta, "Estimation of mass transfer coefficient using a combined nonlinear membrane transport and film theory model," *Desalination,* no. 121, pp. 131-137, 1997.

[55] S.-I. Nakao and S. Kimura, "Models of membrane transport phenomena and their applications for ultrafiltration data," *Journal of Chemical Engineering of Japan,* 1982.

[56] R. Bowen and W. Mohammad, "Diafiltration by nanofiltration: Prediction and optimization," *AIChE Journal,* no. 44, pp. 1799-1812, 1998.

[57] A. Hussain, S. Nataraj, M. Abashar, I. Al-Mutaz and T. Aminabhavi, "Prediction of physical properties of nanofiltration membranes using experiment and theoretical models," *Journal of Membrane Science,* pp. 321-336, 2008.

[58] O. Labban, C. Liu, T. H. Chong and J. H. Lienhad, "Fundamentals of low - pressure nanofiltration: Membrane characterization, modeling, and understanding the multi-ionic interactions in water softening," *Journal of Membrane Science,* no. 521, pp. 18-32, 2017.

[59] M. H. Beale, M. T. Hagen and H. Demuth, Neural Networks Toolbox (TM)- Users Guide, The MathWorks, Inc., 2018.

[60] AWWA M46, "Manual of water supply practices- Reverse Osmosis and Nanofiltration," 1999.

[61] Filmtec Membranes, "Dow water solutions- Filmtec membranes product catalogue," [Online]. Available: www.lenntec.com.

[62] N. Hydranautics, "Product information catalogue," [Online]. Available: www.membranes.com.

[63] R. R. Nair, E. Protasova, S. Strand and T. Bilstad, "Membrane performance analysis for smart water production for enhanced oil recovery in carbonate and sandstone reservoirs," *Energy & Fuels,* pp. 4988-4995, 2018.

[64] ASTM D7678-17, "Standard test method for total oil and grease (TOG) and total petroleum hydrocarbons (TPH) in water and wastewater with solvent extraction using mid-air laser spectroscopy," ASTM International, 2017.

[65] J. Schaep and C. Vandecasteele, "Evaluating the charge of nanofiltration membranes," *Journal of Membrane Science,* no. 151, pp. 123-129, 2001.

[66] J. Tanninen, M. Mänttäri and M. Nyström, "Effect of salt mixture on fractionation with NF membranes," *Journal of Membrane Science,* no. 283, pp. 57-64, 2006.

[67] X.-L. Wang, W.-N. Wang and D.-X. Wang, "Experimental investigation on separation performance of nanofiltration membranes for inorganic electrolyte solutions," *Desalination,* pp. 115-122, 2002.

[68] C. Labbez, P. Fievet, A. Vidonne, A. Foissy and J. Pagetti, "Retention of mineral salts by a polyamide nanofiltration membrane," *Separation and Purification Technology,* pp. 47-55, 2003.

[69] G. Hill and J. Holman, Chemistry in Context, Laboratory Manual, 2001.

[70] M. I. Chaudhari and S. B. Rempe, "Strontium and barium in aqueous solution and a potassium channel binding site," *The Journal of Chemical Physics,* no. 148, 2018.

[71] G. Hagmeyer and R. Gimbel, "Modeling the rejection of nanofiltration membranes using zeta potential measurements," *Separation and Purification Technology,* vol. 15, pp. 19-30, 1999.

[72] A. Yaroshchuk, "Negative rejection of ions in pressure - driven membrane processes," *Advanced Colloid Interface Science,* pp. 150-173, 2008.

[73] J. Gilron, N. Gara and O. Kedem, "Experimental analysis of negative salt rejection in nanofiltration membranes," *Journal of Membrane Science,* no. 185, pp. 223-236, 2001.

[74] X. Xu and H. Spenser, "Dye-salt separations by nanofiltration using weak acid polyelectrolyte membranes," *Desalination,* no. 129, 1997.

Appendices

Appendix 1 – Paper I

Paper I

Membrane Performance Analysis for Smart Water Production for Enhanced Oil Recovery in Carbonate and Sandstone Reservoirs

Remya Ravindran Nair, Evgenia Protasova, Skule Strand, Torleiv Bilstad

Energy & Fuels, 2018, 32 (4), pp 4988-4995

DOI: 10.1021/acs.energyfuels.8b00447

energy&fuels

Article

Cite This: Energy Fuels 2018, 32, 4988−4995

pubs.acs.org/EF

Membrane Performance Analysis for Smart Water Production for Enhanced Oil Recovery in Carbonate and Sandstone Reservoirs

Remya R. Nair,*[,†] Evgenia Protasova,[†] Skule Strand,[‡] and Torleiv Bilstad[†]

[†]Department of Natural Science and Mathematics and [‡]Department of Petroleum Engineering, University of Stavanger, Kjell Arholmsgate 41, 4036 Stavanger, Norway

ABSTRACT: Water with specific ion composition is required for smart water production intended for enhanced oil recovery (EOR) in petroleum reservoirs. Membrane desalination is proposed in a unique configuration to deliver water with varying ionic composition for water injection in both carbonate and sandstone reservoirs. This research is dedicated to improve existing EOR technology and achieve environmentally friendly production of fossil fuels offshore. Present work addresses objectives, such as optimizing the nanofiltration (NF) membrane performance for smart water production from seawater in terms of flux, ion rejection, and power consumption for producing 1 m^3 h^{-1} smart water. The power consumed for smart water production is calculated at 0.7 kWh m^{-3} for carbonates and 5.21 kWh m^{-3} for sandstones. NF membranes were chosen for smart water production over other desalination technologies as a result of their flexibility in altering ionic composition, low energy requirements, low chemical usage, and small footprint along with ease of operation. Smart water production from seawater considerably reduces use of fresh water during offshore water injection and is environmentally friendly.

1. INTRODUCTION

1.1. Smart Water for Enhanced Oil Recovery (EOR). Increased recognition regarding effects of chemicals used in the environment is a major concern for oil companies. Consequently, EOR techniques that have little environmental impact and are simultaneously cost-effective are considered beneficial. Injection of smart water is a relatively new EOR technique that improves oil recovery by wettability alteration toward more water-wet conditions. Increased positive capillary forces improve the microscopic sweep efficiency and increase oil recovery.[1] Compositions of smart water differ between reservoirs and are produced by modifying the ionic composition according to reservoir mineralogy. For carbonate reservoirs, smart water should contain high divalent ion concentrations and low monovalent ion concentrations. Major divalent ions required for smart water are sulfate, calcium (both 2−3 times the amount present in seawater), and magnesium.[1] Smart water in carbonates requires low sodium and chloride concentrations. Total dissolved solids (TDS) between 10 000 and 32 000 mg L^{-1} is preferable for carbonates.[2]

Sandstone reservoirs, in general, require smart water with TDS less than 5000 mg L^{-1}. The presence of divalent ions in the low-salinity brines is not preferred for sandstones because these ions may suppress the increase of pH, which is essential to observe low-salinity effects.[1] Smart water was originally produced by adding required ions (chemicals) to freshwater or low-TDS water.

The focus of this research is to analyze whether smart water can be produced with membranes and the effect of spiked chemicals on nanofiltration (NF) performance for producing smart water. The research also investigates the energy consumed in production of smart water for both carbonate and sandstone reservoirs.

1.2. Choice of Desalination Technologies. Prevailing desalination technologies are categorized mainly into thermal- and membrane-based. Thermal-based desalination includes multi-stage flash (MSF) distillation, thermocompression distillation (TCD), multi-effect distillation (MED), and mechanical vapor compression (MVC). For thermal-based desalination, salty water is heated and salt-free water is collected as a condensate. This process includes a phase change.[3]

NF and reverse osmosis (RO) are the membrane-based desalination technologies used commercially. Both are pressure-driven processes and involve ion separation when water is permeated through the membranes. The permeate stream is desalted, while the reject stream is rich in ions. No phase change occurs during this process.

Selection of desalting technology offshore depends upon footprint, weight, and energy or steam requirements associated with them. Thermal distillation processes require higher energy than membrane processes.[3] The total energy consumed for desalination is shown in Table 1.

1.3. NF Membrane. NF separation is pressure-driven through membranes with a molecular weight cutoff (MWCO) of 200−2000 Da. NF membranes have pore sizes between 0.1 and 1 nm.[4] Most NF membranes are negatively charged. Nevertheless, neutral and positively charged NF membranes are available. Accordingly, the selectivity of NF membranes for dissimilar ions with varying ion size and charge density will differ. NF membranes have applications in numerous fields, such as water and wastewater treatment, food, and pharmacy. NF membranes efficiently separate mono- and divalent ions at low operating pressures and have higher flux compared to RO membranes.

Numerous studies have been conducted on determining the efficiency of NF membranes for separation of mixed salt

Received: February 3, 2018
Revised: March 23, 2018
Published: April 2, 2018

DOI: 10.1021/acs.energyfuels.8b00447
Energy Fuels 2018, 32, 4988−4995

Table 1. Energy Consumption by Major Desalination Technologies[3]

property	MSF	TCD	MED	MVC	seawater RO
total energy consumption (kWh m^{-3})	19.58−27.35	16.26	14.45−21.25	7−12	4−6
final TDS (mg L^{-1})	≈10	≈10	≈10	≈10	400−500

solutions.[5,6] Flux, ion rejection, total salt concentration in feed, and membrane material affect the NF membrane efficiency. The ion rejection by NF membranes is governed by steric hindrance, dielectric exclusion, and Donnan equilibrium.[7,8] Each of these mechanisms contributes to ion separation depending upon the ion concentration and pH of the feed solution, membrane properties, and ion size and charge.[9] Separation of neutral solutes by NF depends upon steric or size exclusion, in which the solute size and shape form the basis of ion partitioning. Donnan equilibrium resulting from the charged nature of the NF membrane contributes to the partitioning effect for charged solutes. The membrane repels solutes having the same charge as the membrane (co-ions) as a result of Donnan equilibrium, whereas the membrane will attract the solutes with opposite charge, counterions.[8]

Flux is generally used to determine the membrane efficiency and is defined as permeate flow through a unit area of the membrane surface. Flux is predicted by Hagen−Poiseuille in eq 1[4]

$$J = \varepsilon d_p^2 P_T / 32 \Delta x \mu \quad (1)$$

where J is the flux in L m^{-2} h^{-1}, ε is the membrane surface porosity, d_p is the channel diameter, P_T is the transmembrane pressure, μ is the absolute viscosity of the fluid, and Δx is the length of the channel or thickness of the membrane.

Equation 2 calculates volumetric flux through a membrane (L m^{-1} h^{-1}) from experimental data

$$J = V/tA \quad (2)$$

where J is the volumetric flux, V is the volume of the permeate, t is the filtration time, and A is the effective membrane area.

The ion rejection is calculated to determine the quantity of ions rejected by the membrane. The rejection of component i is expressed by eq 3

$$R = 1 - C_{pi}/C_{fi} \quad (3)$$

where C_{pi} is the concentration of component i in the permeate and C_{fi} is the concentration of component i in the feed.

If the flux through the membrane is very low, even after proper chemical cleaning, the membrane is permanently fouled and should be replaced. Membrane fouling depends mainly upon feedwater properties and pretreatment performed before membrane experiments. Expenditure of a membrane application is dependent upon many factors, such as flux, operating conditions, cost of pretreatment, plant capacity, membrane installation, and replacement cost, whereas product water quality depends upon pretreatment, percentage rejection, and type of membrane. Membrane cost depends upon market influence and can change with time.

Membrane lifetime depends upon feed composition, operating conditions, such as pressure and temperature, cleaning frequency, and effect of cleaning chemicals. It can be assumed that, with proper feed pretreatment and frequent cleaning, membrane life can be assumed to be 5 years.

1.4. Pure Water Permeability. Pure water permeability determines the ability of the membrane to permeate pure water through it. The permeability of seawater through a membrane will be lower than that of fresh water. A comparison of pure water permeability before and after a membrane experiment indicates the degree of fouling. Pure water permeability is determined using eq 4

$$\text{pure water permeability (L } h^{-1}\ m^{-2}\ bar^{-1}) = V/(tAP) \quad (4)$$

where V is the volume of permeate and P is the pressure.

Pure water permeability is calculated from a flux−pressure graph. When pure water is used, the osmotic pressure difference between the two sides of the membrane is zero and there is a linear relationship between the hydrodynamic pressure, ΔP, and the volume flux, J. The slope of the corresponding flux−pressure curve is the water permeability coefficient.

1.5. Smart Water Production by Membranes. The feed stream enters the membrane and is divided into two streams. The retentate is rejected by the membrane and contains all ions retained by the membrane. The permeate passes through the membrane and is cleaner than the other two streams. NF retentate is used for smart water production in carbonate reservoirs because high divalent ion concentrations together with a TDS between 10 000 and 32 000 mg L^{-1} is preferred. The NF retentate is rich in SO_4^{2-}, Ca^{2+}, and Mg^{2+} and has low Na^+ and Cl^- concentrations when seawater is used as feed. Spiking of chemicals will be made only for smart water in carbonates. Most offshore plants have a RO membrane infrastructure for desalination for potable water production. The permeate from NF can be used as feed for RO membranes. NF permeate is used for smart water production in sandstone reservoirs. NF permeate has low divalent ion concentrations, thus resulting in low TDS. However, one of the main criteria for smart water in sandstones is that it should have a TDS of <5000 mg L^{-1}. Thus, NF permeate should be diluted with RO permeate to tailor required ion consistency. RO permeate has a TDS of <500 mg L^{-1}. Hence, both streams from a NF membrane can be used for smart water production for different reservoirs.

2. MATERIALS AND METHODS

2.1. NF Membrane. NANO-SW-2540 (Hydranautics) was the membrane chosen for this research. According to the manufacturers, this is a thin-film composite polyamide membrane with a spiral wound configuration and an area of 2.3 m^2. It has a defined maximum operating pressure of 41.4 bar, maximum operating temperature of 45 °C, and pH of 3−9.

The feedwater is pre-filtered seawater with TDS of 34.1 g L^{-1}, conductivity of 49 mS cm^{-1}, and pH of 8. The composition of major ions present in feedwater is in Table 2.

2.2. Chemicals and Analytical Instruments. The chemicals used were analytical-grade sodium sulfate anhydrous, calcium chloride dihydrate, magnesium chloride hexahydrate, and magnesium sulfate hydrate.

The pH was measured using VWR Phenomenal pH 1100L. Conductivity, salinity, temperature, and TDS were measured using TDS meter VWR collection CO3100N. Ion concentrations were quantified by ion chromatography (IC, Dionex ICS-3000). The flow rate was measured manually by determining the time required to fill a fixed volume.

DOI: 10.1021/acs.energyfuels.8b00447
Energy Fuels 2018, 32, 4988−4995

Table 2. Composition of Major Ions in Feed Seawater Analyzed by IC

ion	seawater (mM)
HCO^{3-}	2
Cl^-	525
SO_4^{2-}	24
Mg^{2+}	51
Ca^{2+}	9.3
Na^+	450
K^+	10

2.3. Membrane Experiments. Retentate and permeate were recirculated to the feed tank to maintain constant feed concentrations. The NANO-SW-2540 membrane experiments were performed at room temperature with operating pressures between 9 and 18 bar. The membrane stabilization time for each experimental run was 25 min. Figure 1 shows the schematic of the membrane pilot unit used for the experiments. Experiments commenced with seawater and later added chemicals to change the feed concentration, one chemical at a time. Three doses of each chemical were spiked to seawater. Three trials with each concentration of four chemicals were performed. Mass balance error calculations were performed after each experiment to assess whether the measured values was accurate.

Equation 5 defines the mass balance of the membrane experiments

$$Q_f C_f = Q_r C_r + Q_p C_p \quad (5)$$

where Q_f, Q_r, and Q_p are the feed, retentate, and permeate flow rates, respectively, and C_f, C_r, and C_p are the concentrations of the feed, retentate, and permeate, respectively.

2.4. Membrane Regeneration and Replacement. Membrane cleaning was performed after each experiment. Pure water permeated through the membrane after each experiment. Membrane regeneration can also be performed if flux decreases or remains constant with an increase in pressure or when the membrane surface is saturated with dissolved solids. Washing is continued until the membrane flux returned to its initial pure water permeability value. If the flux did not return to its original after washing with pure water, chemical cleaning for removal of metal hydroxides, $CaCO_3$, and other scales should be performed. Conductivity and pH of recirculated tap water were continuously monitored to ensure that no dissolved solids are present in the membrane.

3. RESULTS AND DISCUSSION

3.1. Pure Water Permeability. Prior to ion separation experiments with seawater, pure water permeability tests with NANO-SW-2540 were carried out at varying operating pressure and permeability was calculated using eq 4. The pure water permeability of the membrane was 7.5 L h^{-1} m^{-2} bar^{-1}.

3.2. Seawater Permeability. Figure 2 represents the volumetric flux, and Figure 3 shows ion rejection as a function of the operating pressure using seawater as feed. There is a linear relation between flux and pressure in Figure 2. This linear variation confirms that the membrane surface was independent of fouling and concentration polarization.

Flux and ion rejection increase with operating pressure, according to Figures 2 and 3. This confirms that ions are transported across the membrane because of the force that acts on the ions as a result of pressure acting on NF membranes.

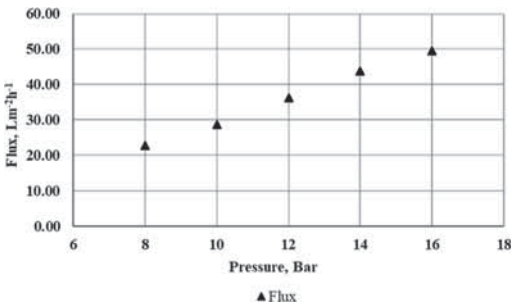

Figure 2. Flux versus pressure with seawater as feed.

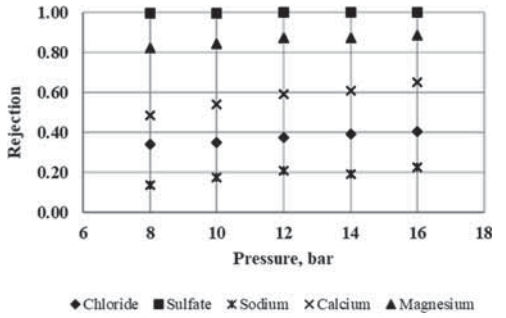

Figure 3. Ion rejection with NANO-SW-2540.

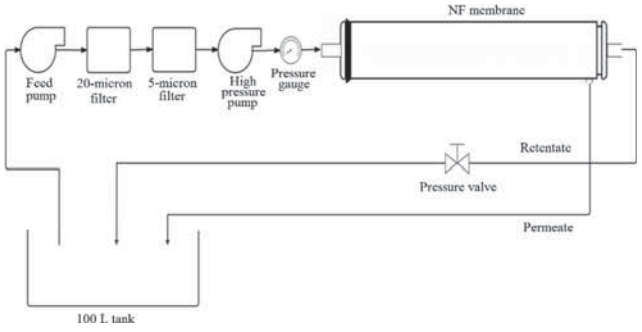

Figure 1. Schematic of the NF membrane pilot unit used for experiments.

DOI: 10.1021/acs.energyfuels.8b00447
Energy Fuels 2018, 32, 4988−4995

The NF membrane is negatively charged and, thus, will attract counterions and reject co-ions as a result of the Donnan effect. Figure 3 shows that the NF membrane exhibits a higher rejection for multivalent co-ions (SO_4^{2-}) than the monovalent co-ions (Cl^-), which is advantageous because the membrane retentate stream is used for smart water production in carbonates that requires a high sulfate concentration and low monovalent concentrations.

3.3. Spiking Chemicals in Feed Seawater. Chemical spiking is not required for smart water production in sandstones as a result of low TDS requirement. For carbonate reservoirs, however, spiking is essential because smart water should contain increased sulfate, magnesium, and calcium concentrations. To achieve a smart water composition with an increased sulfate concentration, Na_2SO_4 was added to seawater at 54 mM or 3.4 g L^{-1} Na_2SO_4 (dose 1), 76 mM or 6.8 g L^{-1} Na_2SO_4 (dose 2), and 95 mM or 8.5 g L^{-1} Na_2SO_4 (dose 3). The corresponding increase in moles of Na^+ measured by IC was 460 mM (dose 1), 510 mM (dose 2), and 572 mM (dose 3).

Figure 4 shows that flux decreased with an increased Na_2SO_4 concentration in the feed. When seawater was spiked with 3.4 g

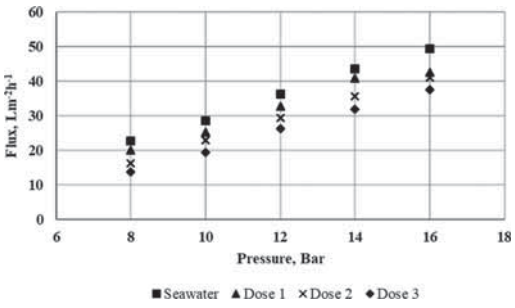

Figure 4. Flux versus pressure for seawater and seawater spiked with Na_2SO_4.

L^{-1} Na_2SO_4, and filtered at an operating pressure of 10 bar, the flux decreased from 29 to 25 L m^{-2} h^{-1}. The flux values were further reduced with Na_2SO_4 concentrations at 6.8 and 8.5 g L^{-1}. At 8.5 g L^{-1} Na_2SO_4, the flux at 10 bar decreased to 19 L m^{-2} h^{-1}. Alternatively, a decrease in flux means that more water is rejected by the membrane. This increases the retentate flow rate, which is beneficial for smart water production in carbonates.

The flux decline is explained by an increase in viscosity with the increased Na_2SO_4 concentrations. The NF pore size is less than 1 nm. Hence, even a very small change in viscosity can lead to a decrease in flux. It is also explained in terms of the osmotic pressure difference across the membrane. According to the van't Hoff equation, the osmotic pressure of water is directly proportional to the concentration of dissolved ions in solution in eq 6

$$\pi = i\frac{C}{M}RT \tag{6}$$

where i is the number of ions, C is the concentration of dissolved ions in solution (g/L), M is the molecular weight of the solute, R is the ideal gas constant, and T is the absolute temperature (K).

Hence, the osmotic pressure difference across the membrane increases when ions are spiked in the feed. The effect of the feed concentration on flux is also well-explained by the mass transfer or the film theory model.[4] According to this model, solute transport to the membrane surface occurs as a result of convection at a rate J_S defined as eq 7

$$J_S = JC_B \tag{7}$$

where C_B is the bulk concentration of the rejected solute.

The concentration gradient causes the solute to back transport to the bulk solution as a result of diffusion, as shown in eq 8

$$J_S = D\mathrm{d}c/\mathrm{d}x \tag{8}$$

where D is the diffusion coefficient and $\mathrm{d}c/\mathrm{d}x$ is the concentration gradient in the boundary layer.

The mechanisms of convective and diffusive transport balance at steady state and eqs 7 and 8 are equated and integrated to form eq 9

$$J = k \ln C_G/C_B \tag{9}$$

where C_G is the gel concentration or the solute concentration at the membrane surface and k is the mass transfer coefficient.

Equation 9 confirms that the flux, J, decreases with an increase in C_B, feed concentration. This effect is independent of the temperature and turbulence.[4]

Figure 5 illustrates rejection of chloride as a function of the pressure with increased sulfate concentrations. Chloride

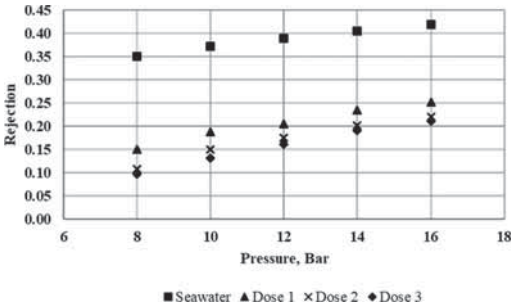

Figure 5. Cl^- rejection versus pressure with an increase in the Na_2SO_4 concentration.

rejection decreases with increased Na_2SO_4 concentrations at any pressure. At an operating pressure of 10 bar, Cl^- rejection with seawater as feed was permeated through the membrane at 0.37, whereas with the added sulfate concentration of dose 3 (8.5 g L^{-1}), the Cl^- rejection decreased to 0.13. A decrease in Cl^- rejection occurs with increasing doses, irrespective of the operating pressure.

If a second co-ion (SO_4^{2-}) is added to NaCl solution (or seawater), the Donnan equilibrium will change. With the addition of Na_2SO_4 to the feed, the system will have more counterions of Na^+, whereas the Cl^- concentration remains unchanged along with a constant membrane charge. This results in an increase in the Cl^- concentration in the membrane or permeate.

Figure 6 shows that the sulfate rejection was at 0.99 for all three doses, irrespective of the operating pressure or increased concentrations. This difference in rejection of SO_4^{2-} and Cl^-

DOI: 10.1021/acs.energyfuels.8b00447
Energy Fuels 2018, 32, 4988−4995

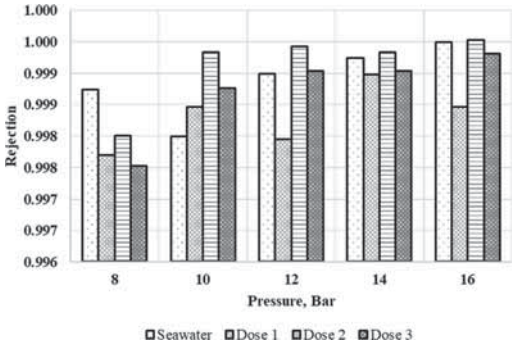

Figure 6. SO_4^{2-} rejection at three added doses of sulfate in seawater.

can be explained with respect to the electrostatic interactions between the two ions and the negatively charged membrane along with the size difference between the two ions.

The hydrated radius of Cl^- is 0.195 and 0.300 nm for SO_4^{2-}.[10,11] Hence, the rejection of divalent SO_4^{2-} will be higher than that of monovalent Cl^-. This effect can also be explained in terms of electroneutrality. When the SO_4^{2-} concentration is increased in solution as a result of the higher hydrated radius, SO_4^{2-} is preferably rejected. To maintain charge balance on the feed side, Cl^- will pass through the membrane. Increased permeation of Cl^- over divalent ions is preferred for smart water production in carbonates because it results in a low Cl^- concentration in the retentate.

Figure 7 demonstrates the rejection of Mg^{2+} with normal seawater and with an increased SO_4^{2-} concentration. This is

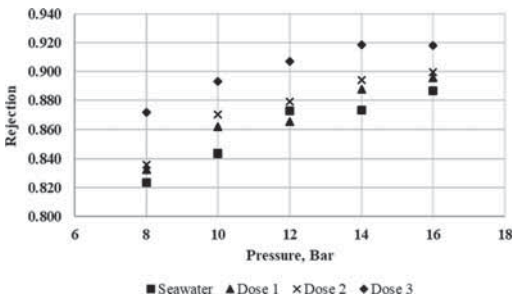

Figure 7. Mg^{2+} rejection with increased SO_4^{2-} concentrations.

contrary to the results for chloride shown in Figure 5 and is explained by the interaction between ions and the membrane. The negatively charged NF membrane attracts divalent positively charged Mg^{2+}, and therefore, the rejection of Mg^{2+} is lower than that of SO_4^{2-}. The hydrated radius for both Mg^{2+} and SO_4^{2-} is 300 nm.[10,11]

Figure 8 shows the rejection of calcium with different doses of Na^+ in the feed when Na_2SO_4 was added in seawater.

Similarly, negative ion rejection is often observed during NF membrane separation of mixed ion solutions.[12] Smart water for carbonates should contain a higher Mg^{2+} concentration compared to seawater. Hence, experiments were performed by adding $MgCl_2$ in feed seawater. Figure 9 shows the effect of an increased $MgCl_2$ concentration on flux. The result is

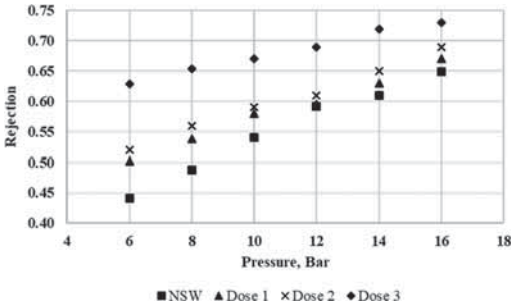

Figure 8. Observed Ca^{2+} rejection with a corresponding increase in the Na^+ concentration.

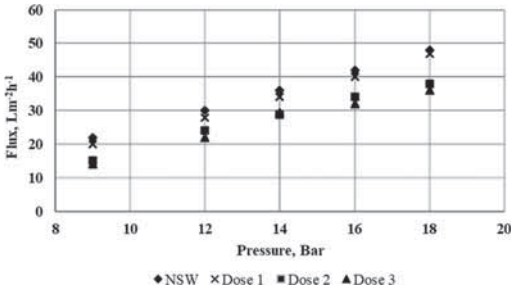

Figure 9. Comparing flux versus pressure for seawater and seawater spiked with $MgCl_2$.

comparable to Figure 4, where flux decreased with an increase in the feed concentration. Similar results were obtained with the addition of $MgSO_4$ to seawater.

Figure 9 confirms that, even though flux decreased with an increased concentration of ions in feed, individual flux shows a linear increase in pressure. This confirms that spiking of chemicals did not initiate membrane fouling.

Figure 10 displays rejection of Na^+ when Mg^{2+} is increased in the feed. The monovalent ion rejections, especially the Na^+ rejection, indicate a negative rejection with an increase of $MgCl_2$ in the feed.

The negative rejection of Na^+ could be due to increased Mg^{2+} concentrations. In an electrolyte mixture, negative

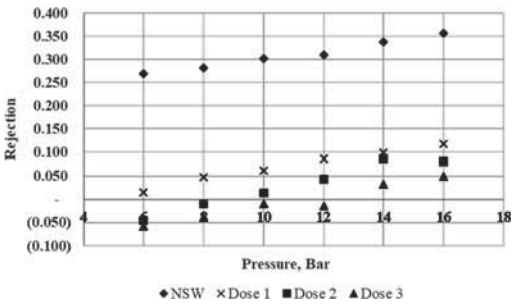

Figure 10. Negative rejection of Na^+ with increased Mg^{2+} in the bulk phase.

DOI: 10.1021/acs.energyfuels.8b00447
Energy Fuels 2018, 32, 4988−4995

rejection is more pronounced for single-charge ions when the augmented number of ions of higher and identical charge is present.[12] Negative ion rejection mainly occurs when ion concentrations in permeate are higher than in the feed solution. When the Mg^{2+} concentration in the feed seawater (51 mM) was increased to 90 mM (dose 1) and further to 110 mM (dose2) and 130 mM (dose 3), more Na^+ ions permeated through the membrane. Mg^{2+} is attracted by the negatively charged membrane, and to maintain the membrane phase electrically neutral, more mobile ions of the same charge permeate, increasing its concentration in the permeate compared to the bulk phase. This phenomenon was observed only at lower pressures, as noted from Figure 10. The rejection of Na^+ was changed to positive at higher flow rates or with an increase in the pressure. According to Figure 10, negative rejection occurred when the Mg^{2+} concentration was increased to 110 and 130 mM. At 6 bar, the rejection was −0.045 for dose 2 and −0.059 for dose 3.

However, no negative rejection was observed for Cl^- ions. Cl^- rejection was decreased when the Mg^{2+} concentration was increased, and there was no difference in Cl^- rejection with a further increase in the Mg^{2+} concentration (Figure 11). At 6 bar, Cl^- rejection with seawater as feed was 0.34, whereas for all other doses, the Cl^- rejection was 0.18−0.19. This confirms that negative rejection occurs for more mobile monovalent ions having the same charge as the ion with an increased concentration in the bulk.

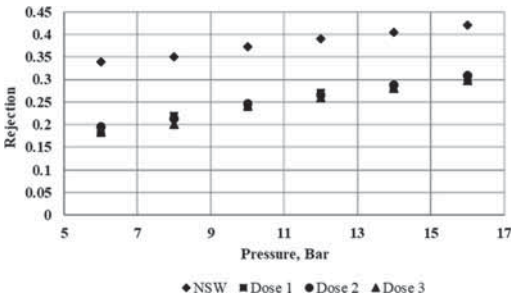

Figure 11. Rejection of Cl^- with an increased Mg^{2+} concentration in the bulk phase.

The calcium concentration was similarly increased from 9.3 mM in seawater to 20 mM (dose 1) and to 30 and 40 mM (doses 2 and 3). Calcium chloride dihydrate was used to spike the Ca^{2+} concentration in seawater. The increase in flux with pressure showed similar results to Figures 4 and 9, a decrease in flux with an increase in the Ca^{2+} concentration.

Figure 12 shows the rejection of Cl^- and Na^+ with different doses of Ca^{2+} at 8 bar. The experimental results in Figure 8 show that the observed rejection of Ca^{2+} increased with an increase of Na^+ in the feed, while Figure 12 shows that rejection of Na^+ decreased with an increase in the Ca^{2+} concentration in the feed. The Na^+ concentration was increased when SO_4^{2-} was spiked with Na_2SO_4. An explanation for the preferential permeation of Na^+ is that the repulsion forces by the negatively charged NF membrane are weak on the cation (Na^+), with lower charge density and Stokes radius (0.184 nm) for Na^+ compared to Ca^{2+}.[13]

Increased ion concentrations confirm that the total feed concentrations and individual ion fractions are important

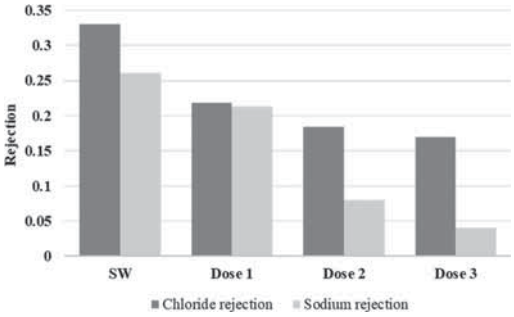

Figure 12. Rejection of Cl^- and Na^+ at 8 bar with different Ca^{2+} concentrations.

parameters affecting rejection of ions and flux through NF membranes. It was confirmed that the proportion of ions in the feed and interaction of electric charges of ions and membrane surface influenced the rejection of specific ions. Numerous reports[14−16] show that, with an increasing feed ion concentration, the effect of membrane charge on ion separation decreases to a minimum as a result of a decrease in the electrical double layer at the membrane surface. This results in the prominent influence of size exclusion and steric hindrance on ion separation compared to Donnan equilibrium. According to the electric double-layer hypothesis, when a charged surface is in contact with an electrolyte solution, an electrical double layer consisting of charged counterions forms at the solid−liquid interface, and this layer effectively shields the NF membrane net charge or neutralizes the membrane charge.[17] This condition results in decreased water flux and decreased retention of monovalent ions.

Seawater is the only freely accessible source of water in offshore environments. Analyzing the membrane properties with respect to the interaction of an ion and the membrane helps in designing a selective seawater ion tailoring technology to meet the injection water chemistry appropriate to a specific reservoir.

From the results obtained, it is confirmed that the addition of chemicals to feedwater influenced membrane performance regarding flux and rejection of ions. Smart water should have 2−3 times increased concentrations of SO_4^{2-} or Ca^{2+} compared to seawater and decreased concentrations of monovalent ions (Na^+ and Cl^-). Spiking of Na_2SO_4, $MgCl_2$, and $CaCl_2$ to feed seawater resulted in (a) decreased retention of Na^+ and Cl^- in the reject, as confirmed by Figures 5, 10, 11, and 12. (b) Resultant flux decreased when chemicals were spiked in seawater (Figures 4 and 9). This leads to an increased retentate flow rate, which is ideal for smart water production in carbonates. (c) Spiking Na_2SO_4 in seawater resulted in increased Mg^{2+} and Ca^{2+} retention, as shown in Figures 7 and 8. Hence, it is important to select proper membranes for specific applications while allowing for the desirable ionic composition causing no membrane fouling, yielding high water recovery.

The results confirm that spiking chemicals in feedwater for smart water production in carbonates are preferred over adding chemicals directly to the retentate because the addition of divalent ions in feed resulted in increased permeation of monovalent ions.

DOI: 10.1021/acs.energyfuels.8b00447
Energy Fuels 2018, 32, 4988−4995

3.4. Power Consumption Analysis. All flow rates and concentrations considered in the calculations were based on experimental results on NANO-SW-2540. NF membranes are suitable for smart water production for carbonates.[18] NF and RO in parallel are suitable for smart water production in sandstones. The efficiency of the pump is assumed to be 80%. The experiments were conducted at room temperature. The NF and RO membranes in Figure 13 operate at 16 and 55 bar, respectively.

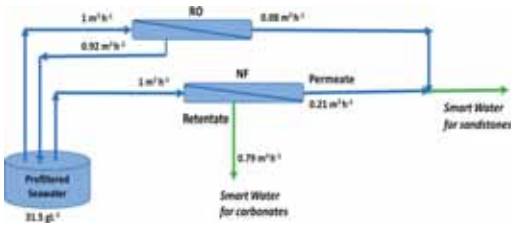

Figure 13. Suggested schematic for smart water production in carbonate and sandstone reservoirs.

Pre-filtered seawater at 1 $m^3\ h^{-1}$ is feed to a NF membrane, resulting in two streams with different ionic compositions. The permeate is rich in monovalent ions (TDS of 20 800−21 000 mg L^{-1}) suitable for sandstones after dilution, whereas the retentate is rich in divalent ions, such as SO_4^{2-}, Ca^{2+}, and Mg^{2+}, and, therefore, suitable for carbonates. TDS in retentate depends upon the pore size and charge of the chosen NF membrane, applied pressure, and temperature.

For sandstone reservoirs, smart water should be low in divalent ions, with TDS less than 5000 mg L^{-1}. TDS in NF permeate with seawater as feed is 21 000 mg L^{-1} and should be diluted with low-TDS water for sandstone applications. A RO membrane is used in parallel to dilute the stream. RO retentate, rich in mono- and divalent ions, can be recirculated to the feed tank.

Table 3 shows power consumption for smart water production by NF and RO for both carbonate and sandstone reservoirs, with flow rates shown in Figure 13. Total power consumed is calculated using eq 10.

Table 3. Power Consumed for Smart Water Production in Carbonate and Sandstone Reservoirs

total smart water produced for carbonates ($m^3\ h^{-1}$)	0.79
total smart water produced for sandstones ($m^3\ h^{-1}$)	0.29
power consumed per m^3 of smart water produced for carbonates (kWh m^{-3})	0.70
power consumed per m^3 of smart water produced for sandstones (kWh m^{-3})	5.21

$$\text{power (W)} = \frac{\text{feed flow rate}\left(\frac{m^3}{s}\right) \times \text{feed pressure (Pa)}}{\text{efficiency } \eta\ (\%)} \quad (10)$$

Power consumed for smart water production in sandstones is higher than that for carbonates in Table 3 as a result of a higher operating pressure for the RO membrane. With an energy recovery factor of 50% for a RO membrane, 50% of the required energy for the feed pump is recovered from the retentate stream. The RO membrane, studied in the process schematic in Figure 13, has 8% permeate recovery, i.e., the ratio of the permeate flow rate to the feed flow rate. The RO permeate flow rate can be increased by selecting an alternative RO membrane with higher recovery. However, TDS in smart water must be formulated with respect to reservoir requirements.

4. CONCLUSION

This research confirms that water with a desired ionic strength, rich in divalent ions or with a desired monovalent/divalent ion ratio, can be custom-made with the investigated technology for smart water flooding applications in both carbonate and sandstone reservoirs. The retentate from a NF membrane can produce smart water for carbonates, while a combination of NF permeate and RO permeate is proposed for tailoring smart water in sandstones.

On the basis of the experiments performed, it is concluded that flux decreased with increasing feed concentrations. This is beneficial for carbonates because reduced flux results in an increased retentate flow rate, with more water used for smart water production. Spiking of chemicals to feedwater for smart water production in carbonates is preferred over adding chemicals directly to the retentate because the addition of divalent ions in feed resulted in increased permeation of monovalent ions. Measured rejections showed a decrease in retention of monovalent ions to negative values, whereas the divalent ions showed a constant or slightly increasing retention when feed concentrations were changed. Rejection of Ca^{2+} increased with an increase of Na^+ concentrations in feed, whereas rejection of Na^+ decreased with an increase of Ca^{2+} concentrations in the feed. Power consumed for smart water production in carbonates is lower than that for sandstones, at 0.70 and 5.21 kWh m^{-3}, respectively.

AUTHOR INFORMATION

Corresponding Author

*Telephone: +47-96816575. E-mail: remya.nair@uis.no.

ORCID

Remya R. Nair: 0000-0001-6102-5031

Notes

The authors declare no competing financial interest.

ACKNOWLEDGMENTS

The authors acknowledge the Research Council of Norway and the industry partners ConocoPhillips Skandinavia AS, Aker BP ASA, Eni Norge AS, Maersk Oil Norway AS, Statoil Petroleum AS, Neptune Energy Norge AS, Lundin Norway AS, Halliburton AS, Schlumberger Norge AS, Wintershall Norge AS, and DEA Norge AS of the National IOR Centre of Norway for support.

NOMENCLATURE

NF = nanofiltration
RO = reverse osmosis
EOR = enhanced oil recovery
TDS = total dissolved solids
MWCO = molecular weight cutoff
TCD = thermocompression distillation
MED = multi-effect distillation
MVC = mechanical vapor compression
MSF = multi-stage flash

DOI: 10.1021/acs.energyfuels.8b00447
Energy Fuels 2018, 32, 4988−4995

IC = ion chromatography

REFERENCES

(1) Austad, T. Water based EOR in carbonates and sandstone: New chemical understanding of the EOR-potential using "smart water". In *Enhanced Oil Recovery Field Case Studies*; Sheng, J., Ed.; Gulf Professional Publishing: Houston, TX, 2013; pp 301−335, DOI: 10.1016/B978-0-12-386545-8.00013-0.

(2) Fathi, J. S.; Austad, T.; Strand, S. Smart water as a wettability modifier in chalk: The effect of salinity and ionic composition. *Energy Fuels* **2010**, *24*, 2514−2519.

(3) Al-Karaghouli, A.; Kazmerski, L. L. Energy consumption and water production cost of conventional and renewable-energy-powered desalination processes. *Renewable Sustainable Energy Rev.* **2013**, *24*, 343−356.

(4) Cheryan, M. *Ultrafiltration and Microfiltration Handbook*; CRC Press: Boca Raton, FL, 1998.

(5) Chaufer, B.; Rabiller-Baudry, M.; Guihard, L.; Daufin, G. Retention of ions in nanofiltration at various ionic strength. *Desalination* **1996**, *104*, 37−46.

(6) Schaep, J.; Vandecasteele, C.; Mohammad, W.; Bowen, R. Modelling the retention of ionic components for different nanofiltration membranes. *Sep. Purif. Technol.* **2001**, *22*−*23*, 169−179.

(7) Van der Bruggen, B.; Schaep, J.; Wilms, D.; Vandecasteele, C. Influence of molecular size, polarity and charge on the retention of organic molecules by nanofiltration. *J. Membr. Sci.* **1999**, *156*, 29−41.

(8) Donnan, F. G. Theory of membrane equilibria and membrane potentials in the presence of non-dialysing electrolytes. A contribution to physical-chemical physiology. *J. Membr. Sci.* **1995**, *100*, 45−55.

(9) Manttari, M.; Pihlajamaki, A.; Nystrom, M. Effect of pH on hydrophilicity and charge and their effect on the filtration efficiency of NF membranes at different pH. *J. Membr. Sci.* **2006**, *280*, 311−320.

(10) Tansel, B.; Sager, J.; Rector, T.; Garland, J.; Strayer, R. F.; Levine, L.; Roberts, M.; Hummerick, M.; Bauer, J. Significance of hydrated radius and hydration shells on ionic permeability during nanofiltration in dead end and cross flow modes. *Sep. Purif. Technol.* **2006**, *51*, 40−47.

(11) Tansel, B. Significance of thermodynamic and physical characteristics on permeation of ions during membrane separation: Hydrated radius, hydration free energy and viscous effects. *Sep. Purif. Technol.* **2012**, *86*, 119−126.

(12) Yaroshchuk, A. E. Negative rejection of ions in pressure-driven membrane processes. *Adv. Colloid Interface Sci.* **2008**, *139*, 150−173.

(13) Hussain, A.; Nataraj, S.; Abashar, M.; Al-Mutaz, I.; Aminabhavi, T. Prediction of physical properties of nanofiltration membranes using experiment and theoretical models. *J. Membr. Sci.* **2008**, *310*, 321−336.

(14) Schaep, J.; Vandecasteele, C. Evaluating the charge of nanofiltration membranes. *J. Membr. Sci.* **2001**, *188*, 129−136.

(15) Wang, X. L.; Wang, W. N.; Wang, D. X. Experimental investigation on separation performance of nanofiltration membranes for inorganic electrolyte solutions. *Desalination* **2002**, *145*, 115−122.

(16) Wang, D.-X.; Su, M.; Yu, Z.-Y.; Wang, X.-L.; Ando, M.; Shintani, T. Separation performance of a nanofiltration membrane influenced by species and concentration of ions. *Desalination* **2005**, *175*, 219−225.

(17) Vezzani, D.; Bandini, S. Donnan equilibrium and dielectric exclusion for characterization of nanofiltration membranes. *Desalination* **2002**, *149*, 477−483.

(18) Nair, R.; Protasova, E.; Strand, S.; Bilstad, T. Produced water treatment with membranes for enhanced oil recovery in carbonates and sandstone reservoirs. *Proceedings of IOR 2017—19th European Symposium on Improved Oil Recovery*; Stavanger, Norway, April 24−27, 2017; DOI: 10.3997/2214-4609.201700296.

DOI: 10.1021/acs.energyfuels.8b00447
Energy Fuels 2018, 32, 4988−4995

Appendix 2 – Paper II

Paper II

Evaluation of Nanofiltration Membranes for Smart Water Production in Carbonate Reservoirs from De-Oiled Produced Water and Seawater

Remya Ravindran Nair, Evgenia Protasova, Skule Strand, Torleiv Bilstad

SPE Productions and Operations (Under Review)

SPE-181588-MS

Evaluation of Nanofiltration Membrane Process for Smart Water Production in Carbonate Reservoirs from De-oiled Produced Water and Seawater

Remya Ravindran Nair, Evgenia Protasova, Torleiv Bilstad, Department of Chemistry, Bioscience and Environmental Engineering, Skule Strand, Department of Energy and Petroleum Engineering, University of Stavanger, 4036 Stavanger, Norway

This paper was prepared for presentation at the SPE Annual Technical Conference and Exhibition held in Dubai, UAE, 26–28 September 2016.

Abstract

This research focuses on membrane separation efficiencies by adjusting the ionic composition of de-oiled produced water (PW) and evaluates the possibility for *Smart Water* production from PW for enhanced oil recovery (EOR) in carbonate reservoirs. Key characteristics of *Smart Water* for carbonate reservoirs are increased concentrations of divalent ions and low concentrations of monovalent ions compared with seawater.

In this research, PW was pretreated with media filters, which resulted in 96 - 98 % oil removal. This de-oiled PW was used as feed for nanofiltration (NF) membranes. Combinations of NF retentate with seawater as feed and NF permeate from PW were considered. PW NF permeate, mixed with seawater spiked with multivalent ions, sulfate or phosphate, is expected to alter wettability of oil reservoirs.

NF membrane performance was evaluated in terms of flux and separation efficiencies of key scaling ions, calcium and barium. The tested membranes removed 60 % of Ca^{2+} and 53 % of Ba^{2+} thereby reducing the scaling tendency. No membrane fouling was observed during the experiments.

NF treated PW was analyzed for solubility of $CaCO_3$. The results showed no calcium dissolution, which could affect chalk reservoir compaction. This research also reflects the use of non-precipitating phosphate for *Smart Water* production from seawater, simultaneously decreasing barium concentration and scaling potential of PW. Results obtained conclude that spiking phosphate below 12 mM showed no indication of chalk dissolution during equilibration tests at room temperature. Experiments performed with 44 mM of phosphate resulted in calcium phosphate precipitation.

A process scheme is proposed for *Smart Water* production by ionic selection from seawater and PW at an operating pressure of 18 bar. Energy consumption analysis for *Smart Water* production prior to membrane treatment concluded NF to be economic over other desalination technologies. Power consumed by NF membranes for *Smart Water* production at 18 bar is calculated at 0.88 kWh/m^3 whereas the power consumed is 51.22 kWh/m^3 and 103.52 kWh/m^3 for reverse osmosis (RO) and multistage flash distillation (MSF).

Keywords: Produced Water, Nanofiltration, *Smart Water*, Phosphate, Scaling, Barium

Introduction

PW is one of the major waste streams from the oil and gas industry and should be managed in an environmentally sustainable manner. PW treatment is concerned with contaminants such as solids and residual oil, together with production chemicals. The current water/oil ratio in oil production is 2:1 to 3:1 worldwide. Onshore treatment costs of PW from the North Sea differ from 0.19 USD/barrel to 3.40 USD/barrel of PW (Duhon, 2012). Assigning a proper water treatment facility for the lifetime of a well is a challenge. Proper characterization of PW is necessary to ensure an optimal treatment process. Discharge, reinjection and reuse are available handling options. However, to reduce emissions, stringent guidelines are imposed by regulatory agencies. In Norway, the maximum allowable oil in water is 30 mg/L for ocean discharge (Norwegian Oil and Gas Industry, 2015). Reinjecting PW is considered a suitable alternative with environmental benefits.

PW composition is complex and varies with reservoir conditions. The components originate from formation water, injected water and chemicals used during oil production. This includes dispersed and dissolved organic compounds, and inorganic compounds including heavy metals, salts and naturally occurring radioactive materials (Norwegian Oil and Gas industry, 2016). The relative significance of each component depends on requirements concerning disposal and discharge and their environmental impact. The concentration of oil in water is the focus of environmental monitoring and design of separation technologies. Reuse of PW requires skillful planning and treatment to reach the quality required for reinjection and to avoid formation damage.

Reinjection of PW for pressure support in reservoirs or as a source of *Smart Water* is an example of converting waste to a resource. Reusing PW reduces environmental risks and negates the need for alternative water sources in environmentally sensitive areas.

Produced Water and Smart Water

Global PW volumes have increased over the last decade and are expected to surge further. The oil and gas industry need to recycle PW for use in stimulation of production i.e., water floods, polymer floods, steam floods etc.

PW for *Smart Water* production requires TDS reduction, removal of heavy metals, oil, and barium ions. Selecting optimal technologies for PW treatment depends on end use; discharge to sea, reinjection for pressure support or as *Smart Water*. The technologies include dual media filtration, membrane separation, hydrocyclones, flotation, skim tanks etc. However, there are several problems that must be accounted for during reinjection including (Statoil, 2017):

- Loss of injectivity
- Uncontrolled fracture growth
- Corrosion
- Scaling
- Reservoir souring
- Erosion.

PW reinjection is only possible if the water is compatible with formation water in the reservoir. Membrane separation could be used for manipulating the ionic composition of water (Nair, et al., 2018; Bilstad, et al., 2015). In this research, NF is considered to be used downstream of oil removal technologies. Diluted oil-free PW treated with NF can be used as *Smart Water* in carbonate reservoirs without any additional steps. In carbonate reservoirs, seawater already behaves as *Smart Water*. Seawater could be made even smarter by modifying the ionic composition (Austad, 2013).

The initial wetting established in the reservoir between pore surface minerals, crude oil and formation water (FW) could be disturbed when injection brine has a different ion composition (Strand, et al., 2006).

Smart Water injection facilitates wettability alteration towards more water wet conditions. *Smart Water* modifies the reservoirs wetting by improving the capillary forces that increases the microscopic sweep efficiency and auguments oil recovery. The ionic modification of seawater includes reducing monovalent and increasing divalent ion concentrations. Seawater with reduced concentrations of Na^+ and Cl^- and spiked with sulfate resulted in enhanced oil recovery by 40 % of original oil in place (OOIP) compared to normal seawater (Austad, 2013). According to Gupta, et.al. (2011) seawater without sulfate but spiked with phosphate also could behave as *Smart Water*.

Smart Water could be produced by adding salts to fresh or low salinity water produced by RO or flash distillation. Therefore, using de-oiled PW as feed to NF will reduce power consumption, footprint and use of chemicals. NF will also remove scale-causing ions from PW and NF permeate can be reinjected into reservoirs as *Smart Water*.

The objectives of this research are to evaluate:

- Ion separation efficiency of membranes for adjusting the ionic composition of de-oiled PW
- The efficiency of media filtration for oil removal from PW as pre-treatment to NF membranes
- The feasibility of using nanofiltration (NF) membranes for treatment of oil-free diluted PW combined with seawater NF retentate for EOR
- The effect of spiking phosphate in *Smart Water* to reduce chalk dissolution
- Assess power consumption for production of *Smart Water* from PW.

Theoretical Aspects

Challenges of Seawater and PW Co-Injection

A main challenge with seawater and PW co-injection is possible scale formation from the interaction between sulfate ions in seawater and barium ions in PW. Typical barium concentrations for the North Sea oil fields are 10 – 200 mg/L. At *South* and *Central Brae* oil fields, barium concentration varies between 800 and 2500 mg/L with depth (Frenier & Ziauddin, 2008). To avoid scale formation, oil production at the *Central Brae* field was supported by injecting low sulfate seawater. NF treatment achieves 97 % sulfate rejection. Injected low sulfate brine has low scaling potential when mixed with formation water and significantly reduces the use of scale inhibitors (Heatherly, et al., 1994).

The volume of PW will continuously increase during water flooding of an oil field. Because of established zero discharge strategy (Norwegian Oil and Gas, 2014) the operating companies in the North Sea are obliged to treat PW before discharge. The separation methods are expensive, and it is of interest to reinject PW into reservoirs. According to Bader (2006) sulfate must be removed to avoid scaling. However, sulfate is the most important wettability alteration parameter in chalk reservoirs and SO_4^{2-} removal will have an adverse effect on EOR. A promising solution is to co-inject divalent ion-rich *Smart Water* and barium-free PW. This process is environmentally friendly and augments oil recovery by wettability alteration of chalk surfaces.

Previous experiments (Puntervold, 2008) were performed by mixing synthetic seawater (SSW) and PW. Table 1 shows the molar compositions of SSW and PW and mixtures used for the experiments linked to Tor field. The results showed that EOR is possible when mixtures of PW and seawater are injected into chalk reservoirs. Nevertheless, Puntervold's experiments confirmed that presence of sulfate was crucial for wettability modification at temperatures greater than 100℃. Figure 1 shows oil recovery when PW, PW1SSW1 (combination of 1- part PW and 1-part SSW), PW1SSW2 (1- part PW and 2- parts SSW), PW1SSW8 (1- part PW and 8- parts SSW) and forced imbibition (FI) were injected into chalk cores. The experiments were performed at 110℃ and the cores were saturated with crude oil having an acid number of 0.70 mg KOH/g oil.

Figure 2 shows $BaSO_4$ precipitation with temperature when SSW and PW were mixed. It is evident that

$BaSO_4$ solubility increases with temperature and is favorable for injection. The reservoir temperature of Tor field is 130℃. According to the brine compositions presented in Table 1, barium and strontium are absent in SSW. Similarly, PW does not contain sulfate. This results in identical curves for PW and SSW in Figure 2.

For co-injection of PW and seawater into the reservoir, it is important to examine the water compatibility to avoid scaling or $CaCO_3$ dissolution. TDS in PW studied in this research is significantly higher than in seawater.

Compaction of Chalk Reservoirs

Various experiments have shown that wettability modification by seawater contributes to compaction in low consolidated chalk during secondary oil recovery, thus resulting in weakening of chalk and loss of production wells. A mechanism of chemical weakening of chalk is defined as a substitution reaction of Ca^{2+} by Mg^{2+} in the presence of SO_4^{2-} (Korsnes, et al., 2008).

When non-equilibrated brine is mixed with $CaCO_3$, chalk dissolution may occur and could be explained by Equations 1 and 2.

$$CaCO_3(s) = Ca^{2+} + CO_3^{2-} \quad (1)$$

$$CO_3^{2-} + H_2O = HCO_3^- + OH^- \quad (2)$$

PW has higher Ca^{2+} concentration than seawater and a mix of this PW and seawater will reduce $CaCO_3$ dissolution. Chalk dissolution increases the concentration of Ca^{2+} in the brine. A PW-seawater mixture with low calcium concentration may initiate $CaCO_3$ dissolution and promote chemical weakening or compaction of chalk.

There is a possibility that replacing sulfate with phosphate might reduce compaction of reservoirs. However, efficiency of phosphate is not well documented especially linked to reservoir temperature and presence of calcium ions. In carbonate reservoirs, Ca^{2+} is always present both in FW and from mineral dissolution ($CaSO_4$/$CaCO_3$) and phosphate will react with Ca^{2+} and precipitate to calcium phosphate. Similarly, limited information is available on PO_4^{3-} interactions with EOR chemicals. Experiments were performed with spiking phosphate in seawater used as feed to NF. Potassium dihydrogen phosphate (KH_2PO_4) with high water solubility is used for spiking phosphate.

Membranes in EOR Applications

NF and RO membranes selectively separate ions from feed water. Cross-flow membrane separation consists of three streams. The feed is driven by pressure over the membrane. The permeate flows through the membrane and has lower TDS compared to the other two streams. The retentate is rejected by the membrane and is concentrated in ions.

NF membranes were used by *Marathon Oil* at *Brae Alpha* field for sulfate removal from seawater to avoid scaling (Heatherly, et al., 1994). NF membranes efficiently remove divalent barium ions from PW resulting in barium-free permeate. Ion separation by NF membranes is based on pore size, porosity and surface charge of the membrane. NF membranes have pore sizes between 0.1 and 1 nm (Cheryan, 1998). Most NF membranes are negatively charged resulting in varying rejection of anions and cations. Ion rejection depends on initial ion concentration, temperature and viscosity of feed. Hydration free energy and Stokes radius of ions similarly influence ion separation. Molecular weight cut-off (MWCO) of a membrane expressed in daltons is another separation property. MWCO is defined as the molecular weight at which 90 % rejection is obtained. The rejection of organic compounds by NF membranes depends on the MWCO. A tight NF membrane has a MWCO of 180 daltons. A loose membrane has a MWCO of 1000 daltons (Wilf, et al., 2007). Compounds with a molecular weight higher than the MWCO of the membrane are rejected. However, separation based on sieving or steric hindrance, electrostatic effect or Donnan exclusion are also common. Flux, ion rejection and permeate recovery of membranes are

important parameters for process optimization. Permeate recovery is important as higher recovery means more PW is available for reuse and less waste is produced.

Equation 3 defines recovery of feed water as permeate.

$$\text{Recovery } \% = \left(\frac{Flow\ rate\ of\ permeate}{Flow\ rate\ of\ feed} \right) * 100 \quad (3)$$

High salt concentrations on the feed side of the membrane, as in PW, results in high osmotic pressure and reduces the available net driving force, consequently reducing the permeate flow.

Fouling of membranes is an obstacle encountered during membrane operations. Fouling occurs in the membrane and will cause pore size reduction by foulants adsorbing on the inner walls of the pores and on the surface of the membrane (Hilal, et al., 2004). Fouling of membranes results in decreased permeate flow. Flux at different pressures is monitored to identify whether fouling occurred during production. Flux is defined as permeate flow rate per unit membrane area.

Oily PW Treatment

Presence of dispersed hydrocarbons in reinjected PW can lead to permeability impairment of the formations (Statoil, 2015). Hence, hydrocarbons should be separated from water before being reinjected into the reservoir. Conventional PW treatment processes include hydrocyclones, flotation, and dual media or nutshell filters. This part of the research is focused on the performance of media filters, which are in common use as pretreatment upstream membranes.

Media Filtration

Usually, a dual media is used for separation of oil in PW. Separation of hydrocarbons is performed by introducing a medium through which water, minute carbon particles and traces of oil can pass. Filtration retains particles that are incapable of following the tortuous channels of the filter media. The media filters are operated with a combination of downward or upward fluid flow; the former used for oil separation and the latter used for backwashing.

During filtration with activated carbon, the oil is adsorbed onto the surface of the media particles. The mechanisms involved in separation include (Ruston, et al., 2000):

- Van der Waals or London force of attraction
- Direct collision
- Surface charge attraction/repulsion
- Diffusion.

Activated carbon filters can also remove some water soluble organics when compared to nutshell filters. A main disadvantage of media filtration is that over time, the bed becomes loaded with oil particles and loses its separation efficiencies. Periodic backwashing of filter media needs to be performed to increase the filtration cycle. However, over time, the media should be replaced as media becomes saturated with oil and lose its separation efficiency even with backwashing.

Experiments and Methods

Synthetic PW treatment included two stages. The first stage was media filtration for oil removal. The second stage consisted of NF membrane treatment of oil-free PW. For the first stage, synthetic PW was prepared by mixing crude oil from Ekofisk and permeate from NF with seawater as feed. The crude oil from Ekofisk has a density of 0.83 g/cc at 15 °C with an API gravity of 38.9 ((Statoil, 2015).

Mixing was performed at six different concentrations (0.1, 0.2, 0.3, 1, 2 and 3 mL oil /L in seawater) at 19000 rpm using *Polytron PT 300* mixer from *Kinematica*. Three trials were performed for each

concentration. Turbidity, conductivity, TDS, and salinity were measured for each feed and effluent using *HACH 2100N* turbidimeter and TDS meter *VWR collection CO3100N*. Turbidity was measured in Nephelometric Turbidity Units (NTU). During the second stage of experiments, oil-free PW was used for NF separation. Compositions of formation water, PW from Tor field (Ekofisk reservoir) and diluted PW used for the experiments are compared with seawater composition in Table 1 (Puntervold & Austad, 2007). Concentration of barium in synthetic PW was increased approximately 40 times the actual concentration in PW of the Tor field.

TDS of Tor field PW was as high as 110,000 mg/L (Puntervold & Austad, 2007). Therefore, diluted brine with approximately 1:3.5 dilution ratio was tested. NF permeate using seawater as feed was used for dilution. The dilution was performed with respect to total TDS and not to individual ion concentrations. Ion Chromatography (IC) using *Dionex ICS-5000*$^{+}$ DP was used to analyze ion concentrations.

The overall liquid and mass balance throughout membrane separation was examined using Equation 4.

$$m_f \times X_f = m_r \times X_r + m_p \times X_p \quad (4)$$

where

m_f is the mass of feed, X_f is the feed flow rate, m_r is the mass of retentate, X_r is the retentate flow rate, X_p is the permeate flow rate and m_p is the permeate mass.

Media Filters

A lab-scale media filtration unit for oil removal was tested for hydrocarbon removal efficiency. The media filtration unit (Figure 3) consisted of anthracite and activated carbon. The unit was designed and constructed at the University of Stavanger with a height of 120 cm and diameter of 25 cm. Pebbles were placed at the bottom of the unit for support. Middle layer consisted of powdered activated carbon with a bed depth of 35 cm and the top layer of 15 cm anthracite. Backwashing of the unit was performed using a 350 W pump with a maximum flow rate of 2500 L/h after each experiment.

Hydrocarbon removal efficiency E_{oil} (%) was calculated in this experiment using Equation 5.

$$E_{oil} = (1-C_p/C_f) \times 100 \quad (5)$$

where

C_p is the concentration of permeate and C_f is the concentration of feed.

The major concern with PW treatment by membranes is fouling by organic compounds. Media filtration was used in this research to obtain realistic data under experimental conditions with oil-free PW samples for treatment with NF membranes. The feed oil concentration was 839 mg/L, higher than compared to effluent obtained from primary and secondary oil separation on a platform. This increased concentration was selected to investigate media filter bed separation efficiency and the oil-fouling tendency of NF membranes if traces of oil is present in feed water. Usually, for an activated carbon filter, the inlet oil concentration is 5-10 mg/L (Statoil, 2017). Alternatively, other oil removal technologies could be used instead of media filters to treat oily PW as pretreatment to NF membranes. The effluent stream from filtration unit was analyzed using *Infrared (IR) Spectroscopy Cary 630 FTIR* from Agilent Technologies.

Extraction of Oil

Oil from synthetic PW and effluent samples from media filtration were extracted with cyclohexane (C_6H_{12}). Process calibration and results of ASTM D7678-11 method correlate to ASTM D3921, D7066, ISO 9377-2, and EPA 1664. These methods are part of the OSPAR agreement 2005 for determination of dispersed oil content in PW (OSPAR Commission, 2005-2015). Extraction with cyclohexane was performed in accordance with ASTM D7678-11 and ASTM D7678-17 procedure described below (ASTM D7678-17, 2017):

- 900 mL of each sample was added to 50 mL of cyclohexane. The samples were shaken for 2 minutes.
- The solution was kept for phase separation for 2 minutes.
- Distilled water was added to this solution until the oil layer reached the top of the bottle, where it was removed with a syringe into a clean vial.
- 2 g of sodium sulfate (Na_2SO_4, drying agent) and 2 g Florisil were added to the vial for cleanup of extracted oil, shaken for 2 minutes and then settle for 5 minutes.
- A 0.45-micron nylon syringe filter of 17 mm diameter was used to filtrate the oil containing cyclohexane into a new vial. Further cleaned up samples were used for IR analysis.

The extraction and analysis of the samples were performed within an hour on non-acidified samples. Preservation of the samples with sulfuric acid or hydrochloric acid to pH 2 and refrigeration is required if samples has to be preserved until extraction (ASTM D7678-17, 2017).

The nominal total oil and grease (TOG) is the hydrocarbon value before clean up, while the total petroleum hydrocarbon (TPH) is measured once the extract is filtered with Florisil (ASTM D7678-17, 2017).

Organic Compound Analysis

IR Spectrometer was used to measure oil content in water. *Fourier Transform Infrared (FTIR)* liquid-liquid extraction was used to analyze aromatics, short-chain, as well as the heavier long chain hydrocarbons.

FTIR measured the methyl group absorbance at wavelengths of 1370 – 1380 cm^{-1} present in the hydrocarbons and lighter aromatics in crude oil, toluene, xylenes, and ethylbenzene. Generally, hydrocarbons containing a methyl group are absorbed at a wavelength of 1378 cm^{-1}. Cyclohexane has no methyl groups and thus is a suitable solvent for this analysis. The IR spectrum of cyclohexane has no absorbance at 1378 cm^{-1}. The oil collected in the cyclohexane during extraction will add to the absorbance at 1378 cm^{-1}. This increase of absorbance is proportional to the concentration of oil and was precisely calibrated using *MicroLab Quant* calibration software (Seelenbinder & Mainali, 2015).

A calibration curve was designed to determine the concentrations of unknown samples. The known concentrations included 0.1 mL/L, 0.2 mL/L, 0.3 mL/L, 0.4 mL/L, 0.5 mL/L and 0.6 mL/L oil in cyclohexane. The results obtained were plotted against absorbance or peak heights. The concentrations of unknown samples were compared to the reference calibration curve.

NF Membranes

An objective of the membrane experiments was to evaluate the ion separation efficiency, flux and permeate recovery by NF membranes. Membrane experiments were performed using diluted synthetic PW of two types; effluent from media treatment and brine with Ba^{2+}. Ion separation was performed with two composite polyamide membranes, NANO-SW-2540 and NF270-2540 with membrane areas of 2.3 m^2 and 2.6 m^2, respectively. The main characteristics of these membranes are presented in Table 2. Two filters with 20 μ and 5 μ pore size were used for pre-treatment upstream of the membranes. Membranes were washed with tap water after each experiment to prevent accumulation of any scaling ions. Membrane water permeability decreases and salt passage increase with time. The membrane performance also deteriorates due to fouling on the membrane surface, presence of abrasive particles in the feed and exposure to cleaning chemicals with extreme pH. If membrane fouls, the flux either will decrease or stay constant with increase in pressure. Alkaline cleaning of the membrane at proper intervals is recommended to prevent organic fouling and to increase membrane life especially when oil-free PW is used as feed.

Seawater spiked with phosphate was tested to improve ion separation and achieving optimal injection water quality for *Smart Water*. Three different chemicals containing phosphate were used; disodium phosphate (Na_2HPO_4), dipotassium phosphate (K_2HPO_4) and potassium dihydrogen phosphate (KH_2PO_4).

The phosphate chemicals were added to seawater and thus the NF feed contained both sulfate and phosphate, contrary to the brine suggested by Gupta (2011). Three trials for every chemical at different doses were performed. It was observed that Na_2HPO_4 and K_2HPO_4 have lower solubility in seawater than KH_2PO_4. Thus, KH_2PO_4 was chosen for further experiments and the dose was increased up to 50 mM without any precipitation in seawater.

Solubility of Chalk in Brines

PW is only a part of the total volume of *Smart Water* injected. The compatibility of barium free PW permeate on calcium carbonate was tested. It was required to verify the solubility of phosphate in brines equilibrated with $CaCO_3$. Calcium carbonate with a molecular weight of 100.09 g/mol was used for the experiments. NF seawater retentate brines with phosphate concentrations of 44 mM, 36 mM, 24 mM and 12 mM were tested. The solubility of $CaCO_3$ mixed with different brines was experimentally verified. A given brine was equilibrated with milled chalk. 10 mL brine was mixed with 2g of $CaCO_3$ for 3 hours at 25 ºC. Equilibration of samples was also performed overnight at 70 ºC. Then the samples were centrifuged by *Damon IEC Model 2K* and the brine composition before and after equilibration was analyzed with IC. Changes in Ca^{2+} concentrations could be linked to $CaCO_3$ dissolution or calcium phosphate precipitation. pH of the solutions was measured using *VWR Phenomenal pH 1100L*.

Results & Discussion

Oily PW Treatment by Media Filtration

Synthetic PW with different oil concentrations was passed through media filters. The influent and effluent samples were extracted with cyclohexane according to ASTM D7678-17 and were analyzed with IR Spectrometer. According to Equation 5, 96 - 98 % hydrocarbon removal efficiency was observed. The oil concentration in the effluent was measured to be between 15-18 mg/L of oil in water for three trials, respectively. Routine cleaning of media filters was required to improve or maintain the performance and prolonged life of the treatment units.
Experiments with media filtration were performed to collect de-oiled water for NF treatment and analyze the efficiency of NF. The experiments were not focused on other aspects of multi media filtration.

Oil-Free PW Treatment by NF Membrane

Based on information provided by membrane manufactures (Dow Water & Process Solutions, n.d.) and other researches (Van der Bruggen, et al., 1999) (Wilf, et al., 2007), it is concluded that a feed with a low concentration of organic compounds can be further treated by NF. The effluent from the media filtration unit was collected and used as feed for NF membrane within an hour to avoid oil/water separation. The maximum applied pressure during the experiments was 18 bar with a feed flow rate of 1050 L/h and a flux of 77 $L/m^2/h$ as shown in Figure 4.

Correlation between flux and pressure was monitored with seawater as feed before and after treating oil-free PW by NF to investigate possible fouling. Flux through a membrane is inversely proportional to fluid viscosity. The flux was lower than that of pure seawater when oil-free PW was used as feed. The flux differences could be due to the presence of minute activated carbon particles in the filter effluent due to attrition. The turbidity of media effluent samples was 2.18 NTU and for seawater was 0.152 NTU. These minute particles would have partially blocked the nanomembrane pores temporarily since the flux retained to its initial values when seawater was used as the feed after PW treatment. The membrane hydraulic permeability did not vary significantly between seawater experiments before and after NF treated PW in Figure 4. Hence, it is concluded that no membrane fouling occurred while oil-free PW was used as feed during an operating time of 4 hours for three trials. However, membrane fouling can occur over time with continuous operation but is not considered in this paper.

Rejection of Major Ions by NF Membranes

Barium and calcium sulfate scaling results when PW is mixed with seawater due to high Ba^{2+} and Ca^{2+} concentrations in PW. Separation of barium and calcium were performed using NF membranes at different pressures using diluted PW. The composition of diluted PW is presented in Table 1.

The permeability of ions through NF membranes has a strong correlation to their hydrated radii. Ions with relatively small crystal radii (Mg^{2+} and Ca^{2+}) have higher hydration free energy and larger hydrated radius. Since these ions hold their hydration shells more strongly, they are effectively retained by membranes (Tansel, et al., 2005). Hydration free energy of Mg^{2+} at -1922 kJ/mol is higher than Ca^{2+} at -1592 kJ/mol (Tansel, 2012) and Ba^{2+} at -1273 kJ/mol (Hill & Holman, 2001). The hydration free energy of Na^{+} and Cl^{-} are -365 KJ/mol and -340 KJ/mol respectively (Tansel, 2012). Ions with lower hydration free energy will easily lose their hydration shell during membrane transport and thus permeate easily. Figure 5 confirms that Mg^{2+} with the highest hydration free energy was rejected the most by the tested membranes followed by Ca^{2+} and Ba^{2+}. The rejection of Na^{+} was lower than Cl^{-} though the hydration free energy of Na^{+} is higher than Cl^{-}. This is explained by the electrostatic attraction of Na^{+} and the negatively charged NF membranes.

The membrane permeate has lower scaling potential allowing mixing with sulfate from untreated seawater. Lower rejection of divalent ions will result in higher divalent ion concentrations in NF permeate which is desirable for *Smart Water*. The rejection of divalent ions by both membranes varies with a change in pressure. Proper membranes must be selected depending on the intended operating pressure for industrial applications.

Recovery for NF Membranes

Important parameters characterizing NF efficiency are flux, ion separation and recovery. Water recovery by a membrane is defined as the ratio of permeate flow rate to feed flow rate. The permeate flow rate depends on membrane pore size, porosity, membrane material, pressure, type of feed and temperature. At constant pressure, an increase in feed concentration results in low permeate flow rate resulting in low recovery. Experiments were performed to measure recovery of NANO-SW-2540 and NF270-2540 with seawater as feed. The recovery was measured at the lowest and highest tested pressures of 9 and 18 bar at 25 ºC. The results concluded that at 9 bar, recovery of NANO-SW-2540 was 11 % higher compared to NF270-2540 with a recovery of 8 %. However, at 18 bar, the recovery was identical (17 %) for both membranes. For *Smart Water* production from PW, a membrane with high recovery at high pressure is recommended.

Fouling of NF membranes

Figure 6 shows an increase in flux with increasing pressure for both membranes. The feed used for both membranes contained barium but no organic compounds. Fouling did not occur during the experiments as indicated by the flux versus pressure graph (Figure 6). The flux obtained at each operating pressure was curve fitted to a linear equation resulting in an R^2 value > 0.99. The membrane hydraulic permeability was determined for each trial and measured as the slope of the linear plot between flux versus ΔP_{TM}. Membrane hydraulic permeability did not vary between trials.

According to specifications of NANO-SW-2540, the maximum operating pressure is 41 bar. Maximum pressure used during the experiments was 18 bar. Flux increased linearly with an increase in pressure from 8 to 18 bar for each trial. When the pressure was reduced, identical fluxes were regenerated i.e., no hysteresis effect.

Solubility Analysis of Chalk with Different Brines

Table 3 shows the results of compatibility analysis of NF permeate with PW as feed after being equilibrated with calcium carbonate. pH and ionic compositions of brines did not change significantly during the experiments, which confirmed that no substantial chalk dissolution occurred. The results confirm that permeate from NF treated PW is compatible with calcium carbonate. A change in ionic

composition would have occurred if the brine were not compatible with $CaCO_3$.

Table 4 summarizes the compatibility analysis of *Smart Water* brines containing 12 mM and 44 mM KH_2PO_4 after equilibration with calcium carbonate. Equilibration was also performed at 24 mM and 36 mM PO_4^{3-} concentrations.

At 12 mM PO_4^{3-}, no changes in PO_4^{3-} and SO_4^{2-} concentrations were observed, confirming that both ions are stable in solution with $CaCO_3$. No major changes in concentrations were observed for other ions. The change in pH was negligible at 12 mM phosphate.

Smart Water brine containing 44 mM of KH_2PO_4 had an initial pH of 4.99 and increased to 5.64 after $CaCO_3$ equilibration. It is observed in Table 4 that there is no change in Cl^-, Na^+, Mg^{2+}, and SO_4^{2-} concentrations. However, significant reductions in Ca^{2+} and PO_4^{3-} concentrations were observed. The calcium concentration was reduced from 11.1 mM to 4.4 mM and the phosphate concentration was reduced from 44 mM to 28.16 mM. The results confirm that calcium phosphate precipitation took place in the solution and initiated chalk dissolution. The dissolution of $CaCO_3$ resulted in producing OH^-, thereby increasing the pH of the brine after equilibration, as mentioned in Equation 2. Chalk dissolution was also observed at 24 mM and 36 mM PO_4^{3-} concentrations. According to these results, the addition of PO_4^{3-} at concentrations higher than 12 mM is not recommended for *Smart Water* production.

Equilibration of 24 mM PO_4 brine with $CaCO_3$ at 70 ºC resulted in an increase in pH from 5.2 to 6 and the PO_4^{3-} concentration was decreased from 24 mM to 10 mM. No significant changes in concentrations of Cl^-, Na^+, Ca^{2+}, $Mg^{2+,}$ and SO_4^{2-} were observed during the process at higher temperatures. However, further research is recommended in this area.

Power Estimation

Requirements for water injection vary for each well. Injection rate at Brae Alpha field by Marathon Oil is used as a reference for calculations. The quantity of water injected is 20,000 bpd or 132 m^3/h (Heatherly, Howell and McElhiney 1994). Efficiency of the pump is assumed at 80 % and pump suction pressure is equal to atmospheric pressure. The operating pressures mentioned in calculations are the difference between applied high pressure and suction pressure. Flow rates used for power calculations are based on the experiments performed. Table 5 shows different diluting techniques and their total energy consumption for *Smart Water* production calculated using Equation 6.

$$Power\ (W) = \frac{Feed\ flow\ rate\ \left(\frac{m^3}{s}\right) \times Feed\ pressure\ (Pa)}{Efficiency\ \eta\ (\%)} \quad (6)$$

Mixing oil-free PW with modified seawater increases oil recovery in reservoirs as previously mentioned. Figure 7 shows schematic of NF membrane combinations using PW and seawater as feed. For *Smart Water* in chalk reservoirs, a low monovalent and high divalent ion concentration is required. However, TDS requirements of injected brines for changing wettability differ between reservoirs depending on rock geology (Austad, 2013).

The power consumption for the above combination was performed with 1 m^3 of PW assuming a TDS content of 90,000 mg/L. Nevertheless, it is a challenge to have very high feed TDS for NF membranes. High feed TDS results in an increase in operating pressure in order to overcome the resulting high osmotic pressure and this pressure may exceed the physical pressure limits of the membrane element. Hence, the feed is diluted before passing through the membrane. After dilution, a maximum feed TDS of 40,000 mg/L was used for calculations.

As mentioned above, scale formation may occur by sulfate ions in seawater and barium ions in PW. The following requirements were focused on the process combination in Figure 7.

1. **Dilution of PW to approximately 40,000 mg/L**: Dilution water should not contain sulfate to avoid scaling when mixed with PW. The options considered for dilution were RO permeate, NF permeate, fresh water from land and multi-stage flash (MSF) distillation process. A maximum TDS of diluted PW of 40,000 mg/L was the objective. All calculations with NF membranes were based on mass and flow balances between different streams.

   Power consumed by each dilution technique is explained using Table 5 and Figure 7. *NF-1* is used for treating diluted PW in all four cases at a constant operating pressure of 18 bar. A membrane recovery of 14 % is kept constant in all four cases. The feed flow rates vary with the type of dilution process. From Table 5 it is evident that the diluting stream with highest TDS content is for *NF-2*. Hence, the amount of water required for diluting PW from 90,000 mg/L to 40,000 mg/L is highest for *NF-2*. Other diluting techniques will replace *NF-2* in Figure 7. The difference in TDS of fresh water, MSF and RO are not significant when compared to TDS in NF permeate. Hence, the required flow rate for dilution is nearly equal for RO, fresh water, and MSF as shown in Table 5.

   Dilution of PW with fresh water does not contain any concentrate disposal issues since it is acquired from a low TDS source onshore, whereas MSF, RO and *NF-2* use seawater as feed. However, the availability of a huge volume of fresh water for water injection is a concern. The concentrated brines from MSF and RO retentate contain high concentrations of monovalent ions and thus cannot contribute to *Smart Water* production. These brines must be disposed of properly without having a negative environmental impact (Al-Karaghouli & Kazmerski, 2013). The retentate from *NF-2* has high divalent and low monovalent ion concentrations and is used for producing *Smart Water,* which does not contribute to disposal issues.

   Dilution water from RO, MSF and freshwater require lower flow rates for diluting PW and only *NF-1* permeate with a flow rate of 0.32 m^3/h contributes to *Smart Water* production. Hence, the final power consumption per cubic meters of *Smart Water* produced is higher for other dilution techniques compared with NF used for PW dilution.

   Table 5 shows that power consumption is the lowest for NF membranes for final *Smart Water* production. A feed pressure of 18 bar was implemented for both NF membranes. MSF distillation has the highest power consumption and footprint (Al-Karaghouli & Kazmerski, 2013). RO membrane power consumption is higher than for NF as shown in Table 5. An operating pressure of 55 bar for RO is used for calculations. If energy recovery factor is applied, 50 % of the energy required for RO feed pump could be recovered from RO retentate stream. For *Smart Water* production with a flow rate of 20,000 bpd, an additional source of water for increased divalent ions concentration should be selected, when RO is chosen for dilution of PW. Fouling is also high with RO membranes compared to NF. Additionally, RO requires pretreatment upstream, increasing the operating and maintenance costs of the total system.

   Table 5 shows that NF membranes for dilution used 10.69 kW. Both streams from *NF-2* (Figure 7) are used for *Smart Water* production. The permeate stream without sulfate is used for PW dilution and the retentate stream with high divalent ion concentration can be used for achieving the required flow rate and divalent ion concentrations for *Smart Water*. *NF-1* (Figure 7) for PW treatment was chosen to reduce the energy consumption and to recover more water for reuse. PW treatment with RO is considered less feasible due to fouling. Fouling can occur during long-term operation with NF membranes. However, this study is limited to evaluating the feasibility of *Smart Water* production by mixing seawater and treated PW, and the estimated power consumption can be considered as an initial data point.

2. **Removal of barium ions from PW**: Barium ions and other divalent ions are partially rejected by *NF-1* (Figure 7) with respect to the rejection trends presented in Figure 5. This step was designed

to avoid barium sulfate scaling when PW and seawater are mixed for *Smart Water* production. The permeate stream from *NF-1* has a low concentration of divalent ions and without sulfate. Thus, this stream must be enriched in divalent ions and sulfate, which is attained either by using retentate stream from *NF-2* or by adding chemicals to permeate from *NF-1*. The preferable option from an economical and environmental consideration is to choose retentate from *NF-2*.

NF can be chosen as the best option for PW dilution and *Smart Water* production over other desalination technologies, considering all these factors.

Based on the material balance shown in Figure 7 and Equation 3, permeate recovery is 14 %. For power consumption calculations, a high PW TDS of 90,000 mg/L is considered. PW with a lower initial TDS will require lower dilution resulting in need of less power.

Chemicals present in PW will permeate through the membrane depending on the MWCO of the chemicals. Reuse of these residual chemicals will be beneficial from an economic perspective. However, this aspect is not considered in the paper.

Management of PW retentate stream with a flow rate of 3.25 m^3/h from *NF-1* has a calculated TDS of approximately 41,600 mg/L. Two options are considered for the disposal of this stream:

1. Retentate can be returned to the PW feed tank for further recovery. The permeate flow rate from *NF-2* should be adjusted depending on the final TDS of PW feed over time if the retentate is recirculated.
2. The retentate can be discharged to sea after additional treatment for removal of residual hazardous chemicals if present.

Nowadays, *Smart Water* is produced by adding chemicals to MSF distillate or to RO permeate. These methods will increase chemical usage, overall power consumption along with concentrate disposal issues. Production of *Smart Water* from seawater and part of PW by NF membranes reduces the environmental impact by reduced usage of chemicals since the divalent ions required for *Smart Water* are obtained from seawater.

Conclusions

Performances by two NF membranes in terms of rejection, flux and fouling were evaluated. NF membranes selectively removed ions prone to scaling from PW prior to mixing with modified seawater. Both membranes tested in this research demonstrated practically comparable divalent ion separation efficiency and have a similar recovery at 18 bar. 53 % barium was removed from oil-free PW. A hydrocarbon removal efficiency of 96 - 98 % was obtained by media filtration. The efficiency may be further improved by altering the depth of the bed and more optimal backwashing.

A compatibility analysis for NF treated PW permeate confirmed that the brine was compatible with calcium carbonate surface. A compatibility test for added phosphate in seawater brine is acceptable at a phosphate concentration at and below 12 mM without initiating calcium dissolution.

Analysis of technical limits of NF membranes showed that NF is an attractive method for ionic selection with respect to quality performance, cost and power consumption. Dilution by NF was considered an effective step for optimization of pretreated PW for reinjection. An economically competitive option for dilution of PW was the use of seawater NF permeate. This decrease of TDS in PW increases NF membrane performance of diluted PW in terms of flux and recovery. Total power consumed during *Smart Water* production by NF membranes was calculated to 0.88 kWh/m^3.

Author Biography

Remya Ravindran Nair is a Ph.D. student at the University of Stavanger with The National IOR Centre

of Norway. Nair's research interest includes membrane technology, environmental technologies and water, and wastewater treatment. Nair has published 2 international journal papers and has contributed with papers and presentations in many desalination/membranes and IOR/EOR conferences. Nair holds an MS degree in Environmental Engineering from the University of Stavanger, Norway.

Evgenia Protasova is a research assistant at the University of Stavanger, where she has worked for 4 years. Protasova's research interests include wastewater treatment, membrane technology, waste recycling, green energy. Protasova has co-authored 6 technical papers. She holds an MS degree in Environmental Engineering from the University of Stavanger.

Skule Strand is an associate professor in reservoir chemistry at the University of Stavanger. Strand's main research work is reservoir chemistry, with a special focus on reservoir wettability and water-based wettability alteration processes for Enhanced Oil Recovery (EOR) by "Smart Water" injection in both sandstone and carbonate reservoirs. Strand is involved in a number of international financed EOR research projects towards the oil industry. Strand has published more than 60 international journal papers and contributed with papers and presentations in IOR/EOR conferences, workshops, and symposiums around the world. Strand holds an MS (1993) and Ph.D. degree (2006) in Petroleum Technology from the University of Stavanger.

Torleiv Bilstad is a professor at the University of Stavanger where he has been working since 1997. Bilstad's research interests include environmental management, wastewater treatment, applied membrane separation, and environmental technologies. Bilstad has authored and co-authored more than 50 technical papers (international publications). He holds a Ph.D. degree in Civil & Environmental Engineering from the University of Wisconsin - Madison, 1977.

Acknowledgements

The authors acknowledge the Research Council of Norway and the industry partners, ConocoPhillips Skandinavia AS, Aker BP ASA, Eni Norge AS, Total E&P Norge AS, Equinor ASA, Neptune Energy Norge AS, Lundin Norway AS, Halliburton AS, Schlumberger Norge AS, Wintershall Norge AS, and DEA Norge AS of The National IOR Centre of Norway for support.

Nomenclature

PW – Produced Water
FW – Formation Water
SSW – Synthetic Seawater
NF – Nanofiltration
EOR – Enhanced Oil Recovery
TDS – Total Dissolved Solids
OOIP – Original Oil in Place
FI – Forced Imbibition
MWCO – Molecular Weight Cut-Off
NTU – Nephelometric Turbidity Unit
MSF – Multistage Flash
IC – Ion Chromatography
IR – Infrared
TOG – Total Oil and Grease
TPH – Total Petroleum Hydrocarbon
FTIR – Fourier Transform Infrared

References

Al-Karaghouli, A. & Kazmerski, L. L., 2013. Energy consumption and water production cost of conventional and renewable -energy-powered desalination processes. *Renewable and Sustainable Energy Reviews, Elsevier,* pp. 343-356.

Anim-Mensah, A. R., Krantz, W. B. & Govind, R., 2008. Studies on polymeric nanofiltration-based water softening and the effect of anion properties on the softening process. *European Polymer Journal*, pp. 2244-2252.

ASTM D7678-17, 2017. *Standard test method for Total Oil and Grease (TOG) and Total Petroleum Hydrocarbons (TPH) in water and wastewater with solvent extraction using mid-air laser spectroscopy,* s.l.: ASTM International.

Austad, T., 2013. Water- based EOR in carbonates and Sandstone: New Chemical Understanding of the EOR-Potential Using ¨ Smart water¨. I: *Enhanced oil recovery field case studies.* s.l.:s.n., pp. 301-335.

Bader, M., 2006. Sulphate scale problems in oil fields water injection operations. *Desalination,* pp. 100-105.

Bilstad, T., Nair, R. R. & Protasova, E., 2015. *American Water Works Association(AWWA).* [Internett] Available at: http://www.awwa.org/portals/0/files/education/conferences/membrane/mtc16/membrane%20papers/tue08%20papers/03-bilstad%20paper.pdf
[Funnet 28.12.2016 Desember 2016].

Cheryan, M., 1998. *Ultrafiltration and Microfiltration Handbook.* USA: CRC Press.

Childress, A. & Elimelech, M., 2000. Relating Nanofiltration Membrane Performance to Membrane Charge (Electro kinetic) Characteristics. *Environmental Science and Technology*, pp. 3710- 3716.

Collins, K. D., 2006. Ion Hydration: Implications for cellular function, polyelectrolytes, and protein crystallisation. *Biophysical Chemistry*, pp. 271- 281.

Davis, R., Lomax, L. & Plummer, M., 1996. membranes solve North Sea waterflood sulfate problems. *Oil & Gas Journal*.

Dow Water & Process Solutions, n.d. *FILMTEC Reverse Osmosis Membranes Technical Manual,* s.l.: s.n.

Duhon, H., 2012. Produced water treatment : yesterday, today and tomorrow. *SPE,* pp. 29-31.

Fathi, J. S., Austad, T. & Strand, S., 2011. Water- Based Enhanced Oil Recovery (EOR) by ¨Smart Water¨ : Optimal Ionic conposition for EOR in Carbonates. *Energy & Fuels*.

Fathi, S. J., Austad, T. & Strand, S., 2010. ¨Smart Water¨as a wettability modifier in chalks: The effect of salinity and ionic composition. *Energy and Fuels*, pp. 2514- 2519.

Fathi, S. J., Austad, T. & Strand, S., 2012. Water-based Enhanced Oil Recovery (EOR) by ¨Smart Water¨ in Carbonate Reservoirs. *Society of Petroleum Engineers*.

Filmtec Membranes, u.d. *Dow water solutions- Filmtec membranes product catalogue.* [Internett] Available at: www.lenntec.com

Fink, J. K., 2012. Enhanced Oil Recovery. I: *Petroleum engineer's guide to oil field chemicals and fluids.* s.l.:s.n., pp. 459-517.

Frenier, W. W. & Ziauddin, M., 2008. *Formation, removal,and inhibition of inorganic scale in the oilfield environment.* s.l.:Society of Petroleum Engineers.

Gupta, R. et al., 2011. Enhanced Waterflood for Middle East Carbonate Cores- Impact of Injection Water Composition. *Society of Petroleum Engineers*.

Heatherly, M. W., Howell, M. E. & McElhiney, J. E., 1994. Sulphate Removal Technology for Seawater Waterflood Injection. *Offshore Technolgy Conference*.

Hilal, N. et al., 2004. A comprehensive review of nanofiltration membranes: Treatment, pretreatment, modelling, and atomic force microscopy. *Desalination,* pp. 281-308.

Hilal, N., Al-Zoubi, H., Darwish, N. & Mohammad, A., 2005. Characterisation of Nanofiltration

membranes using atomic force microscopy. *Desalination,* pp. 187-199.
Hill, G. & Holman, J., 2001. *Chemistry in Context, Laboratory Manual.* s.l.:s.n.
Høgnesen, E. J., Strand, S. & Austad, T., 2005. Waterflooding of preferential oil-wet carbonates: Oil recovery related to reservoir temperature and brine composition. *Society of petroleum engineers*.
Hydranautics, N., u.d. *Product information catalogue.* [Internett]
Available at: www.membranes.com
Korsnes, R. I. et al., 2008. The effects of temperature on the water weakening of chalk by seawater. *Journal of Petroleum Science and Engineering,* Volum 60, pp. 183-193.
Kreig, H. M., Modise, S. J., Keizer, K. & Neomagus, H. W., 2004. Salt rejection in nanofiltration ofr single and binary salt mixures in veiw of sulphate removal. *Desalination, 171*, pp. 205-215.
Manttari, M., Pihlajamaki, A. & Nystrom, M., 2006. Effect of pH on hydrophilicity and charge and their effect on the filtration efficiency of NF membranes at different pH. *Journal of Membrane Science*, pp. 311-320.
Nair, R. R., Protasova, E., Strand, S. & Bilstad, T., 2018. Membrane performance analysis for smart water production for enhanced oil recovery in carbonate and sandstone reservoirs. *Energy & Fuels,* pp. 4988-4995.
Norwegian Oil and Gas Industry, 2015. *Environmental report 2015, Environmental work by the oil and gas industry-Facts and Trends,* s.l.: s.n.
Norwegian Oil and Gas industry, 2016. *Environmental work by the Oil and Gas Industry- Facts and development trends,* s.l.: s.n.
Norwegian Oil and Gas, 2014. *Environmental report,* s.l.: The Norwegian Oil and Gas Association.
Offshore Oil and Gas operators in Denmark, 2009. *Removal of oxygen from injection water at Gorm F,* Denmark: s.n.
OSPAR Commission, 2005-2015. *OSPAR reference method of analysis for the determination of the dispersed oil content in produced water,* s.l.: OSPAR commission.
Puntervold, T., 2008. *Water flooding of carbonate reservoirs - EOR by wettability alteration,* s.l.: s.n.
Puntervold, T. & Austad, T., 2007. Injection of seawater and mixtures with produced water into North Sea Chalk Formation: Impact on Wettability, scale formation, and rock mechanics caused by fluid-rock interaction. *SPE 111237*.
Puntervold, T., Strand, S., Ellouz, R. & Austad, T., 2015. Modified seawater as a smart EOR fluid in chalk. *Journal of Petroleum Science and Engineering*, pp. 440-443.
Ruston, A., Ward, A. S. & Holdich, R. G., 2000. *Solid-Liquid Filtration and Separation Technology.* Wiley - VCH red. Germany: s.n.
Schaep, J., Vandecasteele, C., Mohammad, W. & Bowen, R., 2001. Modelling the retention of ionic components for different nanofiltration membranes. *Seperation and Purification Technology 22-23*, pp. 169-179.
Seelenbinder, J. & Mainali, D., 2015. *Agilent Microlab Quant Calibration software: Measure oil in Water using Method IP 426,* s.l.: Agilent Technologies.
Statoil, 2015. [Internett]
Available at:
http://www.statoil.com/en/OurOperations/TradingProducts/CrudeOil/Crudeoilassays/Pages/EkofiskBlend.aspx
Statoil, 2017. *Lecture handout.* Stavanger, Norway: s.n.
Stosur, G., 2003. EOR: Past, Present, and What the next 25 years may bring. *Society of Petroleum Engineers*.
Strand, S., Høgnesen, E. J. & Austad, T., 2006. Wettability alteration of carbonates-Effects of potential determining ions (Ca2+ abd SO42-) and temperature. *Colloids and Surfaces A: Physicochem.Eng.Aspects,* Volum 275, pp. 1-10.
Tansel, B., 2012. Significance of thermodynamic and physical characteristics on permeation of ions during membrane separation : Hydrated radius, hydration free energy and viscous effects. *Separation*

and Purification Technology 86, pp. 119-126.
Tansel, B. et al., 2005. Significance of hydrated radius and hydration shells on ionic permeability during nanofiltartion in dead end and cross flow modes. *Seperation and Purification Technology 51,* pp. 40-47.
Van der Bruggen, B., Schaep, J., Wilms, D. & Vandecasteele, C., 1999. Influence of molecular size, polarity and charge on the retention of organic molecules by nanofiltration. *Journal of Membrane Science ,* Volum 156, pp. 29-41.
Wilf, M. et al., 2007. *The guidebook to membrane desalination technology.* s.l.:Desalination Publications.

Table 1. Ionic compositions of seawater, PW, Formation water and diluted PW (Puntervold & Austad, 2007)

Ions	Concentration (mole/L)							
	SSW	PW	FW	Diluted PW*	Mixtures PW/ SSW			
					1:1	1:2	1:4	1:8
HCO^{3-}	0.002	0.002	0.002	0.000	0.002	0.002	0.002	0.002
Cl^{-}	0.525	1.564	3.134	0.352	1.044	0.871	0.733	0.640
SO_4^{2-}	0.024	0.000	0.000	0.000	0.012	0.016	0.019	0.021
Mg^{2+}	0.045	0.065	0.116	0.0071	0.055	0.051	0.049	0.047
Ca^{2+}	0.013	0.039	0.882	0.00567	0.026	0.022	0.018	0.016
Na^{+}	0.450	1.340	1.060	0.396	0.895	0.747	0.628	0.549
K^{+}	0.010	0.016	0.043	0.007	0.013	0.012	0.011	0.011
Ba^{2+}	0.0E+00	3.6E-05	2.5E-03	0.0016**	1.8E-05	1.2E-05	7.1E-06	4.0E-06
Sr^{2+}	0.0E+00	5.6E-04	0.016	0	2.8E-04	1.9E-04	1.1E-04	6.3E-05
Li^{+}	0.000	2.853	0.000	0	1.426	0.951	0.571	0.317
TDS (g/L)	33.39	110	177.19	22.32	71.71	58.3	48.72	41.90

** Concentration of diluted PW used for the experiments*
***Original barium concentrations were low and hardly detected by IC. Ba^{2+}concentration in diluted PW was hence increased within non-precipitating range upstream NF, assisting in realistic measurable rejections.*

Table 2. Main characteristics of NF membranes used for experiments according to the manufacturers (Filmtec Membranes, u.d.; Hydranautics, u.d.)

Membranes	Feed spacer thickness (mm)	Maximum operating pressure (bar)	Flux ($L/m^2/h$) at 2000 ppm $MgSO_4$	Recovery (%) at 2000 ppm $MgSO_4$
NANO-SW-2540	0.79	41.4	43.5	15
NF270- 2540	0.86	41	51.3	15

Table 3. Ionic compositions of NF permeate from PW before and after equilibration at 25 ºC

Parameters	PW permeate composition before equilibration	PW permeate composition after equilibration
pH	7.5	7.9
Chloride, mM	475	482
Sodium, mM	500	503
Magnesium, mM	7.8	7.4
Calcium, mM	4.6	4.4

Table 4. Ionic concentrations of phosphate containing *Smart Water* brines before and after equilibration at 25 ºC*

Parameters	Feed 1, before equilibration, 44 mM of phosphate	Product 1, after equilibration 44 mM of phosphate	Feed 2, before equilibration, 12mM of phosphate	Product 2, after equilibration, 12 mM of phosphate
pH	4.99	5.64	5.712	6
Chloride, mM	549.8	537.7	523.8	523
Sulfate, mM	18.8	17.40	17.8	17.8
Phosphate, mM	44	28.16	12	11.8
Sodium, mM	466	466.7	456.8	456.5
Magnesium, mM	52.5	52	52	51.8
Calcium, mM	11.1	4.3	9.25	9.2

*Retentate from membrane experiments was used for equilibration

Table 5. Energy consumption analysis for *Smart Water* production by different dilution techniques

Properties	Fresh Water	MSF*	RO	NF
Operating pressure (bar)	3	-	55	18
TDS of diluting stream, mg/L	300	10	150 (Permeate)	22000 (*NF- 2* Permeate)
Required flow rate for dilution from calculation, m^3/h	1.28	1.25*	1.26 (permeate)	2.78 (permeate)
Retentate flow rate from dilution technique, m^3/h	-	-	14.4	14.3 *(NF-2)*
TDS of the concentrated stream, mg/L		≈ 34500	33732	31550 *(NF-2)*
Concentrate disposal issues from dilution technique	None	High	High	None *(NF-2)*
NF-1 PW permeate flow rate used as *Smart Water*, m^3/h	0.32	0.32	0.32	0.53
Final flow rate used for *Smart Water*, m^3/h	0.32	0.32	0.32	14.83**
Power consumed for dilution, kW	0.13	31.26	14.98***	10.69
Power consumed by *NF-1* after dilution, kW	1.41	1.41	1.41	2.36
Total power consumption, kWh	1.54	32.67	16.39	13.05
Total power consumed for *Smart Water* production per cubic meter, kWh/m^3	**4.87**	**103.52**	**51.22**	**0.88**

* Total average energy consumption of MSF, kWh/m^3 = 25 (Al-Karaghouli & Kazmerski, 2013)
** *Smart Water* flow rate for NF consists of *NF-1* permeate and *NF-2* retentate (Refer Figure 7)
*** Energy Recovery Factor is used

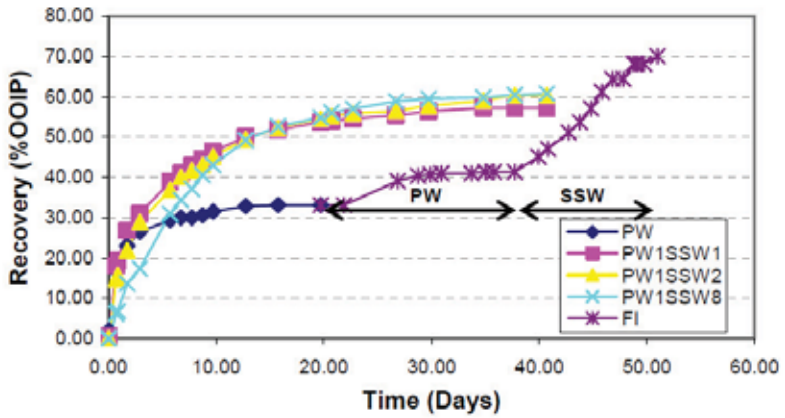

Figure 1. Spontaneous imbibition of mixtures of PW and SSW into chalk cores at 110 °C saturated with a crude oil of acid number = 0.70 mg KOH/g oil (Puntervold, 2008)

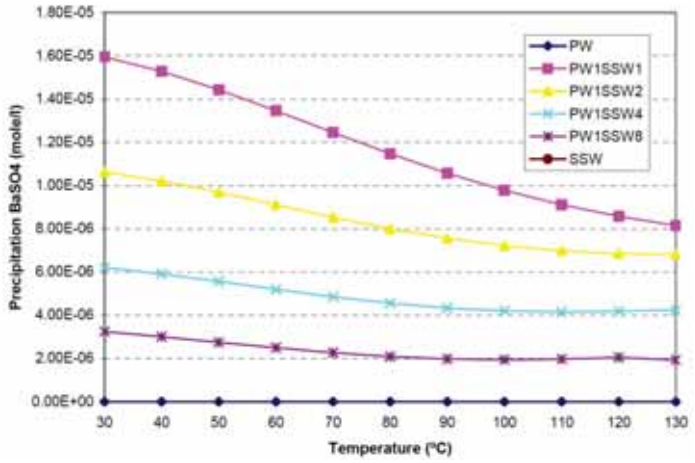

Figure 2. $BaSO_4$ precipitation versus temperature from a combination of SSW and Tor field PW (Puntervold, 2008)
(PW curve lays above SSW curve)*

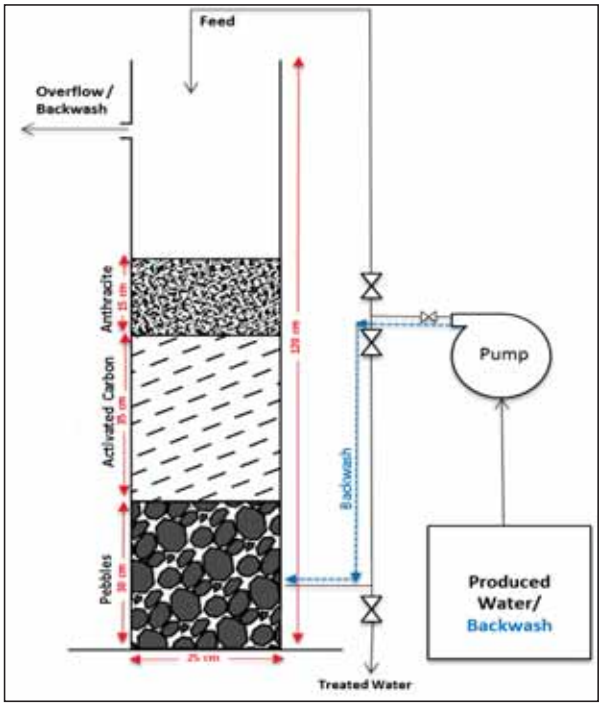

Figure 3. Media filtration unit

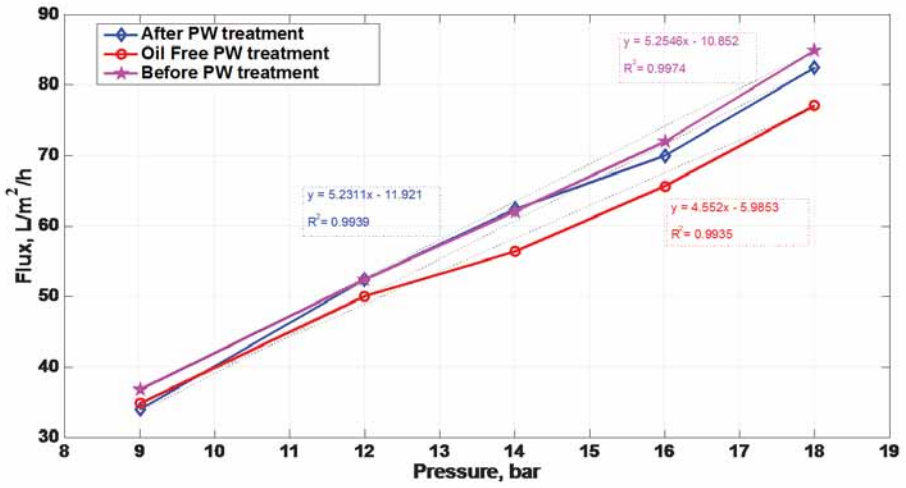

Figure 4. Flux comparison for seawater before and after treating oil-free PW by NF 270-2540

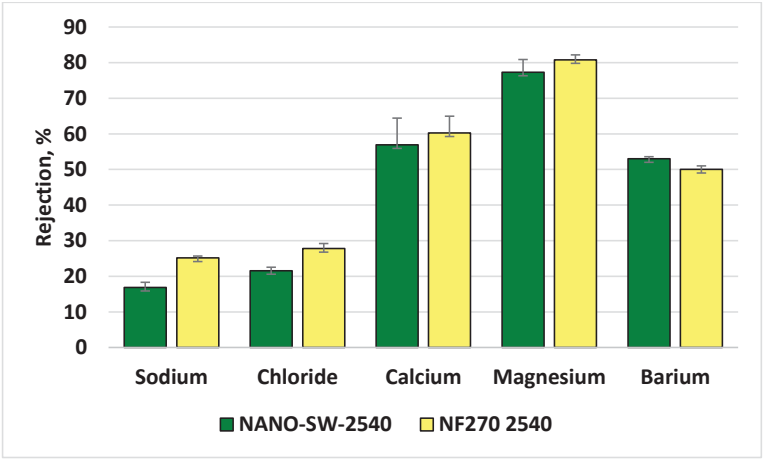

Figure 5. Rejection % by NANO-SW-2540 and NF270-2540 at 18 bar

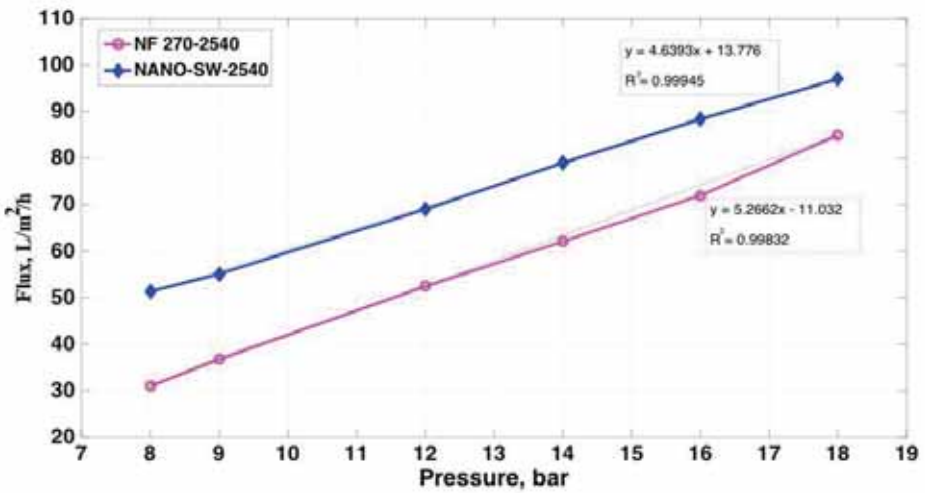

Figure 6. Flux versus pressure for NF270-2540 and NANO-SW-2540

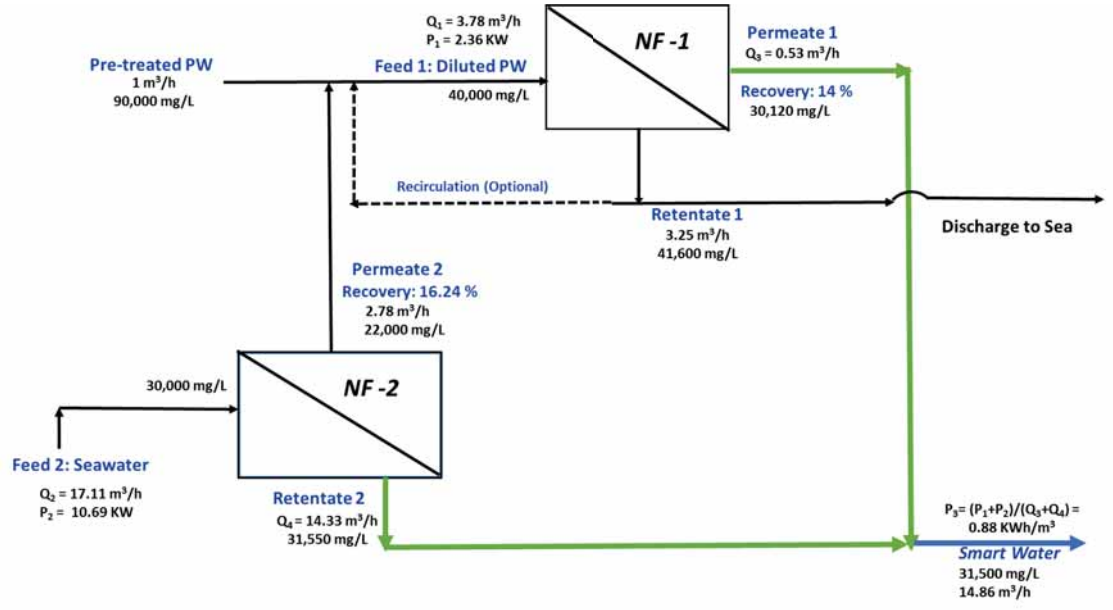

Figure 7. Suggested process schematic for *Smart Water* production

Appendix 3 – Paper III

Paper III

Effect of pH on Produced Water Treatment Using Nanofiltration Membranes: Artificial Neural Network for Performance Assessment and Steric Hindrance

Remya Ravindran Nair, Evgenia Protasova, Skule Strand, Torleiv Bilstad

Desalination and Water Treatment (Under Review)

Effect of pH on Produced Water Treatment using Nanofiltration Membranes: Artificial Neural Network for Performance Assessment and Steric Hindrance Pore Model for Flux Variation Evaluation

Remya Ravindran Nair [a], Evgenia Protasova [a], Skule Strand [b] and Torleiv Bilstad [a]*

a Department of Chemistry, Bioscience and Environmental Technology, University of Stavanger, Kjell Arholmsgate 41, 4036 Stavanger, Norway

b Department of Energy and Petroleum Engineering, University of Stavanger, Kjell Arholmsgate 41, 4036 Stavanger, Norway

remya.nair@uis.no, evgy.pro@gmail.com, skule.strand@uis.no, torleiv.bilstad@uis.no

Abstract

Experimental studies have shown that flux and ion rejection by nanofiltration (NF) are strongly influenced by feed pH. The novelty of this research is using the artificial neural network (ANN) in predicting ion rejection based on multiple variable experimental data for feed pH, pressure, and flux. With a number of independent variables affecting ion rejections, ANN is considered suitable compared to Spiegler-Kedem model for predicting the interrelation between variables with non-linear dependencies in a multi-ion environment. However, Spiegler -Kedem and steric hindrance pore models (SHP) were used for explaining effect of pH on NF flux variations. Experiments were performed to demonstrate reuse of de-oiled produced water (PW) at different pH with salinity similar to seawater as *Smart Water* for enhanced oil recovery (EOR). Flux was higher at basic pH compared to acidic feed pH and varied due to pH-sensitive dissociable groups, which protonated or deprotonated with changing pH. An ANN structure was designed that resulted in a close agreement between ANN predictions and experimental data with an agreement of above 95 % for all membranes. The results are presented, and interpreted with respect to requirements for *Smart Water,* thereby reusing PW, and simultaneously expanding membrane applications in the oil industry.

Keywords- Artificial neural network, Nanofiltration, Spiegler-Kedem, Steric hindrance pore model, Produced Water, *Smart Water*.

1. Introduction

Water injection is performed during oil production for mostly all oil reservoirs for pressure maintenance and to sustain oil recovery. Amount of PW surges as a producing field age and PW volume to be treated is continuously increasing and with high investment for best available technologies.

PW composition is complex and has distinctive characteristics due to organic and inorganic content that differs between reservoirs. The components originate from injected water, formation water and chemicals including dissolved and dispersed organic compounds, inorganic compounds including heavy metals, salts, and naturally occurring radioactive materials.

In 2015, only 22 % of total PW produced on the Norwegian Continental Shelf (NCS) were injected into formations while the rest was discharged to sea after treatment. PW discharges were 150 million standard cubic meter (scm) on NCS while oil production totaled 91 million scm in 2015 [1]. Environmental regulations and sustainable development of scarce resources of water are currently moving the focus towards reusing pre-treated PW as injection water.

EOR by *Smart Water* has become an accepted technology in the oil industry. *Smart Water* is produced by adjusting the ionic composition of injected water that changes the established equilibrium between crude oil, brine and pore surface minerals, modifying the wetting properties of reservoirs [2]. In carbonate reservoirs, seawater and modified seawater brines behave as *Smart Water* while low salinity brines are more efficient in sandstone reservoirs [2, 3].

Smart Water for carbonates requires high divalent ion concentrations (SO_4^{2-}, Ca^{2+}, and Mg^{2+}) and low monovalent ion concentrations (Na^+ and Cl^-). For sandstone reservoirs, low salinity water with TDS < 5,000 ppm and low divalent ion concentrations are preferred [2]. Production of *Smart Water* by NF membranes using seawater as feed for both reservoirs was discussed in our earlier paper [4]. Permeate is used for *Smart Water* production when oil-free PW is treated with NF membranes and is considered as a reuse of PW that simultaneously improve oil recovery and economics [5].

The objective of this research is to focus on PW reuse as *Smart Water* for EOR. It has been suggested that NF membranes can treat oil-free diluted PW and reused for EOR in reservoirs [5]. However, pH of PW is one of the main challenges for treatment by membranes. pH of PW differs from 4.3 to 10 depending on reservoirs and chemicals added [6]. TDS of PW vary from hundreds to 250,000 ppm [7].

Experiments were performed for verifying the feasibility of de-oiled PW and seawater co-injection into reservoirs for EOR or for water flooding [8]. The performance of three NF membranes was experimentally determined with respect to flux and ion rejection under a wide

range of feed pH and pressure values. The experimental results were later used for predicting ion rejections at given pressure, flux and pH using ANN.

A number of mathematical models predict ion transport mechanisms in NF membranes. Prediction of ion rejection was performed by researchers using Spiegler- Kedem model [9, 10, 11] to determine the transport parameters reflection coefficient σ and solute permeability P_s [12]. However, these models are mathematically complex and require a detailed knowledge of membrane characterization and performance.

Artificial neural network (ANN) for predicting ion rejection offers a more attractive alternative to Spiegler-Kedem model and has been applied to predict membrane performance and fouling [13, 14]. Results showed that proper selection of input variables and number of neurons with a set of training data help to optimize the ANN training process resulting in accurate predictions of membrane performance [15].

This research presents an experimental analysis of membrane performance in terms of flux and rejection using three commercially available NF membranes (NF270, ESNA, and HYDRACoRe50) with seawater with varying pH as feed. Spiegler- Kedem model was used to determine the reflection coefficient and solute permeability of ions. A steric hindrance pore model was used to determine the pore size of tested membranes. ANN was used to predict rejections as a function of pressure, pH, and flux for Cl^-, Na^+, Mg^{2+}, and Ca^{2+}.

2. Theory

Treatment of oilfield PW includes processes such as separators, de-oilers, de-sanders, coagulation, media filters, and membranes. Effective PW treatment generally requires a series of pre-treatment operations to remove contaminants. After appropriate pre-treatment, high total dissolved solids (TDS) can be removed from PW by reverse osmosis (RO). RO membranes have no pores and separation is mainly due to solution-diffusion. However, fouling of RO membranes at high feed pressure operation is a challenge. NF is an alternative and is a well-established process in separation and purification of solutions. NF membranes have a pore size in the range of 1 nm and operate at feed pressure from 3 - 20 bar and have higher flow rate than RO and are less susceptible to fouling. By implementing NF membrane treatment, the energy consumption will be less than that for RO and increases water recovery.

Performance of NF membranes as a function of pH is analyzed by flux and solute rejection. Membrane characteristics vary with pH [16] and variations are dependent on membrane material and type and concentration of solute. Solute separation by NF is due to complex

mechanisms including Donnan [17] and dielectric effects and steric hindrance. Ion retention is also determined by the distribution of co-ions between the membrane and solution according to Donnan equilibrium for single salt solutions [18]. However, when pressure is applied across the membrane, Donnan potential repels co-ions and to achieve electroneutrality, counter-ions are also rejected. This is one of the main mechanisms during NF separation [19]. Ion separation also occurs due to sieving (steric) effect based on size differences between ions and membrane pores. Hydrated ions with large size are retained by the membrane while ions with low hydrated radius permeate [19].

2.1 Spiegler-Kedem Model

Solute transport through a membrane can be described by irreversible thermodynamics where the membrane is considered as a black box [20]. According to Speigler and Kedem [20], an expression for relating flux to rejection was developed when high concentration difference occurs between permeate and reject (Equation 1 and Equation 2).

$$R_{obs} = \sigma \frac{(1-F)}{(1-\sigma F)} \quad (1)$$

where

$$F = \exp(-\frac{(1-\sigma)}{P_s} J_v) \quad (2)$$

where R_{obs} is the observed rejection, J_v is water flux, σ is the reflection coefficient and P_s is solute permeability.

The parameters σ and P_s was determined by fitting the experimental rejection data R as a function of flux J_v using a best-fit method. The transport parameter σ measures the degree of membrane semi-permeability. A high σ value ($\sigma \approx 1$) indicates that the solute is highly rejected by the membrane [12].

Membrane efficiency is evaluated by measuring flux J_v through the membrane. Flux is defined as permeate flow through a unit area of the membrane surface with units of $L/m^2/h$ and is calculated by Equation 3.

$$J_v = \frac{V}{t \times A} \quad (3)$$

where V is the permeate volume, t is the filtration time and A is the effective membrane area.

Ion rejection R is another parameter used for investigating membrane performance and specifies the concentration of ions in the retentate or percentage of ions rejected by the membrane using Equation 4.

$$R = 1 - \frac{C_p}{C_f} \quad (4)$$

Where C_p and C_f are permeate and feed concentrations, respectively.

2.2 Steric Hindrance Pore (SHP) Model

According to Nakao and Kimura [21], membrane structural parameters can be estimated using the SHP model. This model was successfully used by many researchers [22, 23], to determine the pore size using neutral and charged solutes. The model explains transport of ions through cylindrical pores hindered by frictional forces and the steric effects are considered. According to this model, the membrane parameters σ and P_s are given as

$$\sigma = 1 - S_F \{1 + (^{16}/_{9})q^2\} \quad (5)$$

$$P_s = D \times S_D (^{A_k}/_{\Delta x}) \quad (6)$$

where

$$S_D = (1 - q)^2 \quad (7)$$

$$S_F = 2(1 - q)^2 - (1 - q)^4 \quad (8)$$

and $$q = {}^{r_s}/_{r_p} \quad (9)$$

D is diffusivity, $A_k/\Delta x$ is the ratio of membrane porosity to membrane thickness, r_s is the Stokes radius of the solute and r_p is the pore radius. S_D and S_F are the steric hindrance factors for diffusion and convection, respectively. Stokes radius of ions is used to calculate the pore radius and is shown in Table 1.

Table 1. Stokes radii of ions [24]

Ions	Cl^-	Na^+	SO_4^{2-}	Ca^{2+}	Mg^{2+}
Stokes Radius (nm)	0.121	0.184	0.231	0.310	0.348

2.3 Limitations of Membrane Process-Based Models

Proper prediction of NF membrane performance is required for process design and optimization. Ion rejections are mainly predicted by Spiegler-Kedem model and by models

based on Nernst-Plank equation. The former is based on a black-box approach that allows the membranes to be characterized based on the transport parameters such as reflection coefficient σ and solute permeability P_s [10, 21]. The latter model describes ion transport in terms of effective membrane charge density and ratio of effective membrane thickness to porosity [25]. Both these models were developed from NF membranes physical properties and performance and require a detailed knowledge of the feed conditions and membrane type that may not be readily available.

However, prediction of ion rejection by ANN only requires readily available inputs with a minimum understanding of the overall complexity of the membrane properties. ANN is user-friendly and suitably accurate for industrial design purposes.

2.4 Artificial Neural Network (ANN)

ANN's are computational models that act as powerful tools to predict output data in complicated systems with several input parameters with a considerable reduction in time and cost. ANN's are used to process data and provide information using a group of integrated process units called neurons. ANN's are adaptive systems that could change its structure based on the information that flows through the network during the training phase. The multi-layer perceptron artificial neural network includes an input layer, a hidden layer, and an output layer. The number of input layers is three and consists of pH, pressure, and flux. Output values are four and include Cl^-, Na^+, Mg^{2+} and Ca^{2+} rejection.

Feedforward back propagation network type is used in this research. In each neuron, the sum of input values is weighted and the sum is transferred through a transfer function. The transfer function calculates the output from an input neuron. The transfer functions mainly used in ANN to solve regression problems are the hyperbolic tangent sigmoid transfer function (tansig), log-sigmoid transfer function (logsig) and the linear transfer function (purelin). The neurons can use any transfer function to create the output. The transfer functions generate outputs for tansig in the range of $-1 \leq f(A_i) \leq +1$, for logsig in the range, $0 \leq f(A_i) \leq 1$ and for linear function from the range $-\infty \leq f(Ai) \leq +\infty$, where A_i is the net input [26]. Different number of hidden layers can be used and the number of neurons in each layer is varied to find the best ANN structure to predict ion rejection.

The ANN inputs present the variables that have an effect on the predicted outputs such as pH, pressure, concentration and membrane type. All these inputs are related to ion rejection, the

ANN output in this research. The structure of the neural network used to predict ion rejection in this research is shown in Figure 1.

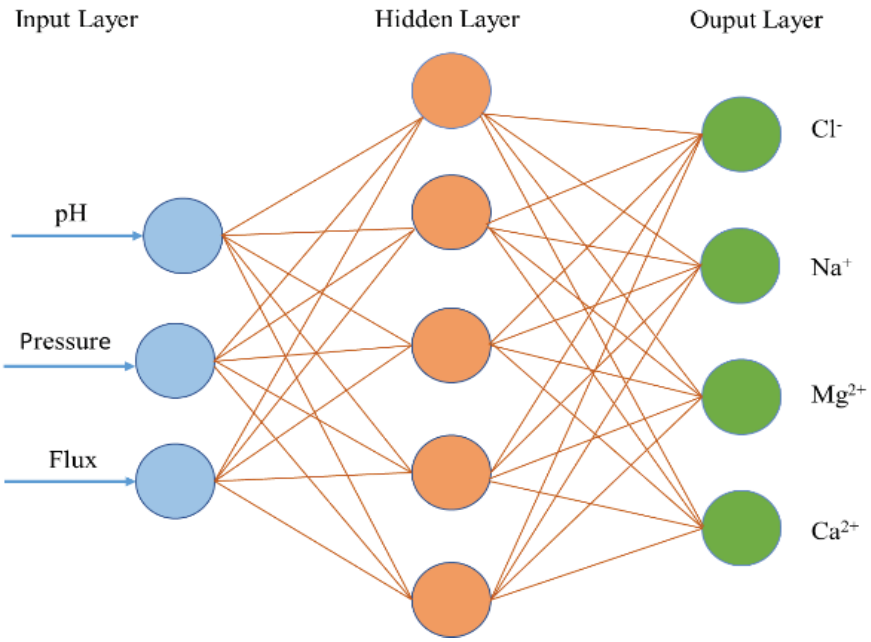

Figure 1. An ANN configuration with 5 neurons in the hidden layer

The output layer should have four neurons since the number of outputs is four. The selected training algorithm is Levenberg-Marquardt. There are mainly four steps involved in ANN modeling that includes collecting the training data for input and output, selecting the network design, training the network and network simulation. The most important phase of building the ANN model is network training. During the training phase, the data supplied will be divided into three sections that include the train data, validation data, and test data. The training process minimizes the error related to the deviations of the ANN predictions from the target values and is calculated as mean square error (MSE). The value of MSE is calculated using Equation 10 [26].

$$MSE = \frac{\sum_{i=1}^{n}(t_i - a_i)^2}{n} \qquad (10)$$

where t_i denotes the i-th target value, a_i is the predicted value and n is the number of data.

The optimum neural network structure was selected based on the smallest difference between the predicted values and the experimental data or in other words, the neural network with the

least MSE and highest R^2 is selected. R^2 is the statistical coefficient of determination and a value higher than 0.95 is considered acceptable.

3. Experimental Methods

3.1 NF Membranes

Three commercial NF membranes were investigated in this study; Nitto Hydranautics ESNA, HYDRACoRe, and Dow Filmtec NF270. Table 2 summarizes the membrane specifications according to the manufacturers. ESNA and Filmtec NF 270 have a polyamide skin layer on a polysulphone /polyester support layer.

Table 2. Membrane specifications according to manufactures

Membrane	Material	Area, m^2	Permeate flow rate, m^3/day
ESNA	Composite polyamide	2.3	4.9
HYDRACoRe*	Sulphonated polyethersulfone	2.3	4.2
Filmtec NF270	Composite polyamide	2.6	3.2

* Molecular Weight Cut off is 1000 Dalton according to the manufactures

Maximum operating pressure and temperature is 41 bar and 45 °C and the pH range is 2 - 11 for all three membranes.

3.2 Experimental Set-up

The experimental set-up consists of membrane modules listed in Table 2, one membrane operated at a time. Membranes were first stabilized by washing with pure water for approximately 4 hours at 25 ˚C and 10 bar. Membranes were operated in a cross-flow mode at room temperature with operating pressure from 9 bar to 18 bar. Feed seawater was pre-treated through a 20 µm and a 5 µm cartridge filter. The retentate and permeate streams were returned to the feed tank securing identical feed concentrations. Samples from both streams were collected and analyzed. The membrane stabilization time for each experimental run at different feed pH was 25 minutes at all tested operating pressures. Flux through the membrane was calculated by measuring the permeate flow rate through the active membrane area. The flow rate was measured immediately after 25 minutes. Three trials were performed for each pH value and the membranes were producing for 3 hours for each trial.

3.3 Feed Solutions and Analytical Instruments

Experiments should be performed with de-oiled PW with high TDS for precise calculations. However, for ease of experimental analysis, the experiments were performed by varying the pH in seawater with ionic composition as shown in Table 3. It was assumed that the feed seawater used for the experiments can be considered as diluted de-oiled PW with no colloids or scaling ions present. Thus, the effect of colloidal fouling and concentration polarization during membrane performance is not considered. PW composition from the Valhall field in the North Sea [8] is likewise displayed to compare the ionic concentrations between PW and seawater. The ions are identical in both PW and seawater, though the ion concentrations differ. Scaling ions such as barium and strontium were not present in the feed seawater.

Table 3. Compositions of major ions in PW and seawater in mol/L

	PW *	Seawater**
HCO^{3-}	0.013	0.002
Cl^{-}	1.096	0.525
SO_4^{2-}	0.001	0.024
Mg^{2+}	0.008	0.052
Ca^{2+}	0.031	0.093
Na^{+}	1.027	0.474
K^{+}	0.005	0.010
TDS(g/l)	64.96	34.1

* PW composition for Valhall field [8]

** Seawater composition from ion chromatography (IC) analysis

Experiments were carried out with pre-filtered seawater at 34,100 ppm TDS and conductivity of 47.3 mS/cm. pH of seawater was adjusted between 2.5 and 10.2 by adding analytical grade HCl and NaOH. 12 feed pH values were used; 2.5, 3, 3.5, 4, 4.5, 5, 6, 7, 8.5, 9.2, 9.7 and 10.2. Experiments were also performed with normal seawater with pH 8. No HCl or NaOH was added at pH 8.

Conductivity, salinity, temperature, and TDS were measured using TDS meter *VWR collection CO3100N*. pH was measured using *VWR Phenomenal pH 1100L*. Ion concentrations were measured using IC (Dionex ICS-5000^{+} DP).

3.4 Membrane Cleaning

Suitable membrane cleaning was performed with tap water after each experiment. Flushing was continued until clean water membrane flux returned to its initial flux. pH and conductivity of recirculated water were continuously monitored to confirm that no fouling occurred on the membrane. Chemical cleaning was performed using Aqua Pro Membrane cleaner for removal of metal hydroxides, $CaCO_3$ and other types of scaling.

4. Results and Discussions

4.1 Effect of Feed pH on Flux or Membrane Permeability

Membrane performance at various feed pH values was interpreted by analyzing flux through the membrane. Flux as a function of transmembrane pressure for three NF membranes is represented in several figures. Figure 2 shows the effect of pH on flux with increasing operating pressure for ESNA.

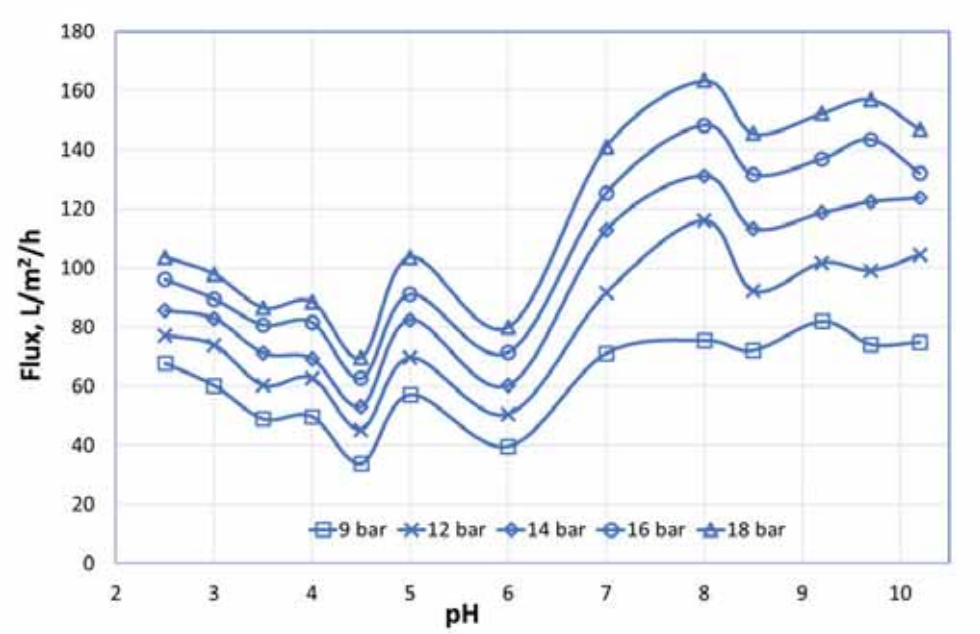

Figure 2. Flux versus pressure for ESNA at different pH

Data presented in the graphs are average values from three trials. Figure 2 shows that the lowest flux was 34 L/m^2/h at pH 4.5 with an operating pressure of 9 bar. Below this pH, flux improved to 68 L/m^2/h at 9 bar for pH 2.5. However, when comparing the membrane performance in all tested pH values, pore size shrinkage occurred significantly at acidic conditions. Highest flux

was observed when normal seawater permeated through the membrane at pH 8. High flux was observed at basic pH for all pressures. Flux increased linearly at all individual pH with an increase in pressure confirming that no membrane fouling occurred during the experiments.

Figure 3 displays flux versus pressure for HYDRACoRe. Low flux was observed at acidic pH and a major change in flux was not observed during the entire tested pH values.

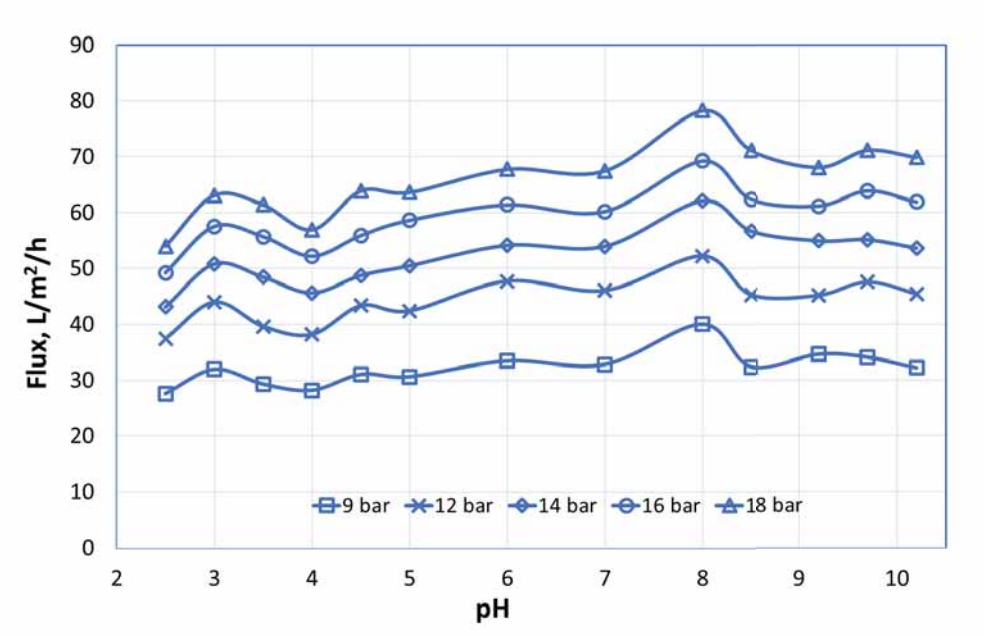

Figure 3. Flux versus pressure for HYDRACoRe with varying pH

Flux versus pressure for NF 270 is presented in Figure 4. Minimum flux was obtained at pH 3. An increase in flux was observed with an increase in feed pH.

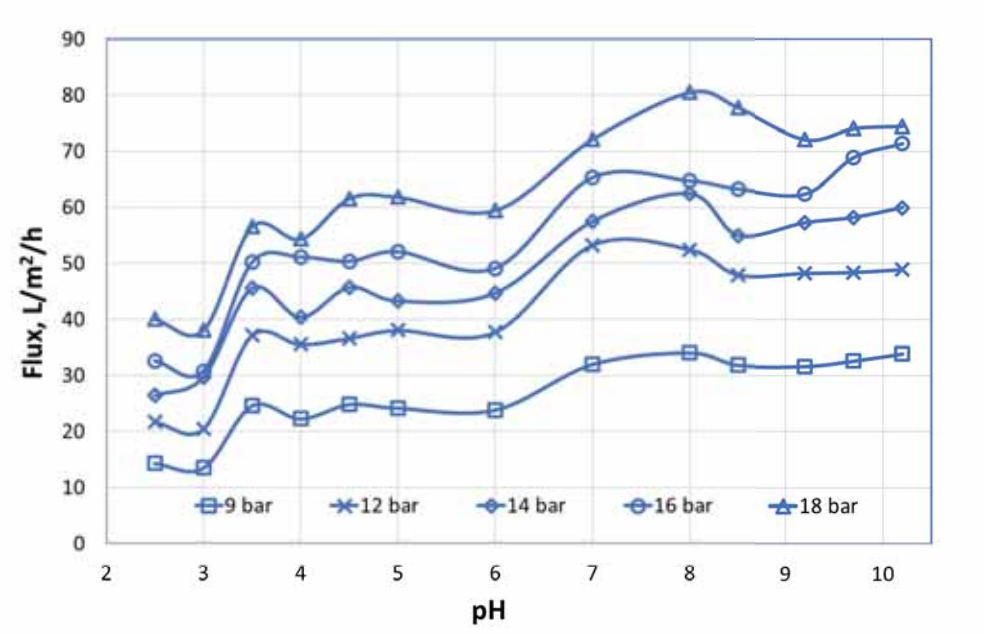

Figure 4. Flux versus pressure for NF 270

Flux for each membrane varies with the type of feed water and increases with increasing pressures. Maximum flux was attained at pH 8 with normal seawater as feed for all three membranes. This confirms that these membranes are designed to produce maximum flux when seawater is used as feed.

Highest flux was 163 L/m^2/h observed for ESNA as presented in Figure 2 and indicates more open pores for ESNA compared to HYDRACoRe and NF 270. ESNA and NF 270 membranes have a polyamide skin layer. However, they have different degrees of crosslinking that gives rise to different surface properties resulting in different flux and ion rejection pattern as a function of pH. Polyamide NF membranes consist of both carboxyl group (≡ COO^-) and amino groups (≡ NH^{3+}) and exhibit positive and negative surface charges depending on pH. At acidic conditions, protonation of amine occurs (≡NH_2 → ≡NH_3^+) resulting in increased pore size, thereby increasing flux. This explains a slight peak in flux in an acidic environment at pH 5 in Figure 2. At high pH, polyamide membrane matrix appears to be more expanded due to deprotonation of carboxyl group (≡COOH → ≡COO-) resulting in higher flux as in the case of ESNA and NF 270.

HYDRACoRe membranes are made of sulfonated polyethersulfone and have −SO_2 groups in the polymeric sulfone. This is quite stable due to attraction of resonating electrons between

adjacent aromatic groups, and the presence of repeating phenylene rings create steric hindrance to the rotation [27]. Both these characteristics lead to molecular immobility and wide pH tolerance [27]. Figure 3 also confirms that permeability of HYDRACoRe was quite stable over the tested pH range, except for a slight increase in flux for normal seawater at pH 8.

4.2 Effect of Feed pH on Ion Rejection

The retention of charged ions depends on ion valency, concentration, charge density, surface charge and chemical nature of the groups present on the membrane surface. Individual ion concentrations at different pressures and pH values in reject and permeate were measured for ESNA, HYDRACoRe and NF 270. An increase in ion rejection with an increase in pressure was observed in all samples.

4.2.1 Rejection of Monovalent Ions

Different membranes showed different rejection patterns even with small pH changes, which could be due to different surface characteristics of the three tested membranes. Figure 5 and Figure 6 display rejection of Cl^- and Na^+ at different feed pH values with increasing pressure for ESNA.

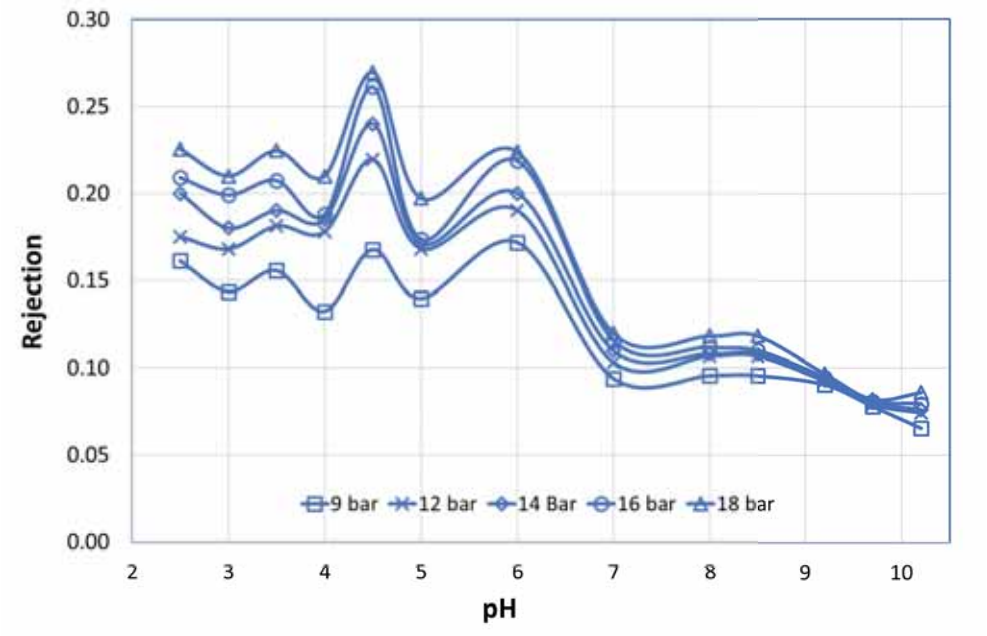

Figure 5. Cl^- rejection for ESNA

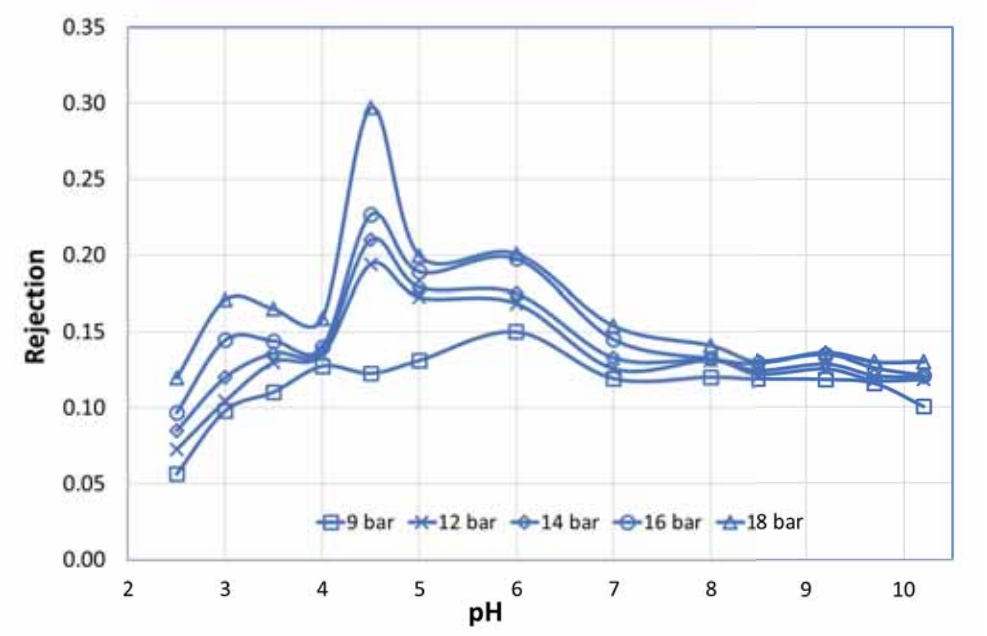

Figure 6. Na^+ rejection with varying pH for ESNA

Figure 5 and Figure 6 present low ion rejections of Na^+ and Cl^- in basic environment. It was observed that when flux increased, ion rejection decreased. In Figure 2, a flux minimum at pH 4.5 was observed whereas a peak in rejection at the same pH for Na^+ and Cl^- was observed in Figure 5 and Figure 6.

Figure 7 and Figure 8 show the rejection of Cl^- and Na^+ with HYDRACoRe.

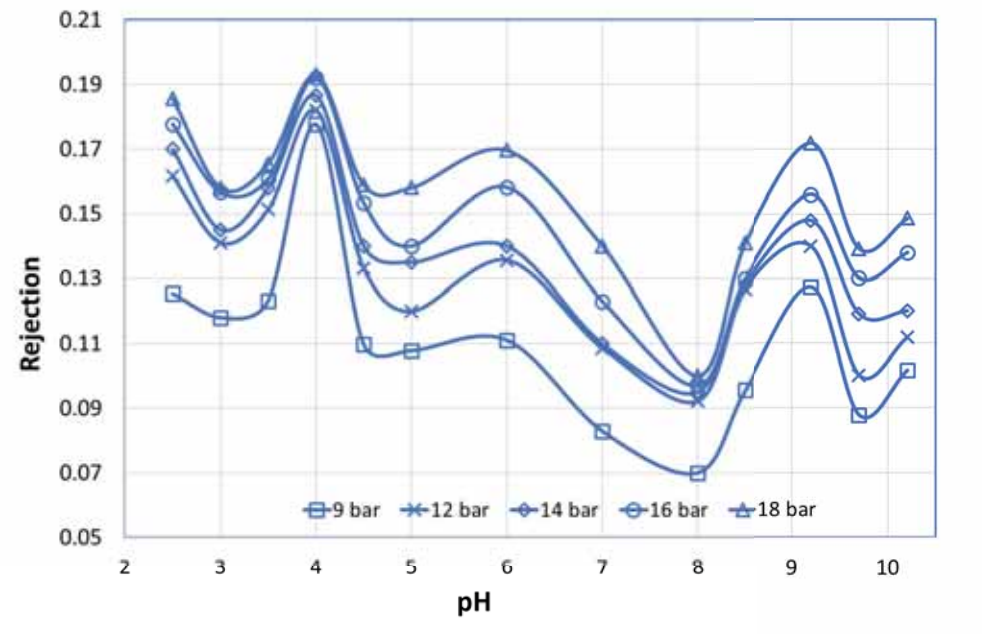

Figure 7. Cl^- rejection for HYDRACoRe at different feed pH

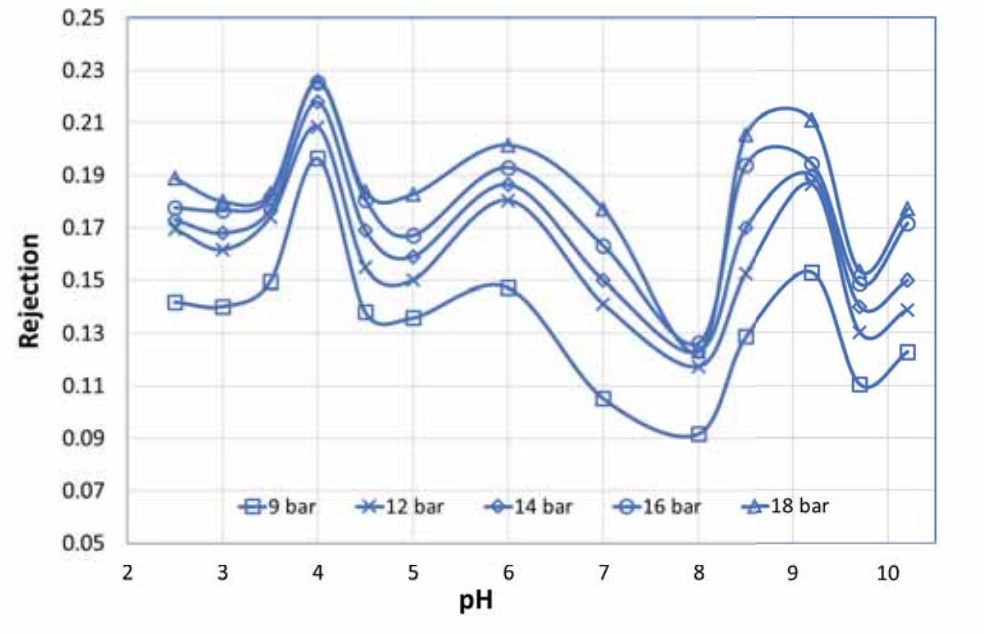

Figure 8. Na^+ rejection at different feed pH for HYDRACoRe

Na^+ and Cl^- rejection by HYDRACoRe show similar patterns. A slight decrease in flux with HYDRACoRe was observed at pH 4. However, a peak in monovalent ion rejections was observed at pH 4. The results confirm that Donnan potential influences ion rejection. In Figure 8, at pH 4, a peak in Na^+ rejection is observed, which could be either due to pore size reduction or by repulsion by the positive charge of the membrane. To maintain electroneutrality at pH 4, more Cl^- is rejected according to Figure 7.

Monovalent ion rejection for NF 270 is displayed in Figure 9 and Figure 10.

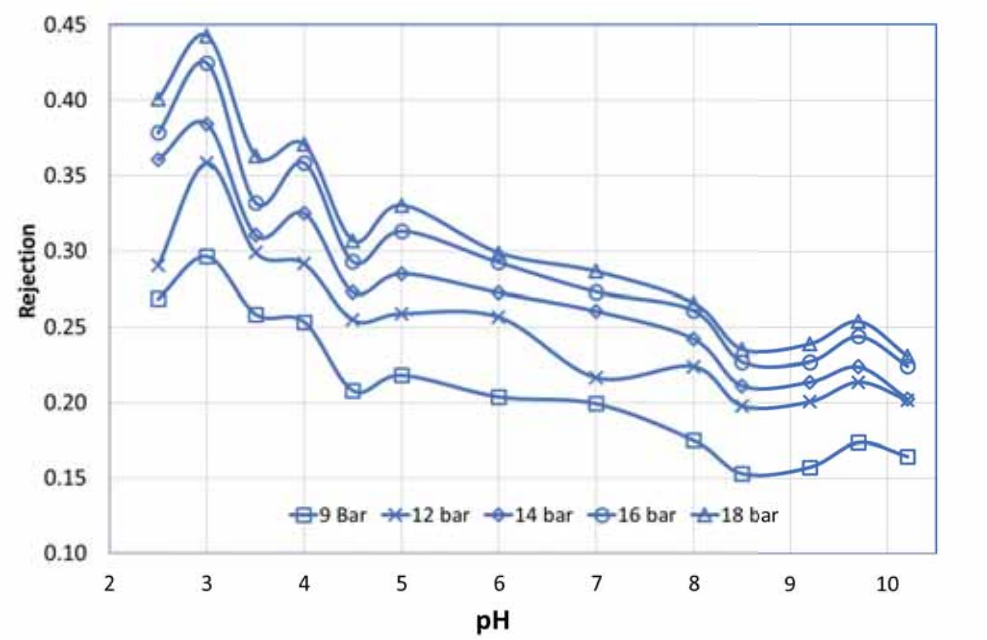

Figure 9. Cl^- rejection at different feed pH for NF 270

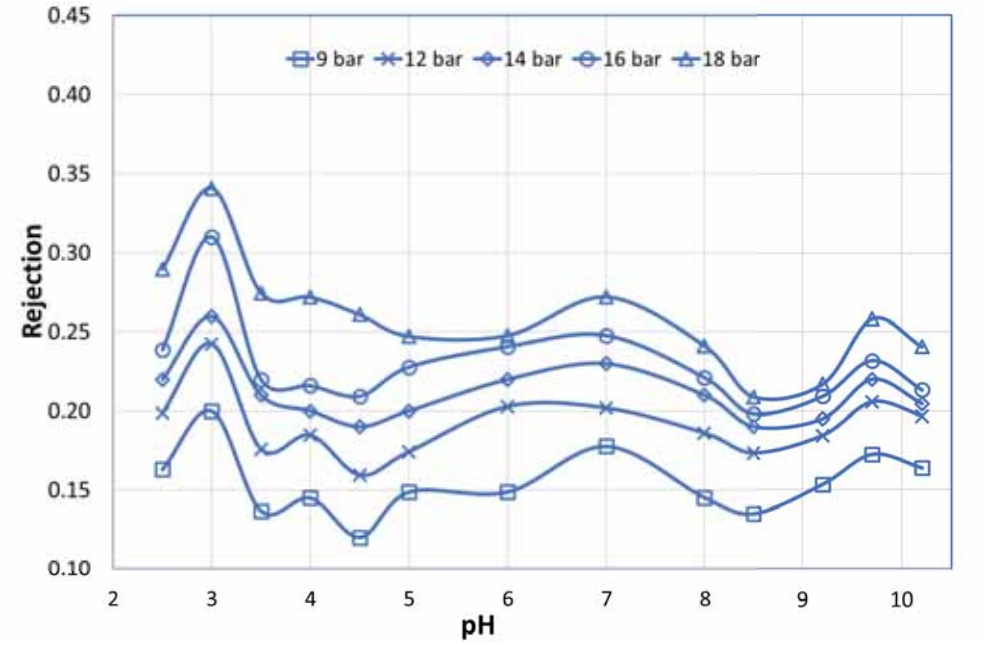

Figure 10. Na^+ rejection at different feed pH for NF 270

It has been confirmed that the isoelectric point for NF 270 is close to pH 5 and salt rejection is minimum at pH 4 [28]. The performed experiments confirmed that Na^+ and Cl^- rejections were low at pH 4.5 for NF 270, close to the isoelectric point.

4.2.2 Rejection of Multivalent Ions

Figure 11, Figure 12 and Figure 13 present the rejection of Mg^{2+} for ESNA, HYDRACoRE and NF 270 membranes.

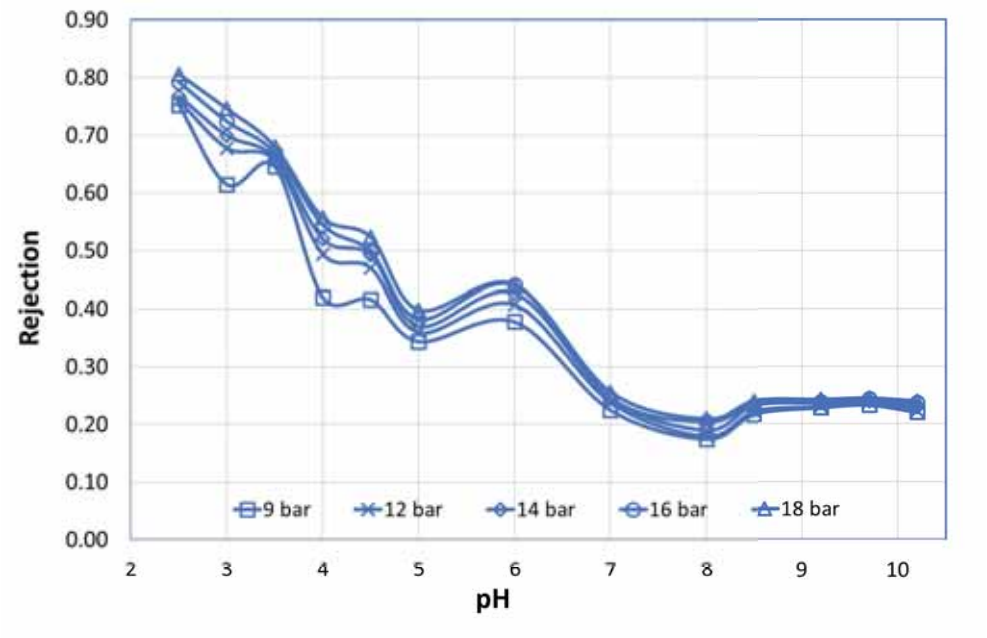

Figure 11. Mg^{2+} rejection at different feed pH for ESNA

Highest Mg^{2+} rejection was observed at the lowest tested pH of 2.5 for ESNA. This confirms that the membrane is highly positively charged at acidic conditions and positive charges are reduced with increasing pH values. Rejection of more positively charged Mg^{2+} resulted in permeation of more Na^{+} through the membrane to maintain electroneutrality between two phases of the membrane. This means low rejection of Na^{+} at acidic pH. This explains the comparatively low rejection of Na^{+} in Figure 6.

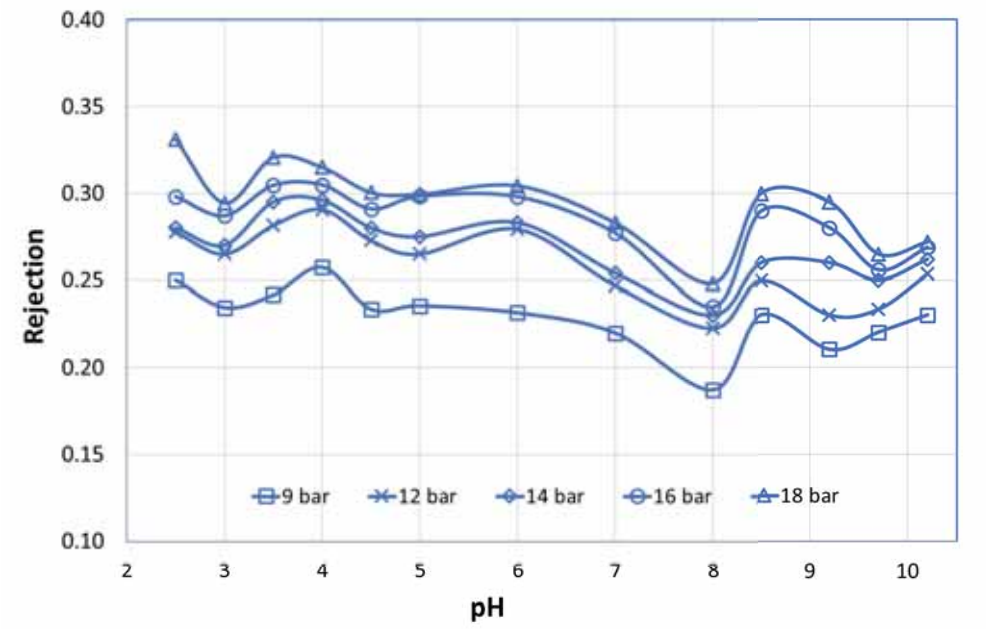

Figure 12. Mg^{2+} rejection at different feed pH for HYDRACoRe

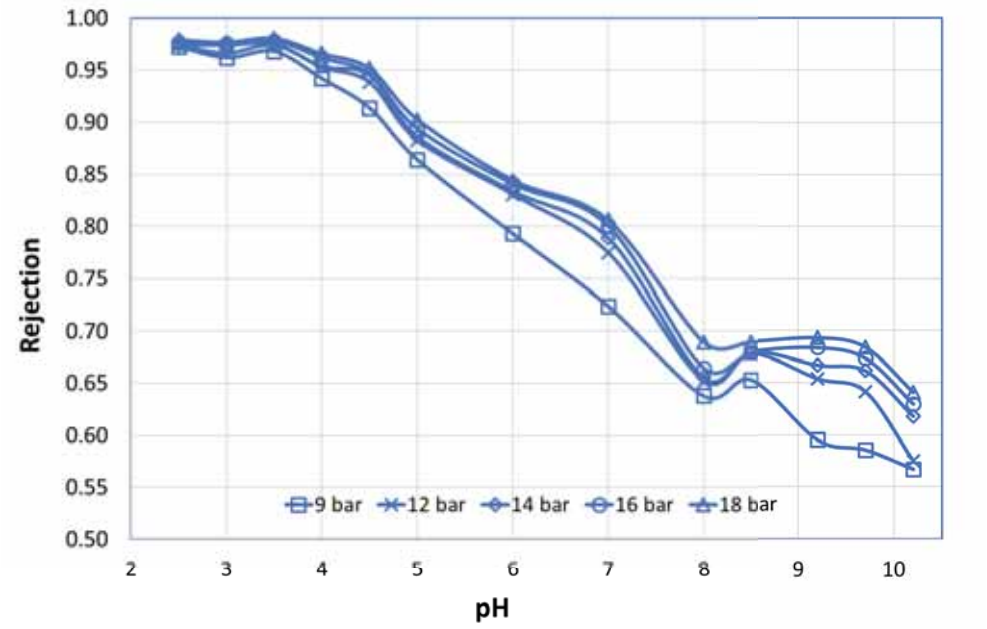

Figure 13. Mg^{2+} rejection at different feed pH for NF 270

Figure 5 - Figure 13 present ion rejections as a function of pH. SO_4^{2-} is generally not present in PW and is not evaluated in this research. Results show that ion rejection by HYDRACoRe was less than 35 % for all ions confirming that the effect of pH on HYDRACoRe was weak or less at all pH. Highest Mg^{2+} rejection was 98 % observed at pH 2.5 for NF 270 and decreased to 56 % at pH 10.2. There was only a slight effect of pressure on Mg^{2+} rejections for ESNA and NF 270 since the rejection was almost the same at all operating pressures, whereas a slight increase in Mg^{2+} rejection was observed for HYDRACoRe.

Figure 14 shows the rejection of Ca^{2+} for ESNA. The highest Ca^{2+} rejection was observed at low pH. A depression in rejection of Ca^{2+} was observed between pH 5 and pH 7. The rejection increased at pH 8 (normal seawater) and slightly decreased at pH > 8.

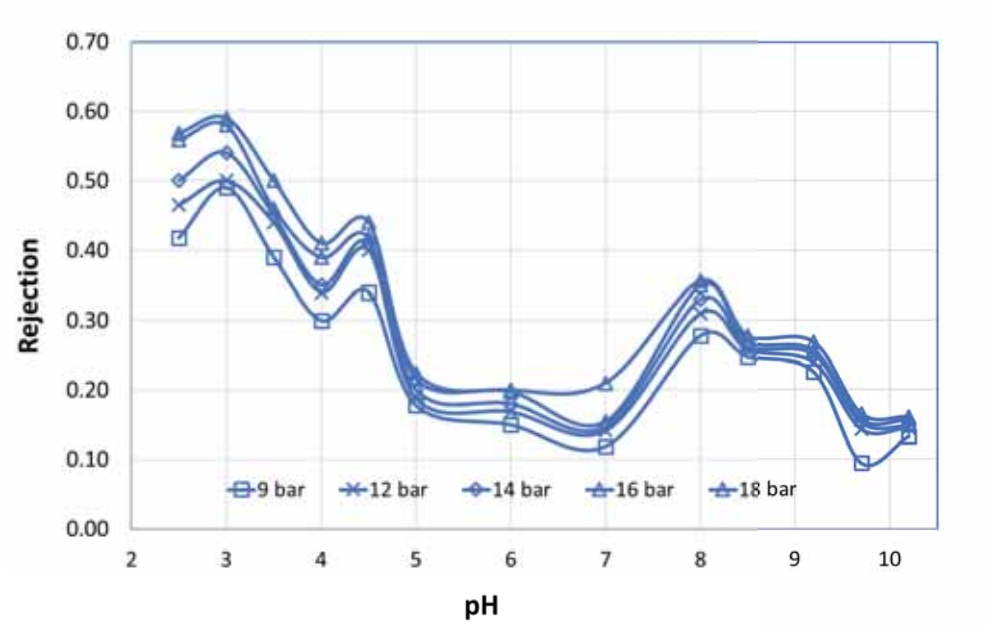

Figure 14. Ca^{2+} rejection observed for ESNA at different feed pH

During membrane performance, electrostatic repulsion between the membrane and cations determines ion rejection. When Na^+, Ca^{2+}, and Mg^{2+} are present in the feed, co-ion rejection competition occurs. Ions with low hydration energy and high mobility are prone to permeate and Na^+ with lowest hydration free energy passes easily through the membrane to balance the charge on both sides. Ca^{2+} has higher hydration energy than Na^+ but lower than Mg^{2+}. Hence, Mg^{2+} will be rejected more than Ca^{2+} as confirmed by Figure 11 and Figure 14. Hydration free

energy of Na^{+}, Ca^{2+} and Mg^{2+} are -365 KJ/mol, -1592 KJ/mol and -1922 KJ/mol, respectively [29]. Similar rejection for Ca^{2+} was observed for HYDRACoRe and NF 270.

Flux and rejections at different pH values may be caused by several mechanisms or combination of mechanisms. These include change in pore size due to change in conformation of the cross-linked polymer structure of the membrane or membrane swelling or shrinkage, difference in osmotic pressure due to addition of HCl or NaOH, changes in electroviscous effect resulting in variation in water permeability, co-ion and counter-ion interactions, Donnan effect, steric or sieving effect, convection and diffusion.

4.2.3 Pore Radius (r_p) Calculations using Spiegler-Kedem and SHP Models

Characterization of the membrane physicochemical properties such as contact angles, surface morphologies, and membrane surface zeta potentials are generally measured to determine the variations in ion rejections and flux permeation. In this research, membrane performance at different pH values has been analyzed by variations in r_p, calculated using Spiegler-Kedem and SHP models where the single independent variable approach was used.

The membrane transport parameters σ and P_s of each ion was calculated by fitting flux versus rejection in Equations 1 and 2 for the three tested membranes. To explain the difference in pore size, Mg^{2+} is chosen as a reference since the Stokes radius and hydration energy of Mg^{2+} is highest when compared to other ions present in seawater and is a divalent cation and thus will be attracted by the membrane surface. Table 4 shows reflection coefficients and solute permeabilities of Mg^{2+} for the three tested membranes at all observed pH values.

Table 4. Reflection coefficient and solute permeability of Mg^{2+} at varying pH

pH	ESNA		FilmTec		HYDRACoRe	
	σ (-)	P_s (m/s)	σ (-)	P_s (m/s)	σ (-)	P_s (m/s)
2.5	0.84	3.578*10^-6	0.98	6.258*10^-8	0.37	6.202*10^-6
3	0.85	6.629*10^-6	0.98	1.181*10^-7	0.32	5.921*10^-6
3.5	0.68	2.177*10^-6	0.98	1.625*10^-7	0.36	6.038*10^-6
4	0.70	9.823*10^-6	0.97	2.761*10^-7	0.33	4.319*10^-6
4.5	0.55	4.399*10^-6	0.97	5.053*10^-7	0.33	6.052*10^-6
5	0.41	6.409*10^-6	0.90	5.96*10^-7	0.33	5.985*10^-6
6	0.47	5.174*10^-6	0.86	9.053*10^-7	0.35	7.212*10^-6
7	0.26	8.316*10^-6	0.75	1.363*10^-6	0.34	8.581*10^-6
8	0.22	1.228*10^-5	0.67	2.088*10^-6	0.38	1.417*10^-5
8.5	0.24	7.763*10^-6	0.69	1.449*10^-6	0.29	4.383*10^-6
9.2	0.24	7.024*10^-6	0.73	3.059*10^-6	0.31	5.46*10^-6
9.7	0.24	5.666*10^-6	0.72	3.17*10^-6	0.28	5.312*10^-6
10.2	0.24	7.407*10^-6	0.65	3.038*10^-6	0.28	4.455*10^-6

Variations in pore size with pH for all membranes with respect to Mg^{2+} was calculated using SHP model by applying σ and P_s on Equations 5 - 9 for the three NF membranes. The resulted r_p for the three membranes are presented in Figure 15.

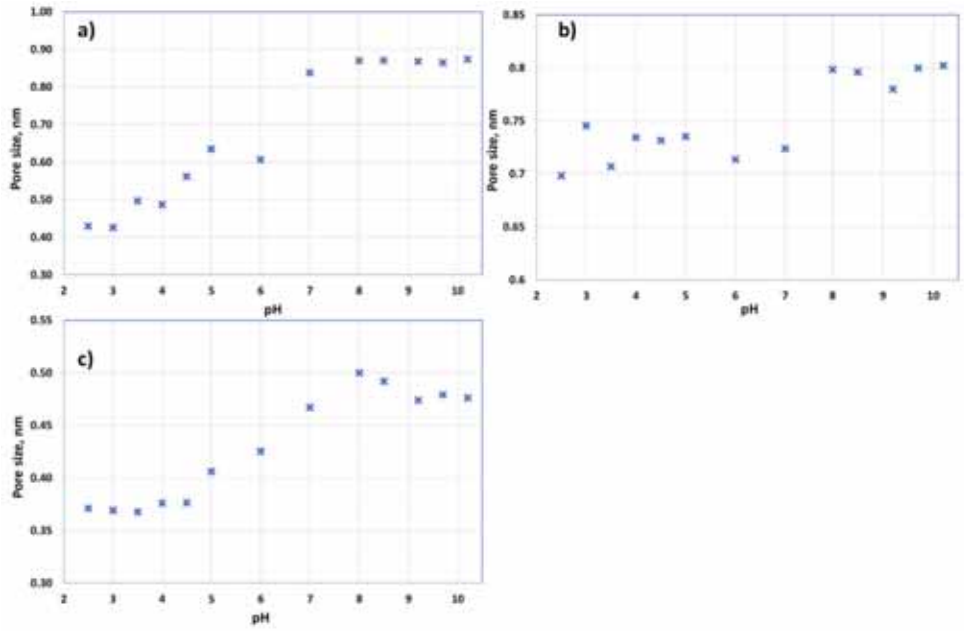

Figure 15. Variations in r_p with pH on a) ESNA b) HYDRACoRe c) NF 270

The results confirm that when pH is varied, pore size was reduced at acidic pH irrespective of the type of membrane, resulting in decreased flux and increased ion rejection. The original r_p is assumed to be at pH 8 when normal seawater was used as feed since all the three NF membranes are designed to operate with seawater. According to Figure 15, r_p is lowest at pH 3 and highest at pH 8 for ESNA. When r_p is lowest, flux is at a minimum with increased rejection. However, there is a deviation in flux and rejection behavior for ESNA. Minimum flux was observed at pH 4.5 with a peak in ion rejections at the same pH. While comparing the difference in pore sizes with pH, it should be noted that for ESNA and NF 270, the effect of pH was more distinct. For ESNA, r_p decreased from 0.87 nm to 0.42 nm while for NF 270, r_p decreased from 0.5 nm to 0.37 nm.

4.3 Effect of PW pH on *Smart Water* Production

Results obtained confirm that feed water with varying pH can be treated with NF membranes to produce permeate with modified ionic composition. Flux is high when feed pH is basic. Basic pH has the advantage of permeating more divalent ions, which are advantageous for carbonate reservoirs and is confirmed by Figure 11 and Figure 13. These figures show that when PW feed pH was high, more Mg^{2+} permeated through the membrane. A power consumption analysis on

the production of *Smart Water* from de-oiled PW for both carbonate and sandstone reservoirs has previously been confirmed [5].

4.4 Modeling Ion Rejection using ANN

In this research, operating pressure, pH, and flux are considered as variables and used as inputs to the ANN network. The number of neurons in each layer is varied for the three NF membranes to find the best ANN structure to predict ion rejection. The hidden layer includes seven neurons with tan-sigmoid function. MSE calculations were performed after each iteration to determine the best possible output and performance of the neural network. Since the data were randomly selected, for every set of neurons, the network was run several times.

Ion rejections are obtained as outputs and the input dataset of 65 samples each for the three tested NF membranes were divided into three sets randomly. 70 % of the dataset (45 samples) were regarded as train data, 15 % of the dataset as validation and 15 % of the data set was regarded for test data (10 samples each). The regression plot for ESNA with 7 neurons in the hidden layer is presented in Figure 16.

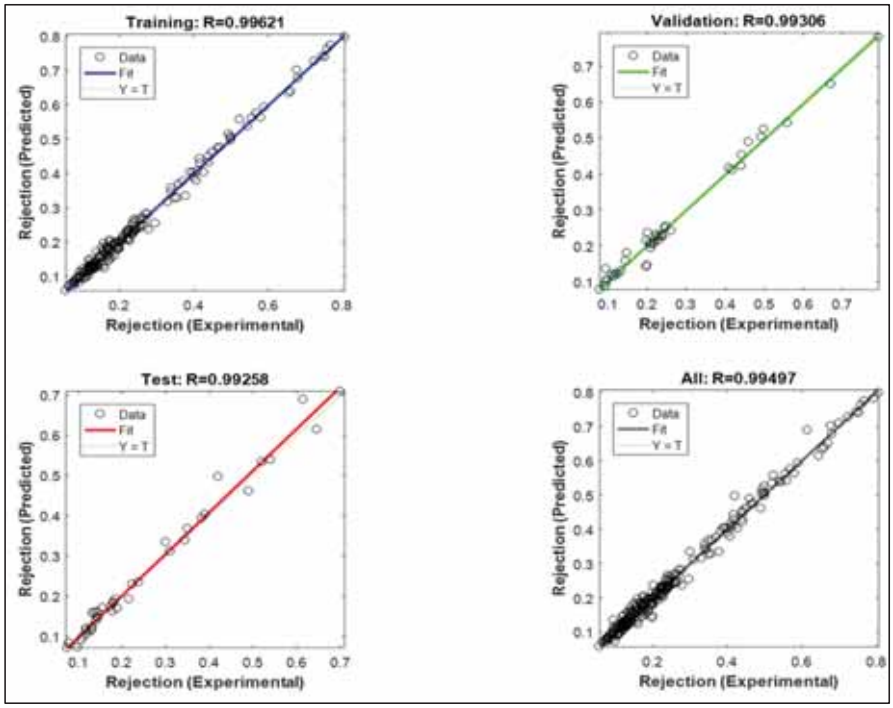

Figure 16. Regression plot between the experimental and predicted rejection values for ESNA with 7 neurons in the hidden layer

Figure 16 displays the network outputs with respect to targets used for training, validation and test. The regression plot shows that the R^2 value is 0.996 for training, confirming that the neural network is well trained with 45 samples. The data should fall along the 45 ° line for a perfect fit where the ANN outputs are equal to the target values provided. R^2 value for test data is also greater than 0.99, confirming that ANN predicted rejection values and experimental values are in close agreement, which signifies the ability of ANN in predicting major ion rejections if flux, pH and pressure are available.

In this work, seven neurons were selected with the highest accuracy and were compared by changing the transfer function between tansig, logsig and purlin functions. To optimize the neural network architecture, the computations started with one neuron as the initial guess and the number of neurons was increased after calculating the MSE according to Equation 10. Performance of ANN model with some selected network structures is presented in Table 5.

Table 5. Performance of ANN with different neuron and transfer functions

Membranes	No. of neurons in each layer	R^2	MSE			
			Cl^-	Na^+	Mg^{2+}	Ca^{2+}
ESNA	4	0.989	0.00014	0.00029	0.00049	0.00096
Filmtec	4	0.97	0.00087	0.00107	0.00086	0.01466
HYDRACoRe	4	0.93	0.00024	0.00035	0.00015	0.00135
ESNA	5	0.98	0.00012	0.00026	0.00056	0.00190
Filmtec	5	0.986	0.00057	0.00068	0.00043	0.00709
HYDRACoRe	5	0.94	0.00024	0.00037	0.00011	0.00100
ESNA	**7**	**0.995**	**0.00011**	**0.00031**	**0.00030**	**0.00053**
Filmtec	**7**	**0.992**	**0.00048**	**0.00052**	**0.00052**	**0.00393**
HYDRACoRe	**7**	**0.956**	**0.00022**	**0.00032**	**0.00011**	**0.00013**
ESNA	10	0.9925	0.00014	0.00029	0.00049	0.00096
Filmtec	10	0.99	0.00038	0.00036	0.00047	0.00374
HYDRACoRe	10	0.92	0.00029	0.00036	0.00015	0.00162

It was confirmed that tansig transfer function works best for predicting ion rejection compared to logsig and purelin transfer functions. The optimal number of 7 neurons in the hidden layer

was chosen (marked in bold in Table 5) after calculating R^2 and MSE for all four ions tested. A hidden neuron layer of 4, 5 and 6 also provided above 92 % for ESNA and NF 270 but a neuron combination of 7 provided highest R^2 for all three membranes and least MSE for ion rejection. ANN approach is data-driven and hence is specific for a particular membrane.

Conclusions

ANN quantitatively predicted the ion rejection without using any membrane properties such as pore radius, effective membrane thickness and membrane charge density. ANN is considered as a simple approach for multiple variables compared to membrane process models. An overall agreement was obtained for ANN predictions and experimental results for all three tested NF membranes.

A significant change in rejection was observed even with small pH changes. For divalent ions, a change in rejection was obvious between acidic and alkaline environments. Flux was higher in the basic environment. When flux increased with an increase in pH, the rejection of charged ions tends to decrease. Highest flux was observed for ESNA indicating a larger pore size than for HYDRACoRe and NF 270. A sharp decrease in Mg^{2+} rejection was observed in the basic environment for ESNA and NF 270. It was confirmed that pore size decreased with a decrease in feed pH using Spiegler-Kedem and SHP models.

Obtained results can be implemented in industrial scale-up for predicting water recovery and ions rejection when PW or other saltwater with varying pH is treated by membranes. These findings are crucial for optimal membrane system design and for a defined ion rejection as required for *Smart Water* production for EOR in carbonate and sandstone reservoirs. pH of PW can be adjusted accordingly for required ion composition in the permeate. For industrial PW applications, the ANN approach to predict NF ion rejection can be used, provided plant operating conditions data for selected feed compositions are available resulting in time and effort savings.

Symbols

R_{obs}	Observed rejection
σ	Reflection coefficient
P_s	Solute Permeability Coefficient, m/s
J_v	Water flux, $L/m^2/h$
V	Permeate volume, L
t	Filtration time, h

A	Effective membrane area, m^2
S_D, S_F	Steric Hindrance Factors for Diffusion and Filtration Flow
D	Diffusivity of i-th ion, m^2/s
r_s	Stokes radius, nm
r_p	Pore radius, nm
$A_k/\Delta x$	Ratio of Membrane Porosity to Membrane Thickness
C_f	Feed concentration, mg/L
C_p	Permeate concentration, mg/L
C_c	Retentate concentrations, mg/L
t_i	i-th target value
a_i	Predicted value
n	Number of data
R^2	Statistical coefficient of determination

Acknowledgment

The authors acknowledge the Research Council of Norway and the industry partners, ConocoPhillips Skandinavia AS, Aker BP ASA, Eni Norge AS, Total E&P Norge AS, Equinor ASA, Neptune Energy Norge AS, Lundin Norway AS, Halliburton AS, Schlumberger Norge AS, Wintershall Norge AS, and DEA Norge AS, of The National IOR Centre of Norway for support.

REFERENCES

[1] Norwegian Oil and Gas industry, "Environmental work by the Oil and Gas Industry- Facts and development trends," 2016.

[2] T. Austad, "Water-based EOR in carbonates and sandstone: New chemical understanding of the EOR-potential using ¨ Smart water¨," in *Enhanced Oil Recovery Field Case Studies*, Sheng, J., Ed.; Gulf Professional Publishing: Houston, TX., 2013, pp. 301-335.

[3] S. Strand, E. J. Høgnesen and T. Austad, "Wettability alteration of carbonates- Effects of potential determining ions (Ca2+ and SO42-) and temperature," *Colloids and Surfaces A: Physicochem. Eng.Aspects,* vol. 275, pp. 1-10, 2006.

[4] R. R. Nair, E. Protasova, S. Strand and T. Bilstad, "Membrane performance analysis for smart water production for enhanced oil recovery in carbonate and sandstone reservoirs," *Energy and Fuels,* vol. 32, pp. 4988-4995, 2018.

[5] R. Nair, E. Protasova, S. Strand and T. Bilstad, "Produced water treatment with membranes for enhanced oil recovery in carbonate and sandstone reservoirs," *Proceedings of IOR 2017-19th European Symposium on Improved Oil Recovery, Stavanger, Norway,* no. DOI:10.3997/2214-4609.201700296, April 24-27, 2017.

[6] J. P. Ray and R. F. Engelhardt, Produced Water-Technological/environmental issues and solutions, 1992.

[7] M. Reed and S. Johnsen, Produced Water-2-Environmental issues and mitigation technologies, 1996.

[8] T. Puntervold and T. Austad, "Injection of seawater and mixtures with produced water into North Sea chalk Formation: Impact on wettability, scale formation, and rock mechanics caused by fluid-rock interaction," *SPE 111237,* 2007.

[9] O. Kedem and A. Katchalsky, "Permeability of composite membranes: Part 1. Electric Current, volume flow and flow of solutes through membranes," *Transactions of the Faraday Society,* pp. 1918-1953, 1963.

[10] O. Kedem and A. Katchalsky, "Thermodynamical analysis of the permeability of biological membranes to non-electrolytes," *Biochimica et Biophysica Acta,* pp. 229-246, 1958.

[11] C. K. Diwara, S. Lo, M. Rumeau, M. Pontie' and O. Sarr, "A phenomenological mass transfer approach in nanofiltration of halide ions for a selective defluorination of brackish drinking water," *Journal of Membrane Science,* pp. 103-112, 2003.

[12] Z. Murthy and S. Gupta, "Estimation of mass transfer coefficient using a combined nonlinear membrane transport and film theory model," *Desalination,* no. 121, pp. 131-137, 1997.

[13] M. Dornier, M. Decloux, G. Trystram and A. Lebert, "Dynamic modeling of crossflow microfiltration using neural networks," *Journal of Membrane Science,* Vols. 263-273, p. 98, 1995.

[14] H. Al-Zoubi, N. Hilal, N. Darwish and A. Mohammad, "Rejection and modeling of sulphate and potassium salts by nanofiltration membranes: Neural network and Spiegler-Kedem model," *Desalination,* pp. 42-60, 2007.

[15] W. Bowen, M. Jones and H. Yousef, "Dynamic ultrafiltration of proteins- A neural network approach," *Journal of Membrane Science,* pp. 225-235, 1998.

[16] S. Bandini, J. Drei and D. Vezzani, "The role of pH and concentration on the ion rejection in polyamide nanofiltration membranes," *Journal of Membrane Science,* pp. 65-74, 2005.

[17] F. Donnan, "Theory of membrane equilibria and membrane potentials in the presence of non-dialysing electrolytes. A contribution to physical.chemical physiology," *Journal of Membrane Science,* no. 100, pp. 45-55, 1995.

[18] W. R. Bowen, A. W. Mohammad and N. Hilal, "Characterisation of nanofiltration membranes for predictive purposes- Use of salts, uncharged Solutes, atomic force microscopy," *Journal of Membrane Science,* pp. 91-105, 1997.

[19] J. Schaep, C. Vandecasteele, W. Mohammad and R. Bowen, "Modeling the retention of ionic components for different nanofiltration membranes," *Separation and Purification Technology 22-23,* pp. 169-179, 2001.

[20] K. Spiegler and O. Kedem, "Thermodynamics of hyperfiltration (reverse osmosis): Criteria for efficient membranes," *Desalination,* pp. 311-326, 1966.

[21] S.-I. Nakao and S. Kimura, "Models of membrane transport phenomena and their applications for ultrafiltration data," *Journal of Chemical Engineering of Japan,* 1982.

[22] X. Wang, T. Tsuru, S.-i. Nakao and S. Kimura, "The electrostatic and steric-hindrance model for the transport of charged solutes through nanofiltration membranes," *Journal of Membrane Science,* pp. 19-32, 1997.

[23] X.-L. Wang, T. Tsuru, M. Togoh, S.-I. Nakao and S. Kimura, "Evaluation of pore structure and electrical properties of nanofiltration membranes," *Journal of Chemical Engineering of Japan,* 1994.

[24] R. Bowen and W. Mohammad, "Diafiltration by nanofiltration: Prediction and optimization," *AIChE Journal,* no. 44, pp. 1799-1812, 1998.

[25] W. Bowen, J. S. Welfoot and P. Williams, "Linearized transport model for nanofiltration: Development and Assessment," *AIChE Journal,* 2002.

[26] M. H. Beale, M. T. Hagen and H. Demuth, Neural networks ttoolbox (TM)- Users guide, The MathWorks, Inc., 2018.

[27] M. Cheryan, Ultrafiltration and microfiltration handbook, USA: CRC Press, 1998.

[28] M. Manttari, A. Pihlajamaki and M. Nystrom, "Effect of pH on hydrophilicity and charge and their effect on the filtration efficiency of NF membranes at different pH," *Journal of Membrane Science,* pp. 311-320, 2006.

[29] B. Tansel, "Significance of thermodynamic and physical characteristics on permeation of ions during membrane separation : Hydrated radius, hydration free energy and viscous effects," *Separation and Purification Technology 86,* pp. 119-126, 2012.

Appendix 4 – Paper IV

Paper IV

Implementation of Spiegler - Kedem and Steric Hindrance Pore Models for Analyzing Nanofiltration Membrane Performance for Smart Water Production

Remya Ravindran Nair, Evgenia Protasova, Skule Strand, Torleiv Bilstad

Membranes, 2018, 8 (3), 78

DOI:org/10.3390/membranes8030078

membranes

MDPI

Article

Implementation of Spiegler–Kedem and Steric Hindrance Pore Models for Analyzing Nanofiltration Membrane Performance for Smart Water Production

Remya R. Nair [1,*], Evgenia Protasova [1], Skule Strand [2] and Torleiv Bilstad [1]

[1] Department of Chemistry, Bioscience and Environmental Engineering, University of Stavanger, Kjell Arholmsgate 41, 4036 Stavanger, Norway; evgy.pro@gmail.com (E.P.); torleiv.bilstad@uis.no (T.B.)
[2] Department of Energy and Petroleum Engineering, University of Stavanger, Kjell Arholmsgate 41, 4036 Stavanger, Norway; skule.strand@uis.no
* Correspondence: remya.nair@uis.no

Received: 8 August 2018; Accepted: 31 August 2018; Published: 6 September 2018

Abstract: A predictive model correlating the parameters in the mass transfer-based model Spiegler–Kedem to the pure water permeability is presented in this research, which helps to select porous polyamide membranes for enhanced oil recovery (EOR) applications. Using the experimentally obtained values of flux and rejection, the reflection coefficient σ and solute permeability P_s have been estimated as the mass transfer-based model parameters for individual ions in seawater. The reflection coefficient and solute permeability determined were correlated with the pure water permeability of a membrane, which is related to the structural parameters of a membrane. The novelty of this research is the development of a model that consolidates the various complex mechanisms in the mass transfer of ions through the membrane to an empirical correlation for a given feed concentration and membrane type. These correlations were later used to predict ion rejections of any polyamide membrane with a known pure water permeability and flux with seawater as a feed that aids in the selection of suitable nanofiltration (NF) for smart water production.

Keywords: nanofiltration; Spiegler–Kedem model; steric hindrance pore model; ion rejection; reflection coefficient; solute permeability; pure water permeability

1. Introduction

Nanofiltration (NF) membranes are pressure driven and selectively separate ions from mixed electrolyte solutes with low energy requirements compared to other desalination technologies. Smart water can be produced by modifying the ionic composition of seawater [1]. Smart water for EOR in carbonate and sandstone reservoirs require different ionic compositions depending on reservoir properties. Divalent ion-rich brine is required for carbonates, whereas a salinity of less than 5000 ppm is preferred for sandstones [1]. Production of smart water from seawater using membranes and the resulting power consumption was discussed in detail in our previous research [2]. However, selection of suitable membranes for smart water production is an extensive process. Thus, predicting membrane ion rejection limited to a couple of steps will avoid intensive membrane experiments.

Application of mathematical models to predict NF membrane performance for selective ion rejection is important for the optimal design and operation of NF membranes for smart water production. However, most modeling studies to date have considered only very dilute solutions and typically containing two or three types of ions. Modeling of concentrated solutions with multi-feed ions, such as seawater, predicts NF performance realistically with regard to industrial applications.

Spiegler–Kedem is a mass transfer-based model that relates flux to the concentration difference of a solute for a given membrane and solvent properties. The experimental data of flux versus

rejection for individual ions for different membranes is used to validate a model. The model is developed using the estimated equation parameters or transport parameters in the Spiegler–Kedem model and is correlated to the structural parameters of a membrane using a steric hindrance pore model. This approach simplifies membrane performance prediction for a given feed ionic composition and provides a consolidated approach to various interacting phenomena that are difficult to define mathematically for mass transport. For the correlations predicted in this research, the model fitting is carried out for a given feed concentration with a certain membrane type (polyamide) so that active mechanisms for all the membranes are similar and can be easily understood. The proposed correlations can be used for predicting ion rejection, thereby aiding the selection of suitable NF membranes for smart water production administered to both carbonate and sandstone reservoirs.

The principal objective of this research is to develop a predictive model to quantify the selectivity of porous polyamide membranes with high feed concentrations for smart water production. To develop such a model, membrane transport parameters and effective pore size were determined using the Spiegler–Kedem model and a steric-hindrance pore model.

2. Theory

2.1. Nanofiltration Membranes

NF membranes permit preferential transport of ions. Separation processes are differentiated based on membrane pore sizes. NF membranes have pore sizes between 0.1 and 1 nm [3] with a molecular weight cut off (MWCO) of 100–5000 Da [4]. Mass transfer through NF includes convection and solution-diffusion [5]. NF selectively separates divalent and monovalent ions. This is mainly due to the strong dependence on the operating parameters, pressure, and feed concentrations, and on the membrane structural parameters such as pore radius and the ratio of membrane porosity to membrane thickness, $A_k/\Delta x$. The separation mechanisms also depend on the hydrophilic/hydrophobic characteristics of the membrane [6].

The performance of the membranes is generally measured in terms of rejection R and flux J_v. Rejection is a measure of the membrane's ability to reject a solute. Membrane rejection is calculated using Equation (1).

$$R = \left(1 - \frac{C_p}{C_f}\right) \tag{1}$$

where C_p and C_f are the permeate and feed concentrations, respectively.

Flux J_v ($\mathrm{Lm^{-2}\ h^{-1}}$) is calculated using Equation (2)

$$J_v = \frac{V}{t \times A} \tag{2}$$

where V is the volume of the permeate collected in a given time interval t, and A is the membrane area.

2.2. Spiegler–Kedem Model

Transport of solutes through a charged membrane can be described using the principles of non-equilibrium thermodynamics where the membrane is considered a black box. This approach allows the membranes to be characterized in terms of only the reflection coefficient σ and solute permeability P_s. In a two-component system consisting of solute and water with flux J_v, the solute flux J_s is related by three membrane coefficients [7]:

1. The hydraulic permeability L_p.
2. The solute permeability P_s.
3. The reflection coefficient σ.

The relation between J_v and J_s and the membrane coefficients is given by Equations (3) and (4) as introduced by Kedem and Katchalsky [8].

$$J_V = L_p(\Delta P - \sigma\Delta\pi) \tag{3}$$

$$J_s = P_s\Delta C_s + (1-\sigma)J_v\, C_m \tag{4}$$

where $\Delta C_s = C_m - C_p$, and C_m is the solute concentration at the membrane surface. ΔP is the pressure difference between the feed and permeate, and $\Delta\pi$ is the osmotic pressure difference of the two fluids. According to Equation (4), the solute flux is the sum of diffusive and convective terms. Transport of the solute by convection is due to an applied pressure gradient across the membrane. The concentration difference on the membrane side and the permeate results in transport by diffusion.

When a high concentration difference exists between the retentate and the permeate, the Spiegler–Kedem model can be used [5], as in this research. The solute permeability coefficient P_s and reflection coefficient σ can be obtained by fitting experimental values of solute rejection versus flux, according to the Spiegler–Kedem model as represented by Equations (5) and (6).

$$R_{\text{obs}} = \sigma\,\frac{(1-F)}{1-\sigma F} \tag{5}$$

where

$$F = \exp\,(-\frac{1-\sigma}{P_s}J_{v)} \tag{6}$$

F is a dimensionless parameter that depends on the reflection coefficient, solvent flux, and solute permeability coefficient. The reflection coefficient represents the rejection capability of a membrane. No rejection occurs when $\sigma = 0$ and 100% rejection occur when $\sigma = 1$ [9]. Also, σ can be considered to represent the maximum rejection at an infinite volume flux.

Permeability can be defined as the flux of a solute or solvent through the membrane per unit driving force. P_s is the overall solute permeability coefficient.

The Spiegler–Kedem model is based on irreversible thermodynamics to describe transport when the membrane structure and transport mechanism within the membrane is not fully understood [10]. The Spiegler–Kedem model is generally applied when there are no electrostatic interactions between the solute and the membrane such as when the membrane is uncharged or when the solute is neutral. NF membranes are mostly negatively or positively charged. Many authors have used this model with charged NF membranes [6,11] and suggested that σ and P_s depend on the effective membrane charge and concentration of the feed solution. The effect of membrane charge is, however, neglected in this research for analyzing membrane performance at high feed concentrations.

The following assumptions were made while using the Spiegler–Kedem model in this research:

(1) The driving forces are pressure and concentration gradients.
(2) The model predicts the transport of the solute and solvent through the membrane irrespective of the type of solute, charge, solvent, and membrane.
(3) Membrane fouling and membrane sensitivity towards chemicals such as chlorine, effects of temperature, and pH are not considered.

2.3. Steric Hindrance Pore Model (SHP)

Structural parameters of the membranes were estimated using the SHP model developed by Nakao and Kimura [12] for the separation of aqueous solutions of a single organic solute by ultrafiltration membranes and was later successfully used for NF membranes by researchers such as Wang et al. [13]. According to the model, transport of spherical ions through cylindrical pores

hindered by frictional forces and the steric effect are considered. Following this model, the membrane parameters σ and P_s are given as

$$\sigma = 1 - S_F \{1 + (16/9)q^2\} \quad (7)$$

$$P_s = D \times S_D(A_k/\Delta x) \quad (8)$$

where

$$S_D = (1-q)^2 \quad (9)$$

$$S_F = 2(1-q)^2 - (1-q)^4 \quad (10)$$

and

$$q = \frac{r_s}{r_p} \quad (11)$$

where S_D and S_F are the steric hindrance factors for diffusion and convection respectively. D is diffusivity, $A_k/\Delta x$ is the ratio of membrane porosity to membrane thickness, r_s is the Stokes radius of the solute, and r_p is the pore radius. The Stokes radii used for calculations [14,15] are presented in Table 1.

Table 1. Stokes radii of major ions used for calculations [14,15].

Ions	Cl^-	Na^+	SO_4^{2-}	Ca^{2+}	Mg^{2+}
Stokes Radius (nm)	0.121	0.184	0.231	0.310	0.348

The stability of membranes is usually tested to assure the reliability of the experiments. This is mainly performed by measuring the pure water permeability ($L_p = J_v/\Delta P$) of the membranes. The pure water permeability L_p is also expressed by Hagen–Poiseuille in the pore model and is defined as

$$L_P = r_p^2\left(\frac{A_k}{\Delta x}\right)/8\mu \quad (12)$$

where μ is the viscosity.

3. Experimental Methods

Experiments were performed with a lab-scale membrane unit consisting of low-pressure and high-pressure pumps, a pressure valve, a pressure gauge, and two prefilters with 20 µ and 5 µ pore size as pre-treatment units upstream of the NF. One membrane is operated at a time and the retentate and permeate were recirculated to a 100 L feed tank to retain identical feed concentrations. The experiments were performed at room temperature with pure water and seawater. The applied pressure across the membranes ranged from 9 bar to 18 bar. Three trials were performed for each membrane with both pure water and seawater as feed. Pre-filtered seawater used for membrane experiments had total dissolved solids (TDS) of 30,400 mg/L, conductivity of 47.5 mS/cm, and pH at 7.9.

Prior to the experiments, the membranes were washed with pure water to remove any membrane preservatives. Eight different membranes with spiral wound configurations from two manufacturers (Nitto Hydranautics, Oceanside, CA, USA and Dow Filmtec, Oceanside, CA, USA) were used for the experiments and the membrane characteristics are provided in Table 2. NF 270 and SR 90 were from Dow Filmtec while all other six membranes were from Nitto Hydranautics. These commercially available membranes were negatively charged since their surface layers were made of polyamide or sulfonated polysulphone.

Table 2. Membrane characteristics as provided by the suppliers.

Membranes	HYDRACoRe10	HYDRACoRe50	NF 270	SR 90	ESNA	NANO-SW	LFC3	HYDRApro501
Material	Sulphonated Polyethersulfone				Composite Polyamide			
pH range	2–11		3–10		2–10	3–9	2–10.6	2–11
Area (m^2)	2.3		2.6				2.3	

MWCO of HYDRACoRe10 and HYDRACoRe50 are 3000 and 1000 Daltons, respectively.

Individual ion concentrations in the feed, permeate, and retentate was measured using ion chromatography (Dionex^{TM} ICS-5000+ DP, from Thermo Fisher Scientific, Waltham, MA, USA). TDS and conductivity were measured using a TDS meter VWR collection CO3100N and pH by VWR Phenomenal pH 1100 L (both from VWR International Limited, Leicestershire, UK)

All membranes, except for HYDRApro 501, had a maximum operating temperature of 45 °C. For HYDRApro 501, the operating temperature was pressure dependent: 41 bar at 65 °C and 14 bar at 90 °C. Maximum operating pressure for the rest of the membranes ranged from 41–41.6 bar according to the manufacturers.

Pure water permeability (L_p) was experimentally determined by plotting flux J_v versus transmembrane pressure ΔP and is represented by Lm^{-2} h^{-1} bar^{-1}. The slope corresponding to each linear line determined the pure water permeability [10]. The hydraulic properties of the studied membranes were analyzed by measuring water flux as a function of pressure. Membrane water permeability was evaluated after achieving a steady-state condition with stable flux after operating the membranes for about 30 min.

4. Results and Discussion

4.1. Pure Water Permeability

Figure 1 shows the dependency of operating pressure on flux through eight membranes. A linear relation was obtained for water flux as a function of operating pressure. According to Figure 1, the pure water permeability of the membranes decreased in the sequence HYDRACoRE 10 > ESNA > NF 270 > HYDRACoRe 50 > SR 90 > NANO-SW > LFC3 > HYDRApro 501.

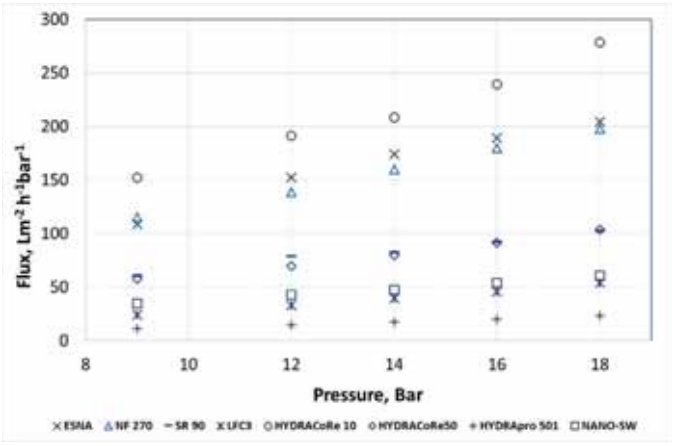

Figure 1. Pure water flux as a function of operating pressure for eight different membranes.

LFC3 is a reverse osmosis membrane while HYDRApro 501 is used specifically for industrial applications with difficult feed streams, according to the manufactures. The permeabilities of these two membranes were lowest among the tested membranes. Thus, only pure water permeability

experiments were performed for LFC3 and HYDRApro 501 membranes and these two membranes were not considered for further calculations of membrane transport parameters.

Relatively high flux was obtained for the other six membranes. High fluxes of these NF membranes at low pressure confirmed that NF membranes can be used as in energy saving compared to reverse osmosis membranes. Table 3 shows the water permeability of membranes when pure water and seawater were used as the feed.

Table 3. The permeability of membranes with different feed solutions.

Membranes	Pure Water (L m^{-2} h^{-1} bar^{-1})	Seawater (L m^{-2} h^{-1} bar^{-1})
HYDRACoRe 10	13.56	9.5
ESNA	10.52	7.9
NF 270	9.38	6.1
HYDRACoRe 50	5.15	3.8
SR 90	4.46	3.3
NANO-SW	3.27	1.9
LFC3	2.85	-
HYDRApro 501	1.32	-

L_p of the tested membranes did not vary throughout the experiments. Hence, the membranes could be considered stable during the experimental period.

The effect of feed concentrations on the membrane flux was evident from the difference in water permeability between the two solutions in Table 3. Pure water permeability was highest through HYDRACoRe10, suggesting more open pores compared to the other tested membranes.

4.2. Calculation of σ, P_s, and r_p Based on the Spiegler–Kedem and SHP Models

Experimental results for rejection and flux during permeation experiments with seawater were calculated using Equations (1) and (2). First, the transport parameters σ and P_s for each ion were estimated using a nonlinear least squares method by fitting the Spiegler–Kedem model by plotting rejection versus flux for six membranes. Coefficients selected were with above 95% confidence bounds. Second, the pore radius based on individual ion rejection data for every membrane was determined from its membrane parameter σ based on the steric hindrance pore model (SHP) using Equations (7), (10), and (11). The value for r_p (determined as = r_s/q) were calculated using the Stokes radius of the solute (r_s) as presented in Table 1.

Membrane parameters were estimated by fitting rejection versus flux using the Spiegler–Kedem equation. Figure 2 shows the dependency of the real rejection on volume flux for Na^+ for NANO-SW. The data points present the rejection values from the experiment and the solid line shows the values calculated using the Spiegler–Kedem equation with the best-fitted σ and P_s. Figure 2 shows that the theoretical curves are in close agreement with experimental values.

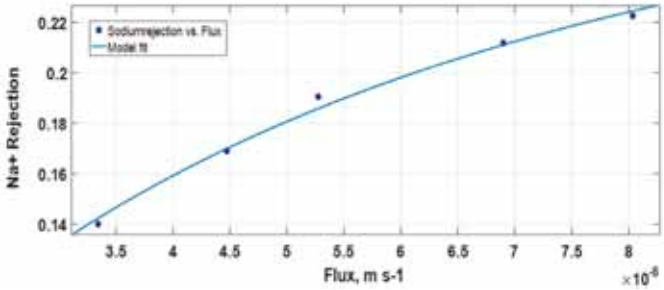

Figure 2. Rejection versus flux (m s^{-1}) for Na^+ for NANO-SW.

The effective membrane pore radius for each ion was calculated from the transport parameters σ and P_s based on the SHP model when seawater was used as the feed and is presented in Table 4.

Table 4. Calculated σ, P_s, and average r_p for ions for all tested membranes.

Membranes	Ions	σ (—)	P_s (m s^{-1})	q	r_p (nm)
ESNA	Cl^-	0.14	3.023×10^{-5}	0.30	0.41
	Na^+	0.14	1.701×10^{-5}	0.29	0.63
	SO_4^{2-}	0.66	6.211×10^{-6}	0.69	0.34
	Ca^{2+}	0.29	1.953×10^{-5}	0.44	0.71
	Mg^{2+}	0.24	1.26×10^{-5}	0.40	0.86
NF 270	Cl^-	0.18	2.105×10^{-5}	0.34	0.35
	Na^+	0.19	1.521×10^{-6}	0.35	0.52
	SO_4^{2-}	0.97	5.341×10^{-7}	0.93	0.25
	Ca^{2+}	0.41	1.879×10^{-5}	0.53	0.58
	Mg^{2+}	0.45	6.154×10^{-6}	0.56	0.62
SR 90	Cl^-	0.36	4.241×10^{-6}	0.50	0.24
	Na^+	0.25	7.313×10^{-6}	0.41	0.45
	SO_4^{2-}	0.99	4.859×10^{-7}	0.96	0.24
	Ca^{2+}	0.82	1.474×10^{-6}	0.79	0.39
	Mg^{2+}	0.92	3.276×10^{-7}	0.85	0.41
HYDRACoRe10	Cl^-	−0.01	-4.844×10^{-7}	-	-
	Na^+	0.03	3.115×10^{-5}	0.13	1.42
	SO_4^{2-}	0.16	1.728×10^{-5}	0.32	0.73
	Ca^{2+}	0.15	7.254×10^{-5}	0.31	0.99
	Mg^{2+}	0.05	5.447×10^{-5}	0.16	2.15
HYDRACoRe50	Cl^-	0.17	1.329×10^{-5}	0.33	0.37
	Na^+	0.24	1.538×10^{-5}	0.40	0.46
	SO_4^{2-}	0.67	3.849×10^{-6}	0.70	0.33
	Ca^{2+}	0.32	5.928×10^{-6}	0.47	0.67
	Mg^{2+}	0.38	1.417×10^{-5}	0.51	0.68
NANO-SW	Cl^-	0.37	9.045×10^{-7}	0.50	0.24
	Na^+	0.29	4.439×10^{-6}	0.44	0.42
	SO_4^{2-}	0.99	3.298×10^{-8}	0.96	0.24
	Ca^{2+}	0.88	2.171×10^{-6}	0.84	0.37
	Mg^{2+}	0.93	3.471×10^{-7}	0.88	0.40

Table 4 shows that reflection coefficients and solute permeability vary for each ion. The pore radii of these membranes were calculated using the Stokes radius of each ion. It was earlier reported by Luo and Wan [16] that the r_p of NF 270 is 0.43 nm. The pore size of NF 270 was previously determined using atomic force microscopy by Hilal et al. [17] and suggested to be between 0.47–0.99 nm with a mean of 0.71 nm. An average pore size of 0.47 nm was determined for NF 270 using the SHP model in this research. The calculated pore size of NF 270 was in the same range as recorded by several researchers confirming the validity of the calculations. The results show that for these membranes, a pore size distribution was more likely than a fixed pore size, and the identification of an effective pore radius does not indicate the presence of geometrically defined pores in NF membranes.

According to Table 4, polyamide membranes showed better rejection for divalent ions since the reflection coefficient was high for divalent ions compared to monovalent ions. According to the obtained results, the Spiegler–Kedem model was able to fit the experimental data of flux versus rejection for all ions and for all membranes except for HYDRACoRe 10. For HYDRACoRe 10, negative Cl^- reflection coefficients were obtained for all performed trials with the model. This could be due to the very low rejection of Cl^- or probably a negative rejection of Cl^- even though it was not observed during experiments. Negative rejection implies that the system has more Cl^- in the permeate compared

to the feed. Negative rejection of an ion occurs when a higher concentration of that ion is present in the smaller permeate volume relative to the larger feed volume. Negative rejection is observed mostly at low operating pressures [18]. The results show that HYDRACoRe 10 membrane has a larger pore size than the usual NF range which explains the poor ion separation of HYDRACoRe 10.

Table 4 shows that membranes with larger pore sizes had lower reflection coefficients. In other words, membranes with higher pure water permeability had lower individual ion reflection coefficients. A relative pore size comparison was performed with Mg^{2+} since it is a divalent cation with the highest Stokes radius compared to other ions tested for pore radius calculations, along with the fact that Mg^{2+} is attracted by the negatively charged membrane (unlike $SO_4{}^{2-}$) and would therefore permeate the membrane easily if the pore size was appropriately large for the ion. Hence, with respect to Mg^{2+}, the pore size of the tested membranes was in the sequence HYDRACoRe 10 > ESNA > HYDRACoRe 50 > NF 270 > SR 90 > NANO-SW.

However, the high feed concentrations and the ionic interactions that occurred among unaccounted ions and major ions in seawater, along with the interactions between ions and the membrane, added to the overall complexity in separation mechanisms of NF membranes. This provides a challenge to any model based on high feed concentrations.

4.3. Selection of NF Membranes for Smart Water Production Using a Predictive Model

The ionic composition required for smart water depends mainly on the type of reservoir. For carbonate reservoirs, an NF membrane with a high rejection of divalent ions and low monovalent ion rejection should be selected. For sandstone reservoirs, low salinity is preferred. Thus, a membrane with moderate flux will be suitable, which results in low divalent ion permeation.

According to Equation (12), pure water permeability is a parameter that combines the structural properties of the membrane and is used as a critical parameter that determines the ion rejection of a membrane. The only other property that influences water permeability is the feed viscosity, as shown in Equation (12). During the experiments, the structural parameters remained the same provided temperature and pH of the feed are controlled. Several researchers [19,20] have established that temperature and pH affect the pore size and change the flux. In this research, the difference in viscosity between pure water and seawater was neglected when L_p was used for correlating the reflection coefficient and solute permeability of membranes.

Thus, according to Equation (12), pure water permeability was directly related to the structural parameters such as effective membrane pore radius, and to $A_k/\Delta x$ (ratio of membrane porosity to membrane thickness). It can be inferred that the transport parameters of a solute are related to the structural properties of a specific membrane, as shown in Equations (7)–(11). Knowing the transport parameters, it is possible to predict the rejection (R_{obs}) of a membrane using the Spiegler–Kedem model.

4.3.1. Relating L_p with σ and P_s

L_p versus σ and P_s of individual ions were plotted to find a relation between pure water permeability, reflection coefficient, and P_s. Transport parameters were calculated for four polyamide membranes, ESNA, NF 270, SR 90, and NANO-SW with varying L_p. These four membranes were chosen since:

(1) Table 4 shows that HYDRACoRe 10 had poor ion separation. HYDRACoRe 50, made of sulfonated polyethersulfone, was not used to have comparable membrane materials for the model.
(2) The L_p chosen for the plot to create the model was in the range required for smart water production. Pure water permeability higher than that of ESNA would have resulted in very low divalent ion rejection. Choosing a membrane with lower permeability than NANO-SW meant a tighter membrane leading to higher rejection for any flux and low recovery thereby increasing power consumption.

Figure 3a shows the pure water permeability of polyamide NF membranes versus σ and Figure 3b presents L_p versus solute permeability P_s of chloride for each membrane.

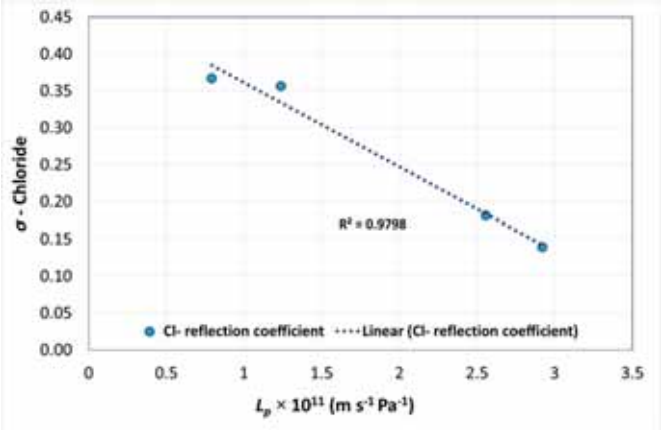

(a)

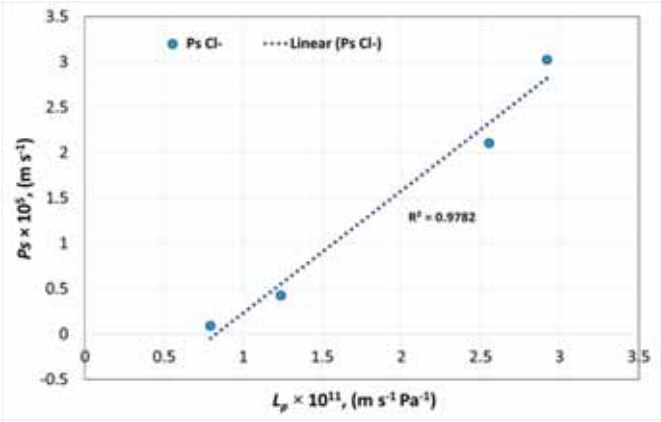

(b)

Figure 3. Pure water permeability versus (**a**) reflection coefficient and (**b**) solute permeability of chloride.

Figure 3a shows that with an increase in water permeability, the reflection coefficient of ions decreased whereas Figure 3b shows that the solute permeability increased. This confirmed that when the effective membrane pore radius increases, permeability increases, resulting in lower ion rejection.

Similarly, Figures 4a and 4b represents the pure water permeability of NF membranes versus σ and P_s of sodium for each membrane, respectively.

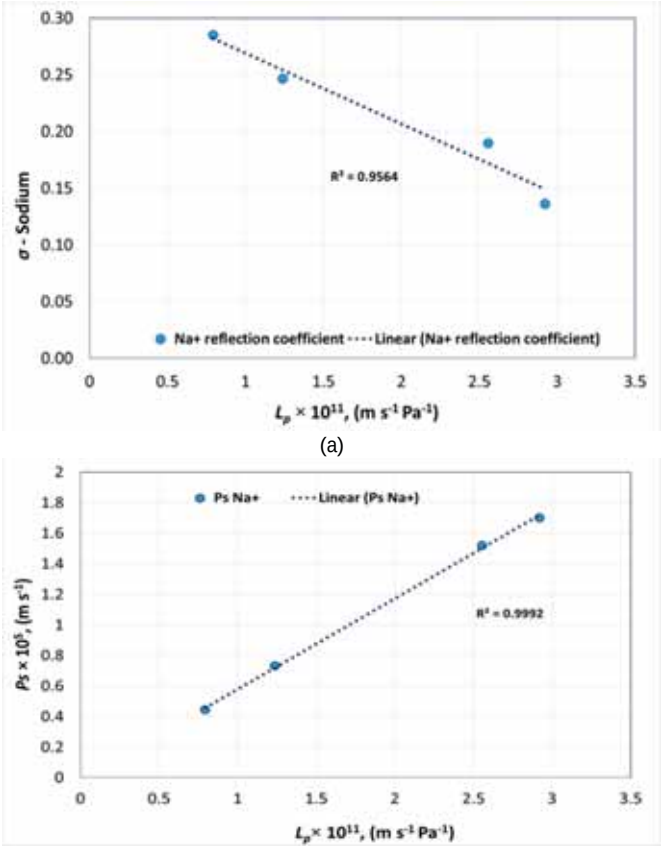

Figure 4. Pure water permeability versus (**a**) reflection coefficient and (**b**) solute permeability of sodium.

Figure 5a presents the pure water permeability of membranes versus σ and Figure 5b presents L_p versus P_s of sulfate for each membrane.

According to Figure 5a, the sulfate reflection coefficient shows a sharp decline with a small change in water permeability. This was mainly because of divalent anion on the negatively charged membrane surface. In Figure 5b showing pure water permeability versus P_s, the sulfate permeability remains unchanged for a range of permeabilities until approximately 2.6×10^{-11} m s^{-1} Pa^{-1}. After this value, a sharp increase was observed similar to the sharp decline in reflection coefficient of sulfate. A deviation in the reflection coefficient and solute permeability of SO_4^{2-} can be explained in relation to the thermodynamic properties of the ion. Ion permeation through a membrane is affected by the hydrated size and hydration free energy of the ions. During membrane transport, the transmembrane pressure creates shear stress that results in ions with low hydration energy being able to easily permeate through the membrane whereas ions with higher hydration energy and hydrated radius will be rejected by the membrane. SO_4^{2-} is a divalent anion with a hydration free energy of -1145 KJ/mol and a hydrated radius of 0.379 nm [21]. When the negatively charged ion is in contact with a negatively charged membrane surface, ion repulsion occurs, resulting in a higher rejection. Similarly, to maintain electroneutrality on both sides of the membrane, anions with a lower hydration energy and hydrated radius permeate through the membrane. Hence, Cl^- will be preferentially permeated compared to

SO_4^{2-} due to a lower hydration energy of −340 KJ/mol and hydrated radius of 0.324 nm. In Figure 5a, for ESNA, the reflection coefficient for SO_4^{2-} was lower at 0.66, whereas for the other three membranes, the SO_4^{2-} reflection coefficient was greater than 0.95. This can be explained with regard to the r_p calculated relative to Mg^{2+} as presented in Table 4. The pore radius r_p calculated was 0.86 nm, thus SO_4^{2-} permeated more for ESNA due to the steric effect resulting in lower σ and higher P_s compared to the other three membranes with a pore size close to 0.4 nm that is in close proximity to the SO_4^{2-} hydrated radius. Hence, a combination of steric effect and divalent anion-membrane repulsion prompted SO_4^{2-} rejection in NANO-SW, SR 90, and NF 270.

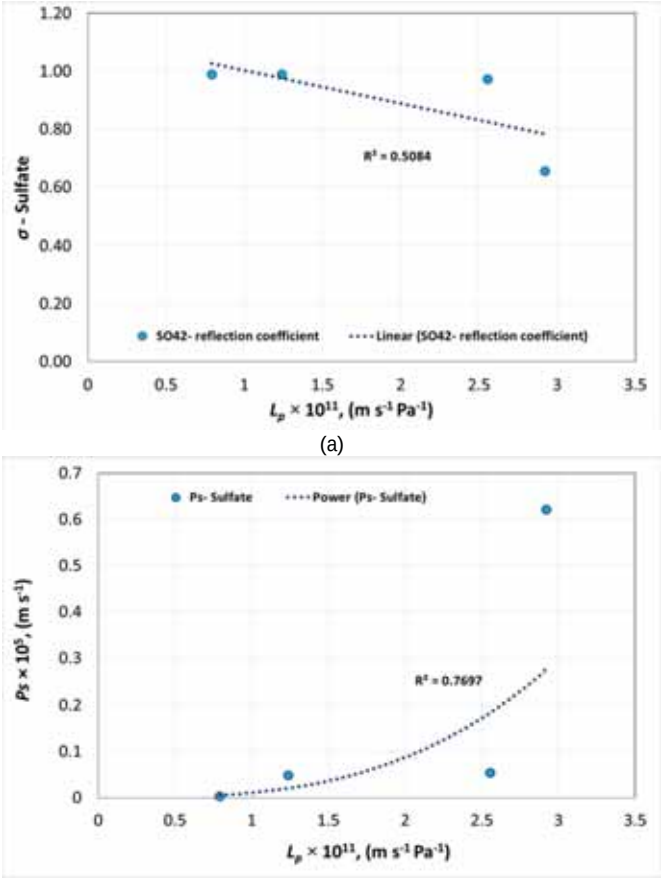

Figure 5. Pure water permeability versus (**a**) reflection coefficient and (**b**) solute permeability of sulfate.

Figure 6a,b shows the pure water permeability of membranes versus σ and P_s of calcium for each membrane, respectively.

According to Figure 6a, the reflection coefficient decreased gradually with increasing permeability. However, a small variation in calcium permeability was observed at lower permeabilities as shown in Figure 6b.

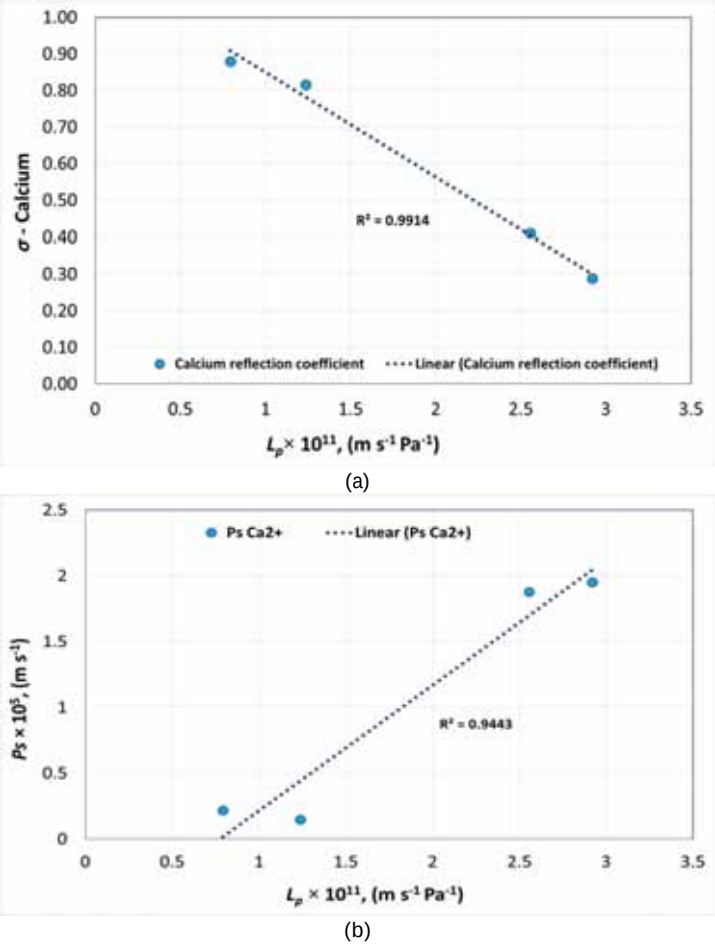

Figure 6. Pure water permeability versus (**a**) reflection coefficient and (**b**) solute permeability of calcium.

Figure 7a,b shows the pure water permeability of membranes versus σ and P_s of magnesium for each membrane, respectively.

According to Figure 7a, the reflection coefficient of Mg^{2+} deviated slightly from linear behavior for membranes with low pure water permeability. Mg^{2+} is a divalent cation with a hydration energy of −1922 KJ/mol with a hydrated radius of 0.470 nm [21]. According to Figure 7a,b, when pure water permeability decreased with respect to pore radius, the reflection coefficient of Mg^{2+} increased, confirming the higher rejection and lower permeation of Mg^{2+}. The deviation from linear behavior was observed for membranes (NANO-SW and SR 90) with a calculated $r_p \approx 0.4$ nm with respect to Mg^{2+}, where r_p is close to its hydrated radius.

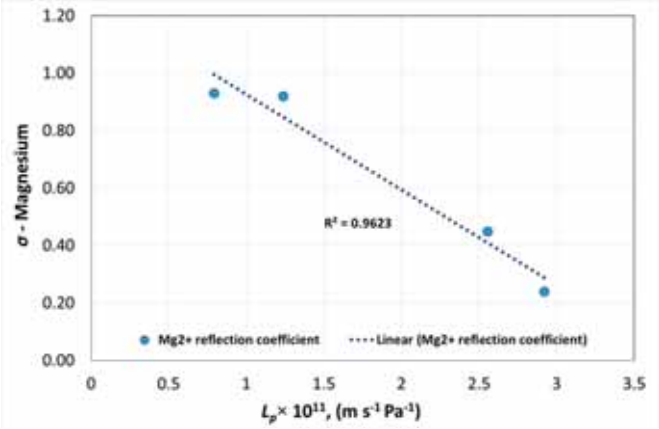

(a)

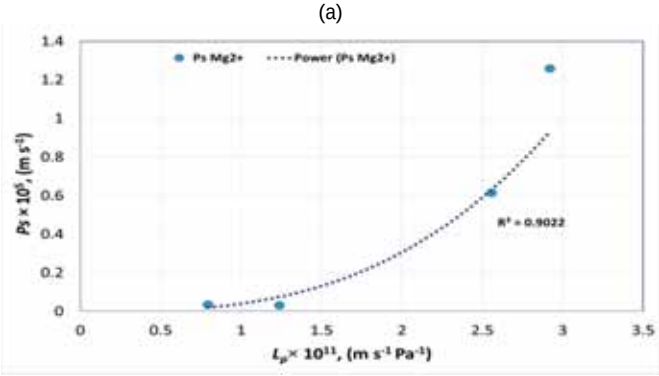

(b)

Figure 7. Pure water permeability versus (**a**) reflection coefficient and (**b**) solute permeability of magnesium.

4.3.2. Correlations for the Determination of σ and P_s of a Polyamide Membranes

The correlation developed was considered valid if the feed is seawater with no change in ionic concentration and viscosity for all tested polyamide membranes.

The following equations were obtained from Figures 3–7, to determine σ and P_s of each ion with a given pure water permeability L_{p0}.

$$\sigma_{Cl^-} = -1 \times 10^{10} \times L_{p0} + 0.4749 \quad (13)$$

$$\sigma_{Na^+} = -6 \times 10^{9} \times L_{p0} + 0.3318 \quad (14)$$

$$\sigma_{SO_4^{2-}} = -1 \times 10^{10} \times L_{p0} + 1.118 \quad (15)$$

$$\sigma_{Ca^{2+}} = -3 \times 10^{10} \times L_{p0} + 1.1354 \quad (16)$$

$$\sigma_{Mg^{2+}} = -3 \times 10^{10} \times L_{p0} + 1.2559 \quad (17)$$

$$P_{s_{Cl^-}} = 1 \times 10^{11} \times L_{p0} - 1.1144 \quad (18)$$

$$P_{s_{Na^+}} = 6 \times 10^{10} \times L_{p0} - 0.0147 \quad (19)$$

$$P_{s_{SO_4^{2-}}} = 4 \times 10^{31} \times {L_{p0}}^{3.0496} \quad (20)$$

$$P_{s_{Ca^{2+}}} = 1 \times 10^{11} \times L_{p0} - 0.7388 \quad (21)$$

$$P_{s_{Mg^{2+}}} = 9 \times 10^{30} \times {L_{p0}}^{2.9414} \quad (22)$$

As previously explained, the correlations represented by Equations (13)–(22) are applicable only for seawater with similar TDS and ionic composition. For a change in feed, the coefficients need to be established through experimental data. Equations (13)–(22) can be used for determining σ and P_s of polyamide membranes with pure water permeabilities between 5×10^{-12} to 3×10^{-11} m s^{-1} Pa^{-1}, which include membranes with a pore size of 0.4 to 0.86 nm, according to Table 4.

The following steps were performed to run the model for predicting transport parameters and rejection.

(1) Using Equations (13)–(22), the model was run to predict $\sigma_{\text{theoretical}}$ and $P_{s,\text{theoretical}}$ for two NF membranes with pure water permeabilities as in Table 5.
(2) Flux for the above-mentioned NF membranes with seawater as feed was calculated using Equation (2). A random flux value at 12 bar was chosen for the model.
(3) The values for $\sigma_{\text{theoretical}}$ and $P_{s,\text{theoretical}}$, and flux at 12 bar was substituted into Equations (5) and (6) to calculate the theoretical rejection ($R_{\text{theoretical}}$).
(4) To validate the calculated equations, ion rejection by the two chosen NF membranes was experimentally determined ($R_{\text{experimental}}$) using Equation (1) for individual ions in seawater. These rejection values were plotted against the respective membrane flux values, and transport parameters were determined by fitting the values using the Spiegler–Kedem equation. Hence, $\sigma_{\text{experimental}}$ and $P_{s,\text{experimental}}$ were determined.

Table 5 shows the results obtained based on the model and on experiments performed by two chosen NF membranes.

Table 5. Comparison of experimental and theoretical values from the Spiegler–Kedem equation.

Pure Water Permeability, m s^{-1} Pa^{-1}	Flux at 12 bar, m s^{-1}	Ions	$\sigma_{\text{theoretical}}$	$\sigma_{\text{experimental}}$	$P_{s,\text{theoretical}}$, m s^{-1}	$P_{s,\text{experimental}}$, m s^{-1}	$R_{\text{theoretical}}$	$R_{\text{experimental}}$
2.56×10^{-11}	2.06×10^{-5}	Cl^-	0.22	0.18	1.44×10^{-5}	2.11×10^{-5}	0.16	0.11
		Na^+	0.18	0.19	1.52×10^{-5}	1.52×10^{-5}	0.13	0.14
		SO_4^{2-}	0.83	0.97	1.99×10^{-6}	5.34×10^{-7}	0.79	0.96
		Ca^{2+}	0.37	0.41	1.82×10^{-5}	1.88×10^{-5}	0.23	0.24
		Mg^{2+}	0.44	0.45	6.27×10^{-6}	6.15×10^{-6}	0.42	0.41
1.24×10^{-11}	8.90×10^{-6}	Cl^-	0.35	0.36	1.23×10^{-6}	4.24×10^{-6}	0.35	0.29
		Na^+	0.26	0.25	7.28×10^{-6}	7.31×10^{-6}	0.17	0.16
		SO_4^{2-}	0.99	0.99	2.18×10^{-7}	4.86×10^{-7}	0.97	1.00
		Ca^{2+}	0.76	0.82	4.99×10^{-6}	1.47×10^{-6}	0.53	0.75
		Mg^{2+}	0.89	0.92	7.44×10^{-7}	3.28×10^{-7}	0.85	0.96

Table 5 shows a close correlation between the model and experimental values of σ, P_s, and rejection of all ions except for Ca^{2+} for the membrane with lower pure water permeability. This validates the robustness of the model. Table 5 indicates that rejection for the divalent anion SO_4^{2-} was highest for all tested membranes indicating the negative surface of the NF membranes. Focusing on the rejection of divalent cations, Mg^{2+} was rejected more than Ca^{2+} due to its larger Stokes radius as shown in Table 1.

The individual ion selectivity is a key parameter for selecting appropriate membrane for smart water production. In this research, the Spiegler–Kedem model was used for determining individual ion transport through the membrane rather than overall solute transport, which has been extensively studied previously. The study is relevant for end users to select proper NF membranes for producing smart water without extensive membrane experiments.

5. Conclusions

Membrane transport parameters were determined by fitting the Spiegler–Kedem equation using flux and rejection values obtained from experiments using six NF membranes. The theoretical rejection

values obtained by fitting the Spiegler–Kedem equation showed good correlations with experimental values for NF membranes with a similar membrane material. It was evident that it was difficult to increase the membrane water flux without losing ion selectivity and membrane flux was directly related to the effective membrane pore radius. The flux was higher for membranes with $r_p > 0.7$ nm. However, membrane ion rejection decreased with higher r_p. The hypothetical pore radii of six membranes were evaluated from permeation experiments with charged ions using a steric hindrance pore model. The pore radii of membranes were estimated from 0.4 nm to 2.15 nm. The experiments concluded that the membranes had a pore size distribution rather than a single pore radius. A sharp change in σ and P_s of sulfate were observed when plotted against pure water permeabilities of polyamide membranes. Hence, choosing an NF membrane for smart water production in carbonates requires much attention when having pure water permeabilities above 2.6×10^{-11} m s^{-1} Pa^{-1} where the SO_4^{2-} rejection will be low. The suggested method helps to predict NF rejection for smart water production from seawater and for feeds with a high concentration and multi-ionic solutions as in softening and desalination.

Supplementary Materials: The following are available online at http://www.mdpi.com/2077-0375/8/3/78/s1, Figure S1: Rejection versus flux for Na^+ for ESNA fitted using Spiegler–Kedem model, Figure S2: Rejection versus flux for Na^+ for HYDRACoRe10 fitted using Spiegler–Kedem model, Figure S3: Rejection versus flux for Na^+ for HYDRACoRe50, Figure S4: Rejection versus flux for Na^+ for NF270, Figure S5: Rejection versus flux for Na^+ for SR 90, Figure S6: Rejection versus flux for Na^+ for NANO SW, Figure S7: Rejection versus flux for Na^+ for all NF membranes.

Author Contributions: Conceptualization, R.N. and T.B.; Methodology, R.N.; Software, R.N.; Validation, R.N., E.P., S.S. and T.B.; Formal Analysis, R.N.; Investigation, R.N.; Resources, R.N., E.P.; Data Curation, R.N.; Writing-Original Draft Preparation, R.N.; Writing-Review & Editing, E.P., S.S., T.B.; Visualization, R.N.; Supervision, S.S., T.B.; Project Administration, T.B.; Funding Acquisition, T.B.

Funding: This research did not receive any specific grant from funding agencies in the public, commercial, or not-for-profit sectors.

Acknowledgments: The authors acknowledge the Research Council of Norway and the industry partners, ConocoPhillips Skandinavia AS, Aker BP ASA, Eni Norge AS, Total E&P Norge AS, Equinor ASA, Neptune Energy Norge AS, Lundin Norway AS, Halliburton AS, Schlumberger Norge AS, Wintershall Norge AS, and DEA Norge AS of The National IOR Centre of Norway for support.

Conflicts of Interest: The authors declare no conflict of interest.

References

1. Austad, T. Water-based EOR in Carbonate and Sandstone: New Chemical Understanding of the EOR-Potential using "Smart water". In *Enhanced Oil Recovery Field Case Studies*; Sheng, J., Ed.; Gulf Professional Publishing: Houston, TX, USA, 2013; pp. 301–335.
2. Nair, R.R.; Protasova, E.; Strand, S.; Bilstad, T. Membrane performance analysis for smart water production for enhanced oil recovery in carbonate and sandstone reservoirs. *Energy Fuels* **2018**, *32*, 4988–4995. [CrossRef]
3. Cheryan, M. *Ultrafiltration and Microfiltration Handbook*; CRC Pres: Boca Raton, FL, USA, 1998.
4. Oatley-Radcliffe, D.; Walters, M.; Ainscough, T.J.; Williams, P.M.; Mohammad, A.W.; Hilal, N. Nanofiltration membranes and processes: A review of research trends over the past decade. *J. Water Process. Eng.* **2017**, *19*, 164–171. [CrossRef]
5. Hilal, N.; Al-Zoubi, H.; Mohammad, A.; Darwish, N. Nanofiltration of highly concentrated salt solutions up to seawater salinity. *Desalination* **2005**, *184*, 315–326. [CrossRef]
6. Gilron, J.; Gara, N.; Kedem, O. Experimental analysis of negative salt rejection in nanofiltration membranes. *J. Membr. Sci.* **2001**, *185*, 223–236. [CrossRef]
7. Spiegler, K.; Kedem, O. Thermodynamics of hyperfiltration (reverse osmosis): Criteria for efficient membranes. *Desalination* **1966**, *1*, 311–326. [CrossRef]
8. Kedem, O.; Katchalsky, A. Permeability of composite membranes: Part 1. Electric current, volume flow and flow of solutes through membranes. *Trans. Faraday Soc.* **1963**, *59*, 1918–1953. [CrossRef]
9. Murthy, Z.; Gupta, S.K. Estimation of mass transfer coefficient using a combined nonlinear membrane transport and film theory model. *Desalination* **1997**, *109*, 39–49. [CrossRef]

10. Jye, L.W.; Ismail, A.F. *Nanofiltration Membranes—Synthesis, Characterization and Applications*; CRC Press, Taylor & Francis Group: Boca Raton, FL, USA, 2017.
11. Diwara, C.K.; Lo, S.; Rumeau, M.; Pontie, M.; Sarr, O. A phenomenological mass transfer approach in nanofiltration of halide ions for a selective defluorination of brackish drinking water. *J. Membr. Sci.* **2003**, *219*, 103–112. [CrossRef]
12. Nakao, S.I.; Kimura, S. Models of membrane transport phenomena and their applications for ultrafiltration data. *J. Chem. Eng. Jpn.* **1982**, *15*, 200–205. [CrossRef]
13. Wang, X.L.; Tsuru, T.; Togoh, M.; Nakao, S.I.; Kimura, S. Evaluation of pore structure and electrical properties of nanofiltration membranes. *J. Chem. Eng. Jpn.* **1994**, *28*, 186–192. [CrossRef]
14. Bowen, R.; Mohammad, W.A. Diafiltration by Nanofiltration: Prediction and Optimization. *AIChe J.* **1998**, *44*, 1799–1812. [CrossRef]
15. Hussain, A.; Nataraj, S.; Abashar, M.; Al-Mutaz, I.; Aminabhavi, T. Prediction of physical properties of nanofiltration membranes using experiment and theoretical models. *J. Membr. Sci.* **2008**, *310*, 321–336. [CrossRef]
16. Luo, J.; Wan, Y. Effect of highly concentrated salt on retention of organic solutes by nanofiltration polymeric membranes. *J. Membr. Sci.* **2011**, *372*, 145–153. [CrossRef]
17. Hilal, N.; Al-Zoubi, H.; Darwish, N.; Mohammad, A. Characterisation of nanofiltration membranes using atomic force microscopy. *Desalination* **2005**, *177*, 187–199. [CrossRef]
18. Yaroshchuk, A. Negative rejection of ions in pressure-driven membrane processes. *Adv. Colloid Interface Sci.* **2008**, *139*, 150–173. [CrossRef] [PubMed]
19. Nilsson, M.; Tragårdh, G.; Ostergren, K. The influence of pH, salt and temperature of nanofiltration performance. *J. Membr. Sci.* **2008**, *312*, 97–106. [CrossRef]
20. Deshmukh, S.S.; Childress, A. Zeta potential of commercial RO membranes: Influence of source water type and chemistry. *Desalination* **2001**, *140*, 87–95. [CrossRef]
21. Tansel, B. Significance of thermodynamic and physical characteristics on permeation of ions during membrane separation: Hydrated radius, hydration free energy and viscous effects. *Sep. Purif. Technol.* **2012**, *86*, 119–126. [CrossRef]